Microwave Mineral Analysis

Prepared by:
Yafas Alahsan Shaikh

A dissertation submitted to the Department of Electrical Engineering, University of Cape Town, in fulfilment of the requirements for the degree of Master of Science in Engineering

Cape Town, January 2004

Declaration

I Yafas Alahsan Shaikh declare that this is my own, unaided work. It is being submitted for the degree of Master of Science in Electrical Engineering at the University of Cape Town. It has not been submitted before for any degree or examination in any other university.

Signature of Author Signed by candidate

Cape Town
December 2003

Terms of Reference

The Namakwa Sands Mineral Processing Company, located 500 km north of Cape Town on the West Coast of South Africa, is responsible for extracting minerals from the earth for various industrial purposes. The most extensively extracted mineral is **Zircon,** an **insulator.** It has two major impurities, **Rutile** and **Leucoxene** which are **conductors.** Namakwa Sands Mineral Processing Company proposed and commissioned this thesis at the University of Cape Town on the 15 of February 2003. Professor Downing specified that the purpose of this thesis was to design and build an **inexpensive mineral analyzer,** resulting in a great improvement in process control and thus efficiency at the mineral processing plant. This system should be able to identify the percentage purity of Zircon (a sand sample used for the manufacturing of ceramic tiles) in a sample of impurities. This thesis was conducted in fulfillment of the requirements towards a Master of Science in Electrical Engineering degree at the University of Cape Town.

Professor Downing's specific instructions were to:

- **Design and fabricate a low cost prototype system** - The design must be cost effective, as a number of systems may be built and installed in each stream of the plant.
- **Suitable dynamic range** - The system should be able to measure a full scale range from 50% to 100% of Zircon. However, it should it have an error of no more than ± 4% between the range of 70% to 100% Zircon.
- **Provision of a suitable calibration standard** - The system should incorporate a fast, simple and accurate method of calibration.
- **Temperature** - The system should be able to withstand a maximum temperature of 50° C in summer.
- **Humidity** - The measurements should not be affected by day to day changes in relative humidity.

Abstract

The Namakwa Sands Mineral Processing Company, located 500 km from Cape Town up the West Coast, is responsible for extracting minerals from the earth for various industrial purposes. The most extensively mined mineral is **Zircon**. It is used in the production of ceramic tiles, sanitary ware, a wide range of advanced ceramics, refractories and jewellery. It is also used in electronic appliances such as TV screens and computer monitors.

Zircon itself is an **insulator** but when mined it contains two major impurities: **Rutile** and **Leucoxene.** These are **conductors**. A cheap and rapid method is required to measure the proportions of these impurities in the final mixture.

There are currently two methods used at the mine to measure the components of the initial Zircon mixture. The first is **X-ray analysis** and generates results with a high degree of accuracy. However, this measurement technique takes a long time and is very costly and thus only a limited number of samples are measured. The second method used is **physical grain counting** and is also very accurate. The major drawback of this technique is that it is extremely labour intensive and time consuming (taking approximately ten days).

The capacitive measurement technique was consequently investigated and appeared to be the most viable. This was tried and tested to aid in the analysis as an additional quick and inexpensive method (as an addition to the above methods). However, it was found that the measurements were greatly influenced by day to day changes in the relative humidity of the atmosphere, as the mine is located near the sea shore.

Due to the limitations of the current methods, we were approached by the mineral sands producer to investigate alternative analytical techniques. The main requirements were that the system chosen should be an **inexpensive, easy to use analyser.** It should not be affected by the day to day change in humidity and hence would result in a great improvement of process control and thus efficiency.

After analysing numerous available techniques, the **microwave attenuation technique** was selected, as it was the most favourable compromise between cost and accuracy.

The attenuation characteristics of a range of sand samples (including the effect of relative humidity) were measured. The optimum frequency was found to be 10.5GHz. This frequency was largely determined by the availability of commercial components at minimum expense. The range of attenuation measurements was found to be about 30dB, an easily manageable dynamic range within which good accuracy can be achieved.

The proposed transmitter was a switched power supply for a 10.5GHz Gunn oscillator at a modulated frequency of 1KHz. This allowed the use of AC amplification at the receiving end. The receiver circuit used a simple low-level microwave detector diode to pick-up the attenuated signal. A rectangular waveguide proved a suitable transducer to propagate the waves from the transmitter to the receiver as none of the energy escaped into the surroundings.

The prototype was built and tested. The results obtained gave a clear correlation between the attenuated signal and percentage impurity, and displayed an accuracy of $\pm$ 2 %. A suitable system for calibration was then found and later programmed into a chip as a look-up table that drove an LCD screen, which was used as a display. The system proved to be unaffected by changes in atmospheric conditions.

Although this system worked well, the waveguide transducer had to be quite long in order for the microwave signal to be attenuated sufficiently. In order to reduce the size of the transducer a microwave resonant cavity technique was developed. The optimum frequency proved to be 1.598 GHz. A rectangular cavity operating at T_{101} mode, gave the best results. The system was very successful with tests showing that the complex permittivities of the dielectrics could be measured repeatedly with a high degree of accuracy. The results of measured mineral powder are presented and discussed. These results showed substantial variation in both the dielectric constant and the loss factor for

the different mineral. The results were plotted on a plane of complex permittivity that clearly illustrates the potential of using cavity perturbation techniques for mineral differentiation and sorting.

Microwave measurement techniques do not offer the same accuracy and versatility as existing sophisticated analysis techniques (eg. X-ray spectroscopy, NMR, ESR), but they are a simple, quick and low cost measurement systems for applications of this sort.

Acknowledgements

I hereby would like to express my sincere words of thanks to my supervisor, Prof. B. Downing, for assisting, advising and for his tireless effort of supporting me during the course of this thesis. I also wish to thank Mr. Schire for his advice on electronic circuitry. A special thanks also goes to my best friend Javaneh Mahmoudi for being by my side at all times. I would like to also thank my family and specially my mother for her love and support, without whom this thesis would not been a success.

TABLE OF CONTENTS

List of Illustrations

Chapter 1

1. Introduction

1.1 Process Overview

The Namakwa Sands Mineral Processing Company, located 500 km north of Cape Town on the West Coast of South Africa, is responsible for extracting minerals from the earth for various industrial purposes. The most extensively extracted mineral is **Zircon,** which is an **insulator.** It has two major impurities, **Rutile** and **Leucoxene** which are **conductors**. The minerals are extracted in the form of slurry from sand dunes formed near the sea shore and then pumped into a concentrator. The heavy and light minerals are separated using a gravimetric technique, then stockpiled. The heavy mineral concentrate is taken to the mineral separation plant [1].

At the plant, the heavy mineral concentrate is re-slurried (mixed with water). The slurry is then passed over a magnetic bed (Figure 1.1) to extract a mineral called **Ilmenite** which is used as feedstock for the smelter as can be seen in Figure 1.3. This is an overview of the process [1]. Ilmenite is roasted and mixed with **charred** Anthracite (heated and dried in another process) to form an iron oxide. This is then fed to electric arc furnaces where it is reduced to high purity iron and **Titanium Dioxide rich slag** as a by-product. The Titanium slag is used in paints, plastics, paper, sweets, cosmetics and toothpaste due to its non-toxic and biologically inert properties [2]. The high purity iron (pig iron) is used as a raw material to reproduce ductile iron castings used in automotive parts (brake callipers and steering knuckles).

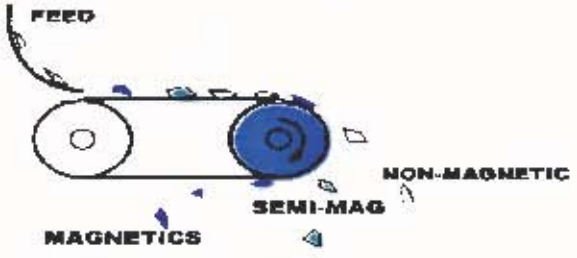

Figure 1.1 Magnetic Separation [3]

Zircon, **Rutile** and **Leucoxene** and other non-magnetic minerals are then sent to the drier where they are dried and separated, (using a high voltage electrostatic field) into **insulators (Zircon)** and **conductors (Rutile** and **Leucoxene)** as shown in Figure 1.2. Zircon is further purified to produce a higher grade product [1].

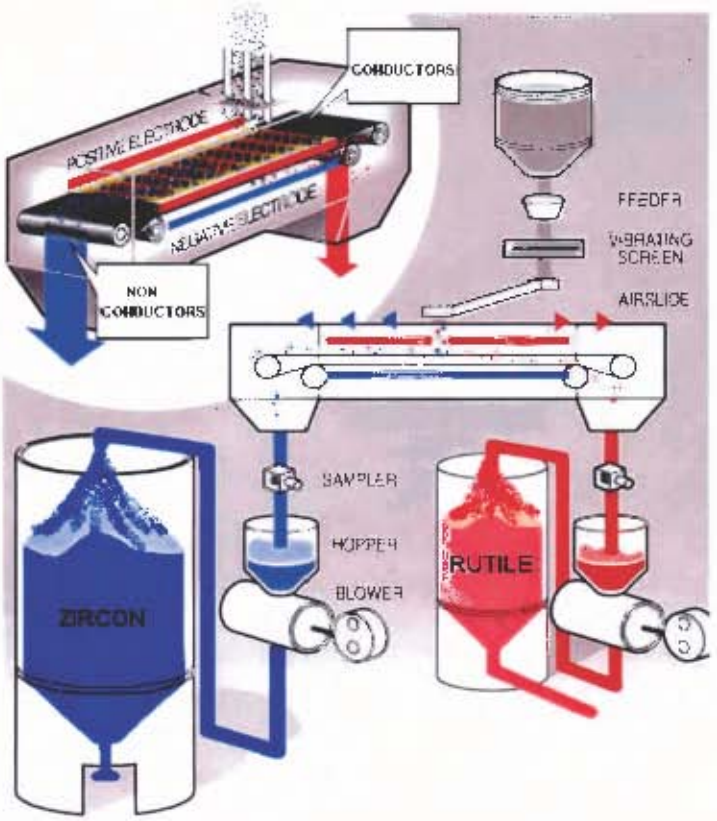

Figure 1.2 Electrostatic Separation [28]

Rutile and Leucoxene are mainly used in welding rod fluxes. Due to their strength, corrosion and heat resistance properties, they are also used in aerospace, and aviation industries, and in the manufacture of artificial hip joints, heart pacemakers and spectacle frames [2].

Zircon is used in the production of: ceramic tiles; sanitary ware; a wide range of advanced ceramics; refractories; jewellery; electronic applications; a component in TV screens and computer monitors; and many other industrial and domestic products [2]. An overview of the process is seen in Figure 1.3.

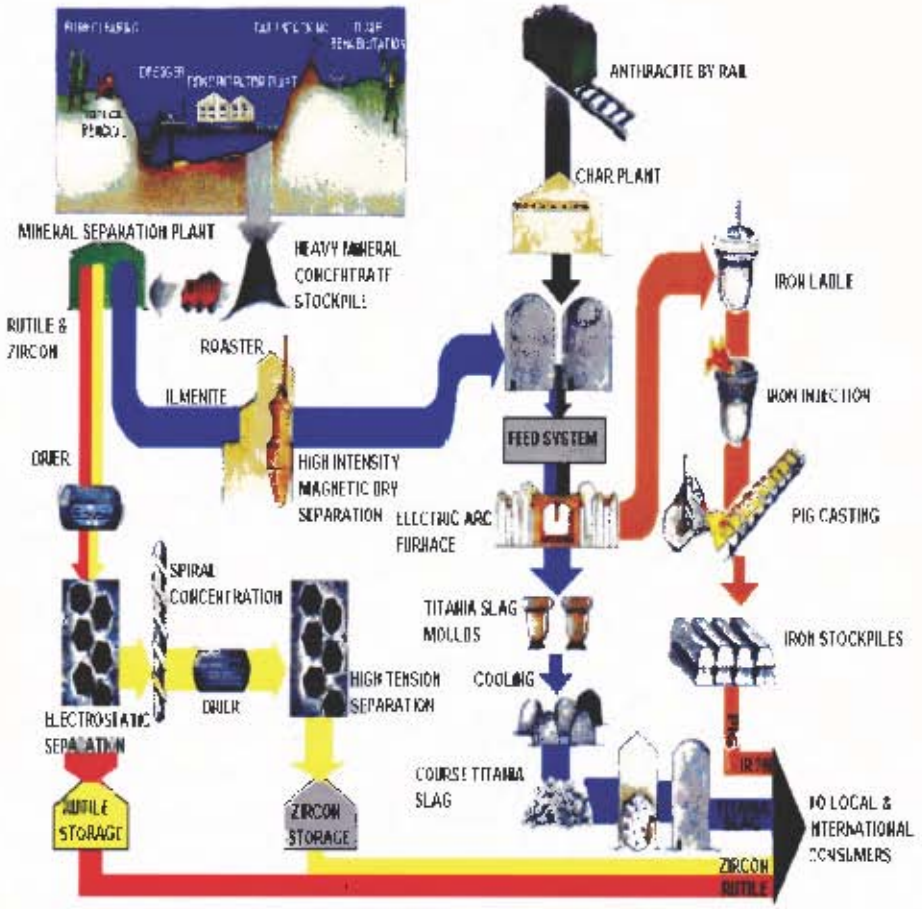

Figure 1.3 Process Overview [1]

1.2 Problem Statement

The major problem faced by the mine is measuring how pure the extracted minerals are in the final mixture. Currently, there are two methods of doing this.

1. X-ray analysis, which achieves results with a high degree of accuracy. However, the measurement equipment is very costly and thus only a limited number of samples are measured. It also takes about 30 minutes to complete a measurement.
2. Physical grain counting. This is also very accurate but is extremely labour intensive and time consuming (taking approximately ten days).

Capacitive measurement was tested as a viable alternative method. However, it was found that the measurements were greatly influenced by day to day changes in the relative humidity of the mines atmosphere; this was due to the hygroscopic nature of the mineral, absorbing moisture from the atmosphere. The resulting relative permittivity of the mineral was shown to change appreciably with moisture absorption.

1.3 Objective

Existing methods of analyzing the proportions of minerals in the final mixture are unable to do this quickly at a low enough cost. Hence, we were approached by the mineral sands producer to investigate alternative techniques. The main requirement of the producer was that the system should be an **inexpensive mineral analyzer**, resulting in a great improvement in process control and thus efficiency.

1.4 Namakwa Sands Specific Requirements

The specific requirements were:

- **Design and fabricate a low cost prototype system** - The design must be cost effective, as a number of systems may be built and installed in each stream of the plant.
- **Suitable dynamic range** - The system should be able to measure a full scale range from 50% to 100% of Zircon. However, it should it have an error of no more than ± 4% between the range of 70% to 100% Zircon.
- **Provision of a suitable calibration standard** - The system should incorporate a fast, simple and accurate method of calibration.
- **Physical dimensions** - The system should be no larger than 600mm × 600mm × 600mm.
- **Temperature** - The system should be able to withstand a maximum temperature of 50° C in summer.
- **Humidity** - The measurements should not be affected by day to day changes in relative humidity.

- **Robust system** - Although sensitive to mineral properties, the system should be robust with very little maintenance required.

1.5 REVIEW OF EXISTING TECHNIQUES

There are several existing techniques that could be used to measure the percentage of impure minerals in a Zircon mix. This section briefly outlines of some of them and describes their advantages and disadvantages.

1.5.1 Infra-red Spectroscopy

Every element in a compound is joined to another element by a chemical bond. These bonds vibrate at specific resonant frequencies and are dependent on the size and the mass of the atoms involved [4]. Taking this property into account, an infrared beam of specific frequency is passed through the sample under investigation and the spectrum of reflected (or absorbed) light is measured as can be seen in Figure 1.4. This information is then compared to a look-up table and hence the concentration of each compound in the sample is identified.

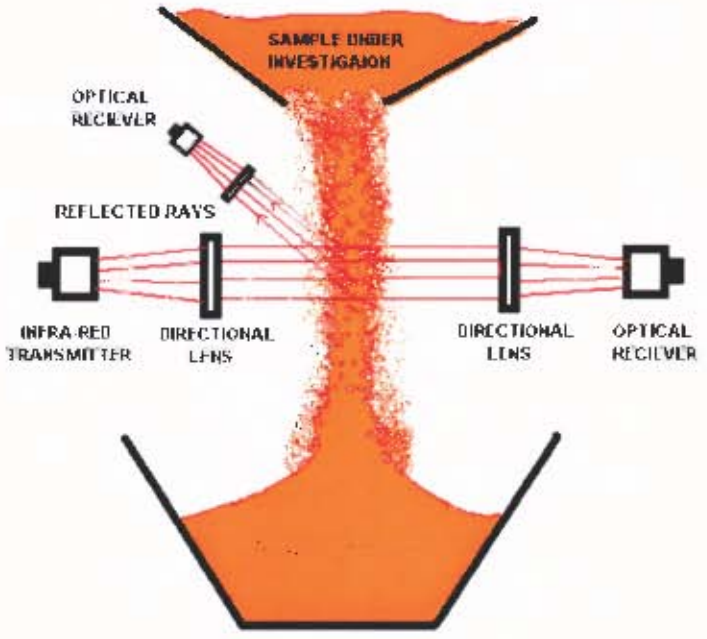

Figure 1.4 Infra-Red Analysis

The advantages of the technique are:

- The system is compact and thus versatile.
- It is fairly accurate.
- It is not temperature dependent as it relies on the optical characteristic of the sample.

The disadvantages are:

- It is very costly.
- Since it is an open structure, the presence of moisture has significant influence on readings.
- It would be difficult to implement this application due to environmental considerations, such as dust created when pouring sand samples [9].

1.5.2 X-ray Fluorescence Spectroscopy (XRF)

This technique is shown in Figure 1.5, and is presently used at the mineral processing plant.

Figure 1.5 XRF Analysis [6]

X-ray beams are passed through the sample in a vacuum chamber. This induces kinetic energy in the electrons and induces them to jump to a higher energy band causing the sample to produce fluorescent X-rays [5]. The fluorescent energy is measured to provide spectral information about the elements in the sample.

The technique has the following advantages:

- The system is very accurate.
- Moisture error is easily avoided since the sample is placed in a vacuum.

The disadvantages are:

- The X-ray can be easily absorbed by the sample in the electrons excitation process, resulting in errors [7].
- Highly skilled labour is required.
- The capital equipment is very expensive.

1.5.3 Nuclear Magnetic Resonances (NMR)

The sample under investigation is placed in an external magnetic field and radio waves are applied to it. At a certain frequency, the radiation is absorbed by the atomic nuclei and the nucleus enters an excited state. In this excited state the nuclei undergoes an electron spin effect, thus changing the orientation of spin in the nuclei. The atom then goes back to its original orientation (relaxation) and in doing so releases radiation. This re-emitted radiation is measured with respect to (time) and quantity, to determine the concentration of elements in a sample. A diagram of the technique is shown in Figure 1.6.

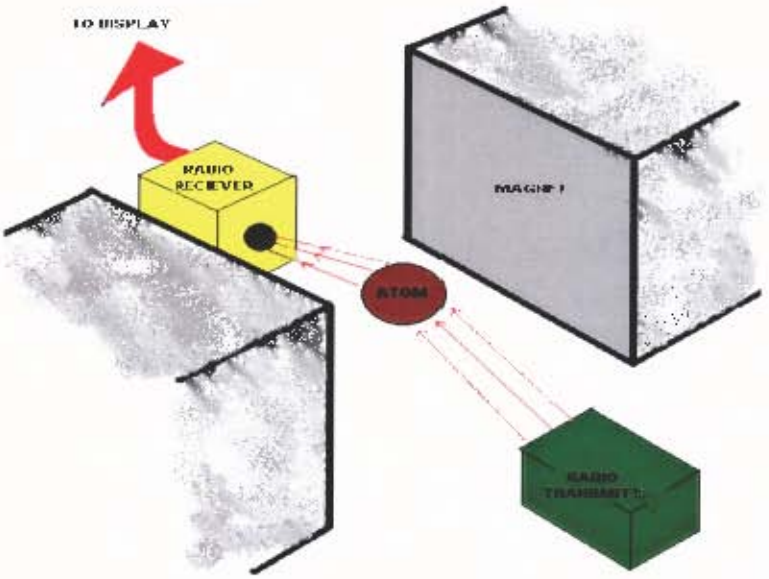

Figure 1.6 NMR Spectroscopy

The main advantage of NMR is that it is very accurate and external environmental conditions are easily accommodated. However, the system is extremely labour intensive and, like the XRF spectroscopy previously mentioned, the capital equipment is extremely expensive.

1.5.4 Microwave Technique

Microwaves lie in the region of 1GHz to 100GHz of the frequency spectrum. The advantages of microwaves are that they pass right through insulators (Zircon) without affecting the material, and the effects of moisture can easily be detected and accommodated for. Microwaves of specific frequency are passed through the sand sample and the power absorbed is measured. This would give an indication as to how much of the impurities (conductors) are in the sand.

1.6 Choice of Approach and layout of Thesis

After reviewing the system requirements, and due to the limitations mentioned in the above processes, it seemed that the use of microwaves would be an appropriate choice. Various mineral samples were tested using a microwave network analyser. The attenuation measurements carried out gave a good correlation between attenuation values and percentage impurities i.e. they were almost linear. The measurements also indicated a good dynamic range of 3dBs to 30dBs.

The dielectric properties of the mineral samples were then investigated in order to understand the interaction of microwaves and the minerals concerned. Chapter two provides a brief overview of dielectric permittivity and the effects of moisture on microwave measurements.

Chapter three describes the different components that could be used in building the measuring instrument with their advantages and disadvantages.

The planned approach is to have a 10.5GHz transmitter which was amplitude modulated at a frequency of 1KHz. The receiver circuit will be connected to the system and will display the attenuation measurement in voltage form. A look-up table will be created from which the percentage impurities could be recorded. The method of propagation of the microwaves could be waveguides or antennae. The implementation of the preferred method is described in Chapter four and the results and conclusions from the measurements using this system are provided in Chapter five.

The literature review for the second measuring technique, Cavity Perturbation technique, is given in Chapter six and the implementation of the second system is described in Chapter seven. The results and analysis of data found is provided in Chapter eight. Finally, the thesis is concluded in Chapter nine.

Chapter 2

2. Characteristics of Dielectric Materials

The term dielectric describes materials that exhibit definite properties when placed in an electric field, even though they are good insulators. These properties are best understood through consideration of their effect on capacitors.

Suppose a voltage V is applied to two parallel plates of a capacitor of capacitance C: the charged stored Q is given by the relationship Q = CV [10]. Filling the plates with a dielectric increases the capacitance from C_o to C_i. The relative permittivity ε_r is given by:

$$\varepsilon_r = \frac{C_i}{C_o} \tag{2.1}$$

Thus, a capacitor made of rectangular parallel plates of area A and separated by distance d, filled with a dielectric with a relative permittivity ε_r will be defined by the following relationship [10]:

$$C = \frac{\varepsilon_r \varepsilon_0 A}{d} = \frac{\varepsilon A}{d} \tag{2.2}$$

ε = *Absolute Permittivity of dielectric medium*

εo = *Permittivity of vacuum* ($8.85 \times 10^{-12} F/m^2$)

Dielectric materials are considered to be good insulators implying that they do not have any free electrons for conduction and giving a net charge of zero. However, at molecular level the positive and negative charges of dielectric materials do not perfectly align themselves to completely cancel out each other. Such materials are thus regarded as polar and possess a permanent dipole moment about their axis. The magnitude of the dipole ρ

is equal to the product of the charge q and the distance d between the positive and negative charges of the atom. This shown in Figure 2.1.

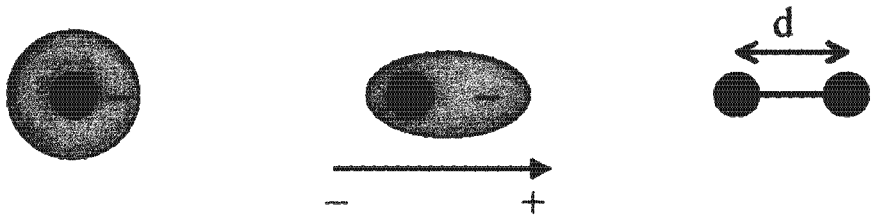

Figure 2.1 Effect of Charge on Polar Molecules [10]

2.1 Polarisation and Electric Susceptibility in Dielectrics

Under the influence of an external electric field the charge is redistributed in such a way that the negative charges align themselves near the positive plate and the positive charges at the negative plate, as shown in Figure 2.2. This effect is known as polarisation and is defined as the net charge Q' per effective area A of plates (P = Q'/A).

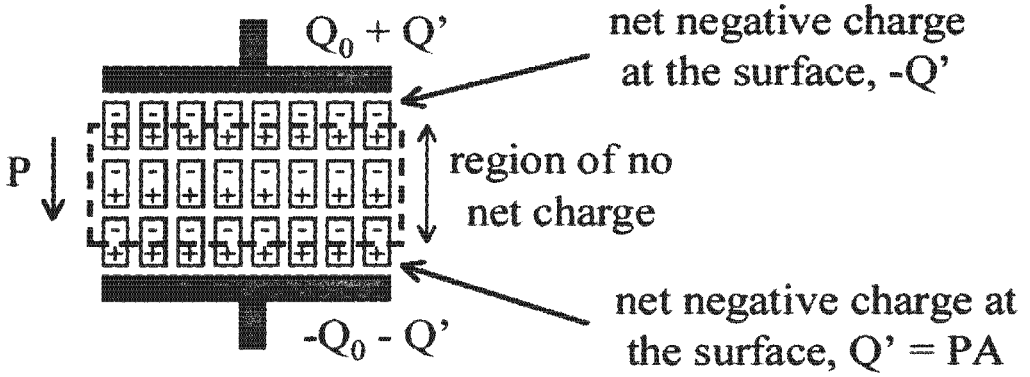

Figure 2.2Effect of Electric Field on Polar Molecules [10]

At this stage one can easily see that the greater the electric field intensity E the greater the polarisation as described by the following Equation:

$$P = \epsilon_o \chi_e E \qquad (2.3)$$

χ_e is the dielectric susceptibility and is a Figure of merit which describes how easily the material will be polarised. The relative permittivity can also be written in terms of electric susceptibility:

$$\epsilon_r = 1 + \chi_e \tag{2.4}$$

From Equations (2.3) and (2.4) it can be easily be seen that the easier the material is polarised, the larger the relative permittivity.

2.1.1 Types of Polarisation

There are three common types of polarisation:

2.1.1.1 Electronic Polarisation

Figure 2.3 Electronic Polarisation [10]

This occurs in all materials and is due to induced dipole moment created through non-symmetrical positioning of the electrons and protons at any given point (see Figure2.3). This type of polarisation is fairly weak and is associated with the bonding between air molecules [10].

2.1.1.2 Ionic or Induced Polarisation

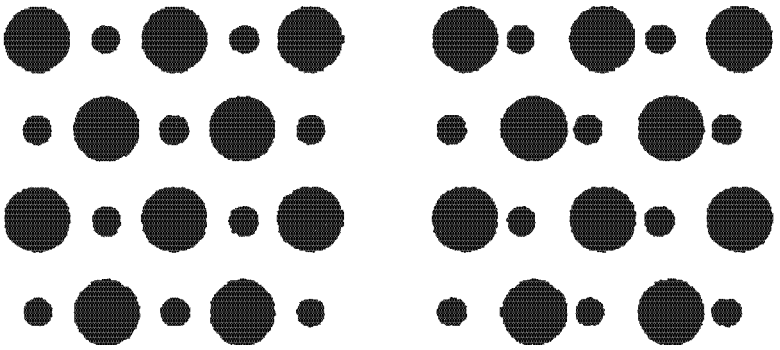

Figure 2.4 Ionic Polarisation [10]

Ionic polarisation occurs in ionic compounds where the cat-ions and an-ions are attracted to the opposite charged plates when an electric field is applied, as can be seen in Figure 2.4. A good example is the electrolysis process [10].

2.1.1.3 Molecular or Orientation Polarisation

Figure 2.5 Orientation Polarisation [10]

Molecular polarisation occurs in materials that have permanent dipole moments. On application of an electric field, the molecules align themselves, resulting in strong polarisation (see Figure 2.5). A good example is water molecules and associated Van Der Waal forces.

2.2 Complex permittivity

When an **alternating** electromagnetic field is applied to a dielectric, a current, i, will flow [11].

$$i = j\omega\varepsilon_r c_0 v \tag{2.5}$$

ω = *operating frequency*
ε_r = *relative permittivity*
c_0 = *capacitance*
v = *alternating e.m.f*

This forces the dipoles to align themselves in the direction of the E-field.

At this stage "it is more convenient to work with the electric displacement vector D, rather than polarisation" [12] when dielectric permittivity is concerned and is defined by the following Equation:

$$D = \varepsilon_0 E + p \tag{2.6}$$

ε_0 = *permittivity in free space*
E = *alternating electric field*
P = *polarisation*

The attempt of the dipoles to align themselves to the alternating field results in the polarisation lagging the electric field [13]. The displacement vector is thus:

$$D = \varepsilon^* E\cos(\omega t - \phi) \qquad ,\phi > 0 \text{ since lag.}$$

Or using phasor notation

$$D = \varepsilon^* e^{-j\phi} E\cos(j\omega t)$$

where $\varepsilon^* e^{-j\phi}$ represent the phase difference. Thus the complex permittivity is given as [12]:

$$\begin{aligned}\varepsilon_r &= \varepsilon^* e^{-j\phi} \\ &= \varepsilon^*(\cos\phi - j\sin\phi) \\ &= \varepsilon' - j\varepsilon'' \end{aligned} \tag{2.7}$$

ε' = *DC or capacitive measurement*

ε'' = *Dielectric loss factor*

Substituting Equation (2.7) into Equation (2.5) gives:

$$\begin{aligned} i &= j\omega(\varepsilon' - j\varepsilon'')C_0 v \\ &= j\omega\varepsilon'' C_0 v + j\omega\varepsilon' C_0 v \end{aligned} \tag{2.8}$$

where the real part of current is defined by the imaginary part of complex permittivity. This represents the '**loss**' component of current which is proportional to **attenuation**. The imaginary parts of current in Equation (2.8) are defined by the real part of complex permittivity and are proportional to the phase shift.

2.3 Effects of Moisture on Microwave Attenuation

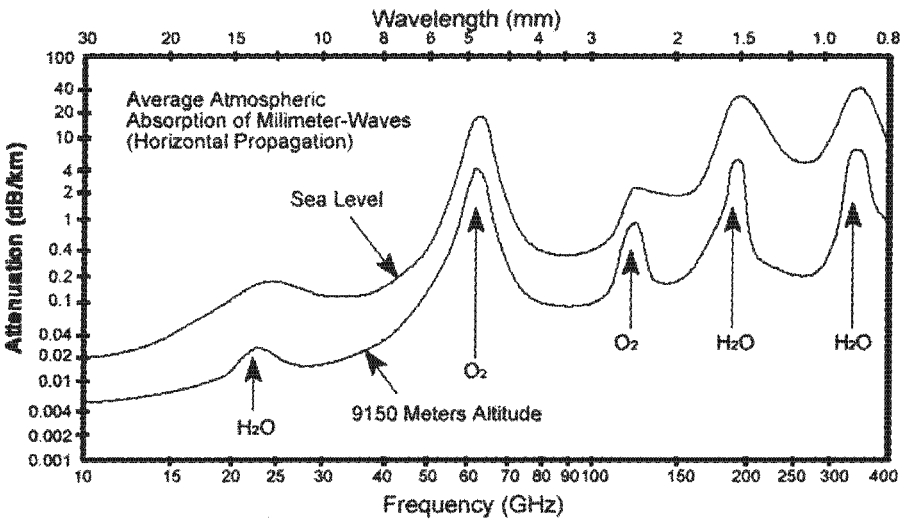

Figure 2.6 Atmospheric Attenuation at Sea Level [8]

The mineral samples are hygroscopic and they absorb moisture from the atmosphere. Thus it is important to study the effects of relative humidity at microwave frequencies. From the Figure 2.6 it can be predicted that for microwave frequencies anywhere between 1.5GHz – 10.5GHz, moisture has very little effect on the attenuation measurements and has a maximum attenuation Figure of 0.02dB/km with average humidity and temperature at sea level. This value is hardly detectable by the network analyser. Thus attenuation will change with changes in humidity and temperature. The mineral samples are hygroscopic and the moisture absorbed from the atmosphere will increase at higher levels of humidity.

Figure 2.7 below shows the effects of rainfall on attenuation. At a frequency of 10GHz the maximum attenuation due to tropical downpour is 1dB/km. This is equivalent to passing microwaves through a cup of muddy water. The mineral samples under investigation, however, are in the form of dry sand. Therefore the moisture content should have very little effect on microwave measurements.

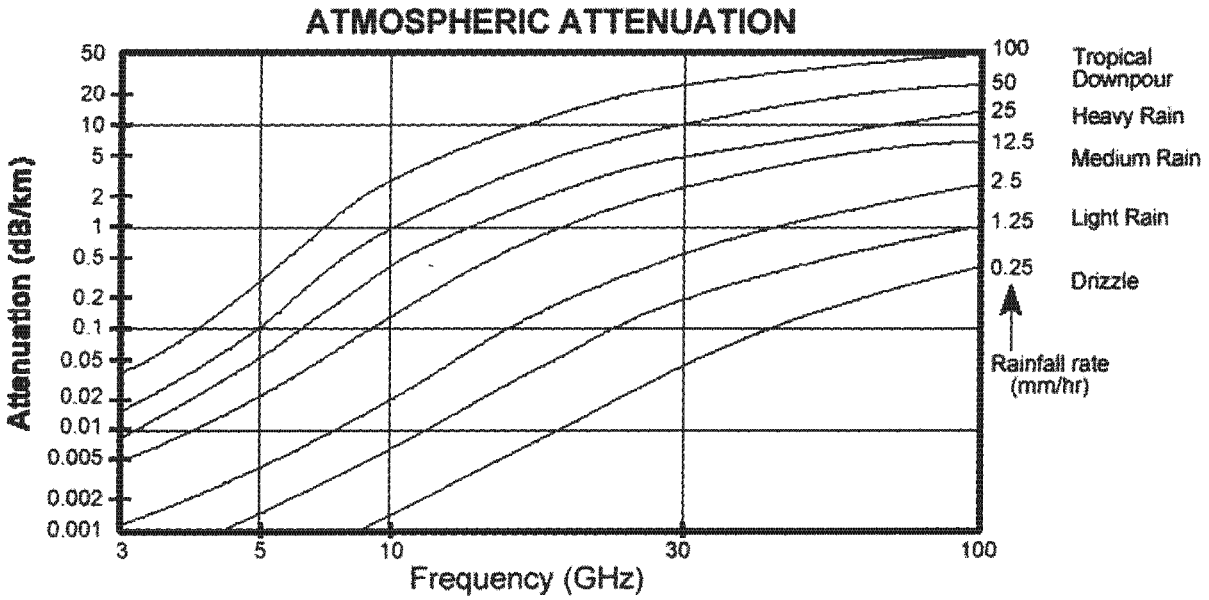

Figure 2.7 Atmospheric Attenuation Due to Rainfall [8]

It should be noted that extensive research has not been carried out on the relationship between the hygroscopic nature of sand samples and changes in relative humidity. Consequently, from the discussion above one cannot conclude that moisture has **no** effect between 1GHz and 10GHz but can argue that it has **very little effect** on the proposed measurements for the following reasons:

- The samples under investigation are relatively dry
- The imaginary part of complex permittivity is measured with the equipment developed in this thesis and not the real part, which is related to capacitive measurements and is greatly influenced by water content.

Nevertheless this can only be finally proved once the instrument has been fabricated and tested in a mining environment.

Chapter 3

3. Microwave Transmitter and Receiver Units

There are several devices that can be used in the transmission and reception of microwaves. A few of the most relevant devices are discussed and the disadvantages and advantages will be considered.

3.1 Selection of Optimum Frequency

Attenuation measurements are related to frequency in such a way that the higher the frequency the greater the attenuation. Thus, to select a suitable frequency, one must consider the following [14]:

- Size of sample under investigation
- Availability of components at that frequency
- Cost of components
- Dynamic range of attenuation

In order to ensure a microwave signal propagates through the mineral sample, a closed structure is used. Frequencies from 2GHz to 12GHz were considered. Circuits using waveguides, coaxial and microstrip with high frequency semiconductors are used. Waveguide circuits are the most attractive as they do not rely on precision connectors to launch microwave power into the test samples .

At frequencies of 10.5GHz, commonly known as the X-band, components are readily available at an affordable price. The range of attenuation measurements was shown to be about 30dB at this frequency using a network analyser. This is an easily manageable dynamic range to achieve using a simple detector diode with good accuracy. The advantage is that the thickness of sample has to be only about 6 cm [14].

Frequencies higher than this would result in an unacceptable increase in the cost of the microwave components. For frequencies lower than this, the size of the waveguide would be too large for the application.

3.2 Transmitter Devices

This section will briefly discuss the theory of two transmitter devices, the Impatt diode and the Gunn diode.

3.2.1 Impatt Diode Oscillator

The Impatt diode works with the physical properties of impact ionization [2], avalanching and time drift. Referring to the Figure 3.1 [16], the reversed bias conditions of the P-N junction exhibits negative AC resistance, which is used to sustain oscillations in a resonant circuit.

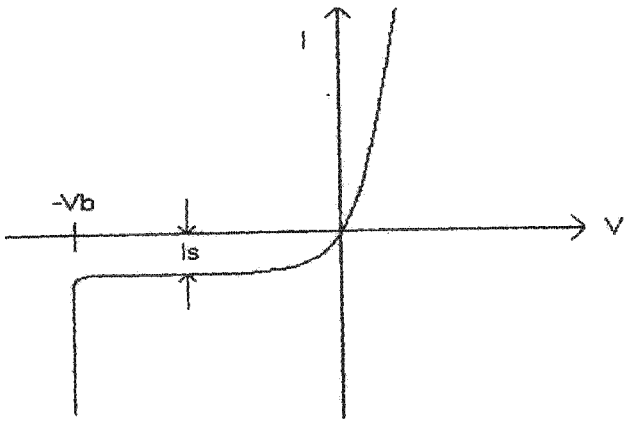

Figure 3.1 Avalanche Characteristic of an Impatt Diode

At voltage -Vb a breakdown results in an avalanche multiplication of holes and electrons. With the formation of electrons and holes, sufficient kinetic energy is gained to further ionize atoms upon collision, resulting in a reverse current (Is) being produced [16]. When a microwave resonant circuit is connected to the Impatt diode, the diode swings in and

out of the avalanche condition. Impatt diode oscillations are relatively noisy, sensitive to bias conditions and unreliable.

3.2.2 Gunn Diodes

The theory of Gunn Diodes will be discussed in greater detail than that of the Impatt diode. They will be used for the transmitter circuit as they are easily available at frequencies of 10.5GHz, can be obtained at lower power consumption and are inexpensive. For this reason it is important to understand how they work. The properties of Gallium Arsenide (material used to make Gunn diodes) are discussed first.

3.2.2.1 Negative Resistance Devices (Gallium Arsenide)

In general, electrons in an atom are set according to quantized energy levels known as conduction bands. If the electrons obtain sufficient energy, they are able to escape their respective bands and move freely through the lattice. In gallium arsenide, electrons in the first conduction band have a higher mobility than in second. Thus, when a voltage is applied to the lattice, electrons in the second conduction band possess drift velocities, so they respond more slowly to any increase in voltage than electrons in the first band [29].

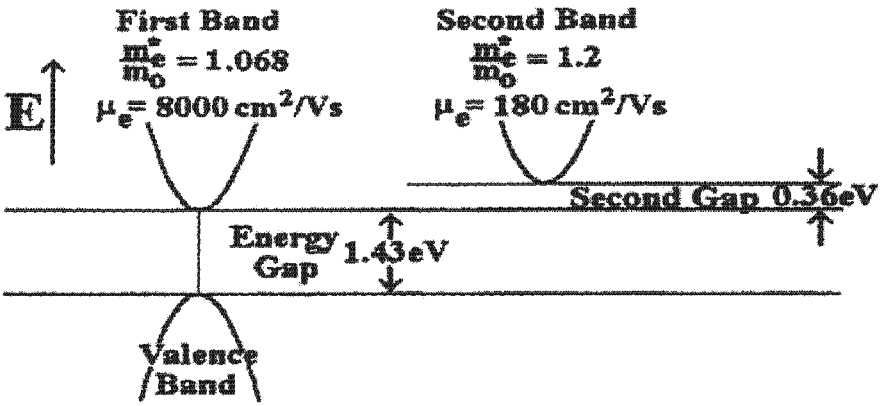

Figure 3.2 Energy Band for GaAs

When an external field is applied to the lattice, the mobility constant, μ_L in the lower band is given by:

$$\mu_L = \frac{v_d}{E} \tag{3.1}$$

v_d = *drift velocity*
E = *electric field*

If the electric field is increased, all the electrons gain enough kinetic energy and jump to the next quantization level with mobility constant, μ_U ,of:

$$\mu_U = \frac{v_d}{E} \tag{3.2}$$

3.2.2.2 Domain of Gallium Arsenide

With the field increased above the threshold field for negative resistance behaviour, electrons near the cathodes move into the upper conduction band, losing mobility as they do so. All electrons move towards the anode but those that jump into the upper band are delayed, forming an electron rich region known as the **domain**. This domain drifts towards the anode and increases the field strength as it does so, increasing in size as it hits the upper band. Finally it terminates at the anode and releases the energy in the form of a current pulse (refer to Figure 3.3) [29].

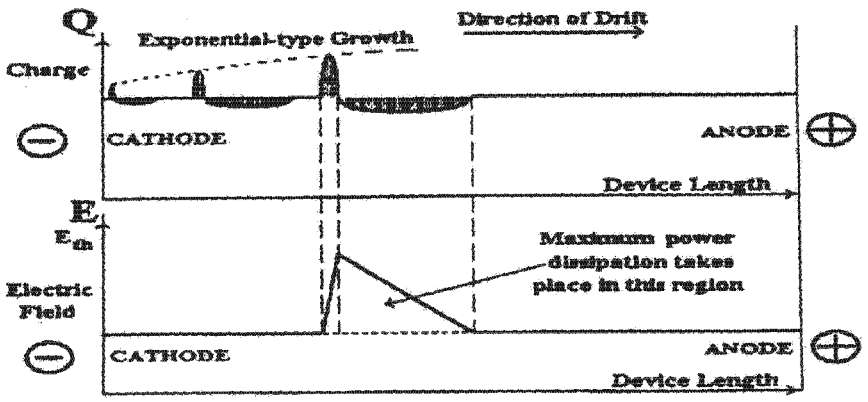

Figure 3.3 Charge and Field Distribution in a Travelling Domain

3.2.2.3 Commercial Gunn Oscillators

A large commercial market exists for Gunn oscillators, mainly as power sources for domestic intruder alarms. These oscillators or power sources use Gunn diodes operating as a negative resistance device in the delayed domain mode. The commercial Gunn oscillator used at the transmitter in this project required a D.C supply of 10V and 0.5A. The output power was nominally 50mW, which is only about 1% efficient.

3.3 The Detector

A microwave signal may be detected using a detector diode (commonly known as a level detector). When the signal is detected, the non-linearities of the diode cause a current to flow as a result of rectification. The diode acts as a square law detector (see Figure 3.4) and converts the low-level amplitude of the received signal to DC [17]. One should note that if high levels of power are applied the diode saturates, limiting the dynamic range [18].

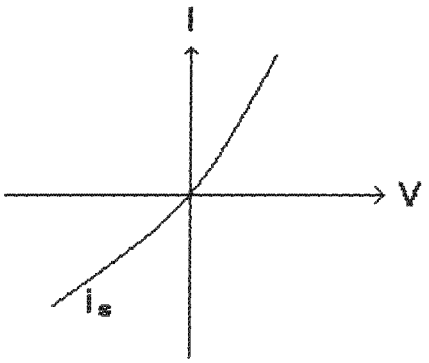

Figure 3.4 Diode Characteristic Curves

Figure 3.5 shows a typical construction of a Schottky barrier diode. This has a wide dynamic range of -55dBm to +15dBm in a 1KHz bandwidth and has a power measurement accuracy of approximately 0.1dB with a frequency range from 0.01GHz to 20 GHz [19], [20].

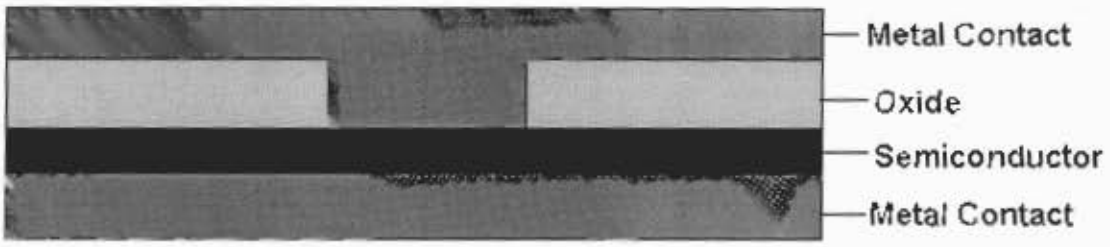

Figure 3.5 Schotty Barrier Diode

3.4 Methods of Propagation

This section covers two methods in which microwaves can be propagated between the transmitter and receiver.

3.4.1 Microwave Horn Antenna

Although relatively easy to make and use, the Horn antenna has a major problem with signals that escape into its surroundings and are reflected back. This is known as multi-path reflection and drastically affects attenuation measurements and reduces the accuracy of measurement.

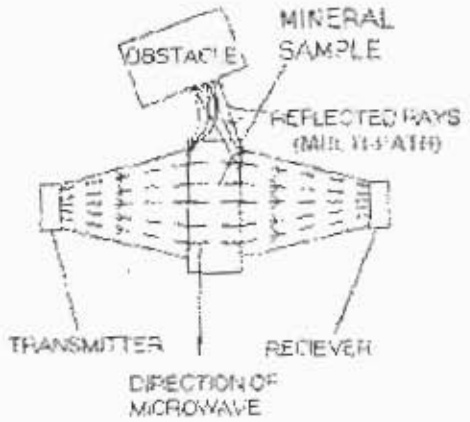

Figure 3.6 Propagation of Microwaves Using Horn Antennae

3.4.2. Waveguides

In this method the waveguide is filled with the dielectric and direct measurements are made. Since the waveguide is an entirely closed structure, the multi-path reflections are eliminated. The proposed method of propagation is the TE_{10} fundamental mode rectangular waveguide. This is the propagation of waves along a rectangular waveguide with its sidewalls of width one H-loop (the H field refers to magnetic field). The 1 in TE10 mode means that the propagated wave is only one H-loop wide and the 0 indicates that the E-field (electric field) is vertical and the H-field is horizontal along the waveguide [29] (see Figure 3.10.).

Fundamental TE_{10} mode rectangular waveguides was used in preference to other waveguide shapes and other higher order modes for the following reasons:

- Ease of launching
- Limited chance of higher order modes being generated by operating below their cutoff frequency
- Reduces waveguide size

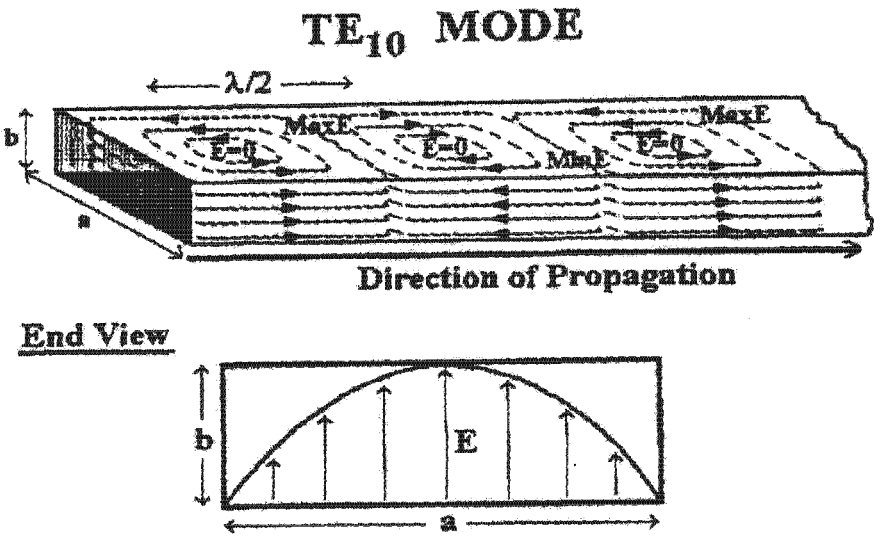

Figure3.7 TE_{10} Mode

The advantage of using the waveguide is that none of the energy is lost to the surroundings and there are no reflections from the surroundings.

When a waveguide is filled with a mineral (sand) sample, an air gap is created as the mineral settles down. Thus a wave passing from a dielectric medium to air medium causes a relative phase change in the wave, which is different from the phase of the input wave. This results in reflections. This problem can be solved by using an isolator (which absorbs reflected waves) or an attenuator in between the Gunn diode and waveguide. Isolators are quite expensive and not easily available. Attenuators reduce the power at the receiving end but are cheaper and more easily available.

However, measurements were carried out to find the optimum operating region of the detector diode (Chapter 5, Figure 5.1) and it was found that the power levels transmitted by commercially available Gunn oscillators were too high. An attenuator is therefore ideal as it reduces the impedance mismatch and results in the reduction of power level available to the detector diode to the optimum level.

4. Design of the Microwave Systems

An operating frequency of 10.5GHz was used. The system used to transmit this frequency was a Gunn diode, also discussed in Chapter 3, mainly due to the low cost as this device is commonly used for an alarm power source. The Gunn diode was driven by a circuit producing a 10V square wave supplying a current of 600mA. The square wave modulated power supply was used in order to use an A.C amplifier at the detector. The receiver made use of the Schottky low-level detector operating in the square law region. Finally, the voltage output is read using the ICL 7107chip(A/D converter) and displayed on a LED screen.

4.1 The Transmitter Circuit

The block diagram of a 1KHz transmitter is shown below.

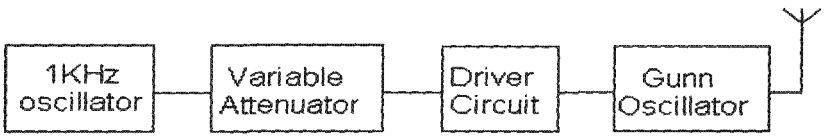

Figure 4.1 Block Diagram of Transmitter Circuit

4.1.1. The 1KHz Oscillator

To provide the required duty cycle, a CMOS 555 timer circuit is used. The frequency of oscillations is set by resistors R1 and R2 according to the formula [17], [21]:

$$\text{Frequency (Hz)} = 1/ (0.693*(R1+2R2)\ C1) \qquad (4.1)$$

R1 and C1 were chosen to be 2.2KΩ (see Figure 4.2). The 5KΩ potential divider is used to fine-tune the oscillations. Capacitors C3 and C4 are used for the smoothing of the power supply and to filter out any high frequency spikes.

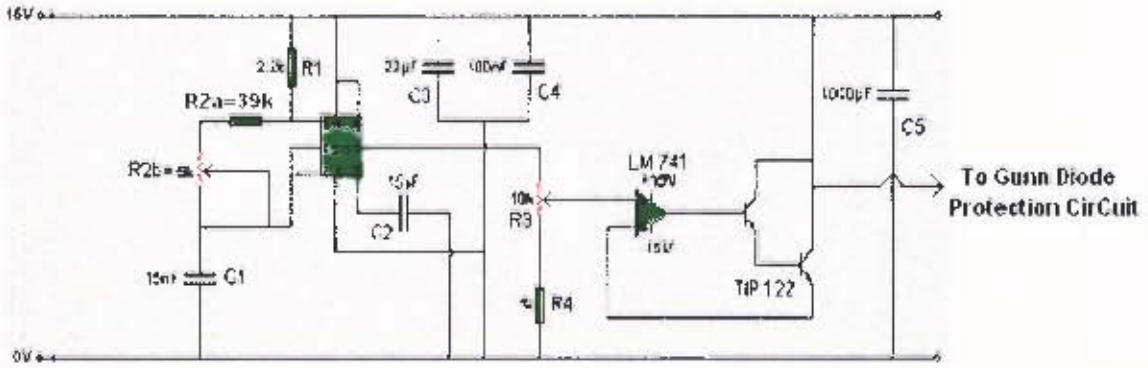

Figure 4.2 Circuit Diagram of 1KHz Oscillator

4.1.2 The Variable Attenuator and Driver Circuit

As can be seen in Figure 4.2 the CMOS 555 is connected to a variable attenuator R3 that sets the square wave voltage to 10V. Series resistor R4 is used to improve the stability of the voltage attenuator. The output of the attenuator is fed to an LM741, connected as a voltage comparator to maintain the output at the same level as the input. The LM741 drives the base of a transistor, which is connected to a power transistor set up in Darlington configuration. This set-up allows a current of up to 2A to flow into the Gunn diode [17], [21].

4.1.3. The Gunn Diode Protection Circuit

Gunn Diodes can be permanently damaged with a reverse bias or over voltage supply and hence require reverse bias and over voltage protection. Thus it is essential to use a protection circuit as shown in Figure 4.3 [17].

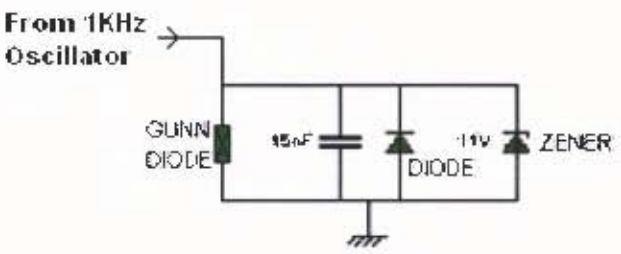

Figure 4.3 Protection Circuit

4.2. The Receiver Circuit

The block diagram of the receiver circuit is given below in Figure 4.4 and the circuit diagram shown in Figure 4.5.

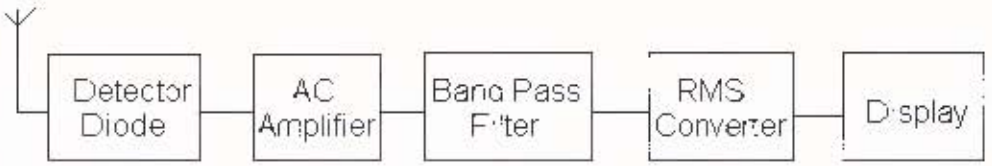

Figure 4.4 Block Diagram of Receiver

The output of the detector diode is connected to an AC amplifier (LM411). Capacitor C1 is used to remove any DC offsets. Potential divider R1 is used to control the amplification of the LM411 such that the maximum output voltage of the LM411 op amp is 4V. The signal is then passed through a band pass filter with centre frequency of 1KHz and band pass frequency of 200Hz to remove any unwanted noise [17]. It is then attenuated to 2Vp, as this is the maximum input voltage allowed into the RMS converter and display chip. Finally it is fed to the AD 536A RMS to DC converter [21] (Figure 4.6)

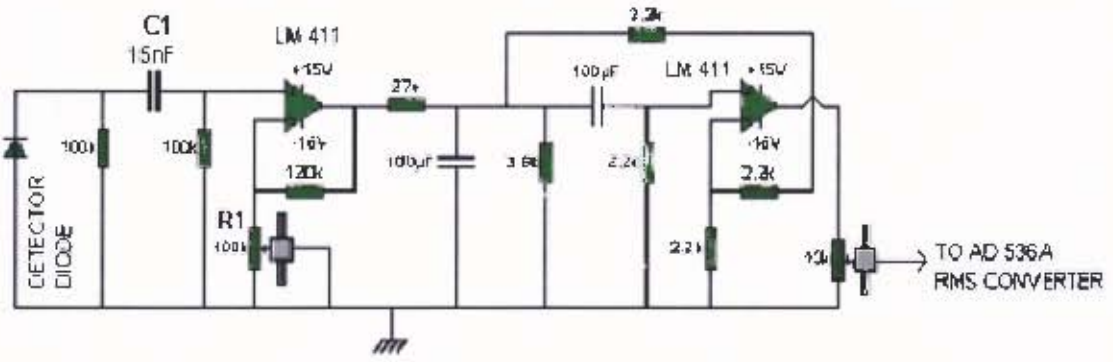

Figure 4.5 Circuit Diagram of Receiver

The AD 536A is used because it has the advantage of being a true RMS to DC converter up to 0.1V with a max error of 0.5% (Figure 4.6).

is equal to the product of the charge q and the distance d between the positive and negative charges of the atom. This shown in Figure 2.1.

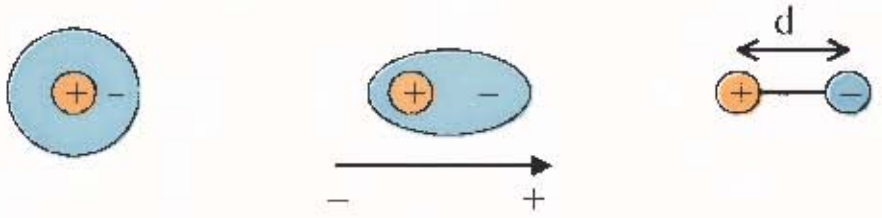

Figure 2.1 Effect of Charge on Polar Molecules [10]

2.1 Polarisation and Electric Susceptibility in Dielectrics

Under the influence of an external electric field the charge is redistributed in such a way that the negative charges align themselves near the positive plate and the positive charges at the negative plate, as shown in Figure 2.2. This effect is known as polarisation and is defined as the net charge Q' per effective area A of plates (P = Q'/A).

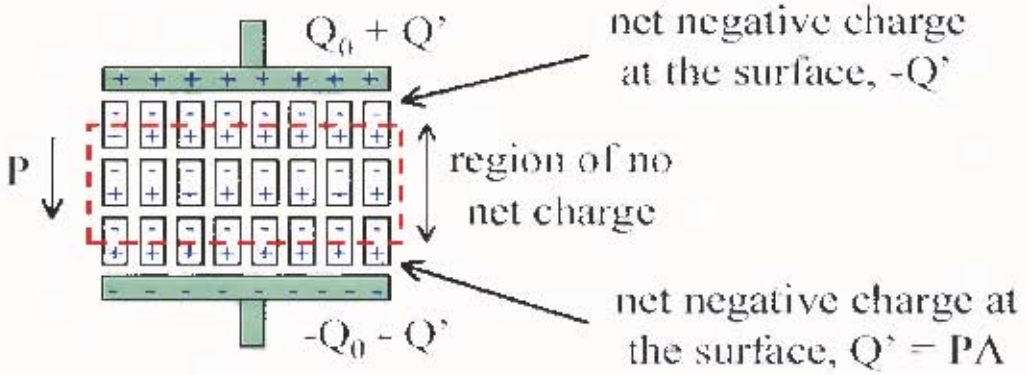

Figure 2.2Effect of Electric Field on Polar Molecules [10]

At this stage one can easily see that the greater the electric field intensity E the greater the polarisation as described by the following Equation:

$$P = \epsilon_0 \chi_e E \qquad (2.3)$$

χ_e is the dielectric susceptibility and is a Figure of merit which describes how easily the material will be polarised. The relative permittivity can also be written in terms of electric susceptibility:

$$\varepsilon_r = 1 + \chi_e \tag{2.4}$$

From Equations (2.3) and (2.4) it can be easily be seen that the easier the material is polarised, the larger the relative permittivity.

2.1.1 Types of Polarisation

There are three common types of polarisation:

2.1.1.1 Electronic Polarisation

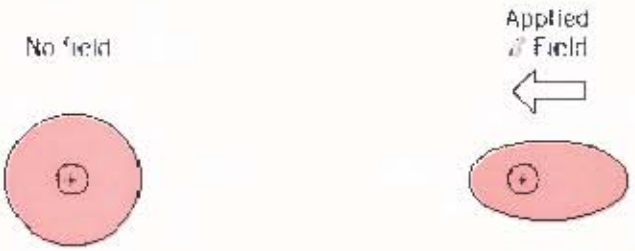

Figure 2.3 Electronic Polarisation [10]

This occurs in all materials and is due to induced dipole moment created through non-symmetrical positioning of the electrons and protons at any given point (see Figure2.3). This type of polarisation is fairly weak and is associated with the bonding between air molecules [10].

2.1.1.2 Ionic or Induced Polarisation

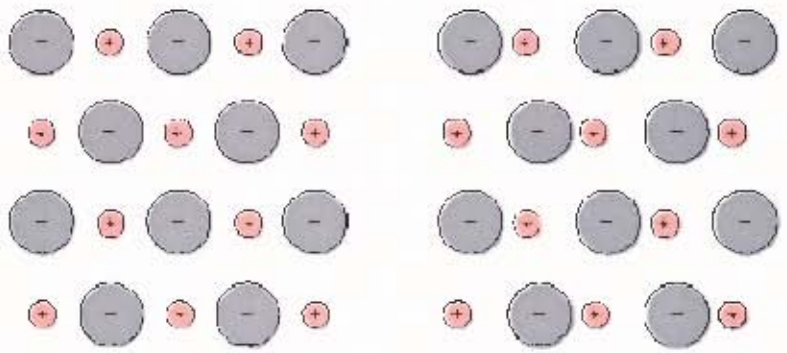

Figure 2.4 Ionic Polarisation [10]

Ionic polarisation occurs in ionic compounds where the cat-ions and an-ions are attracted to the opposite charged plates when an electric field is applied, as can be seen in Figure 2.4. A good example is the electrolysis process [10].

2.1.1.3 Molecular or Orientation Polarisation

Figure 2.5 Orientation Polarisation [10]

Molecular polarisation occurs in materials that have permanent dipole moments. On application of an electric field, the molecules align themselves, resulting in strong polarisation (see Figure 2.5). A good example is water molecules and associated Van Der Waal forces.

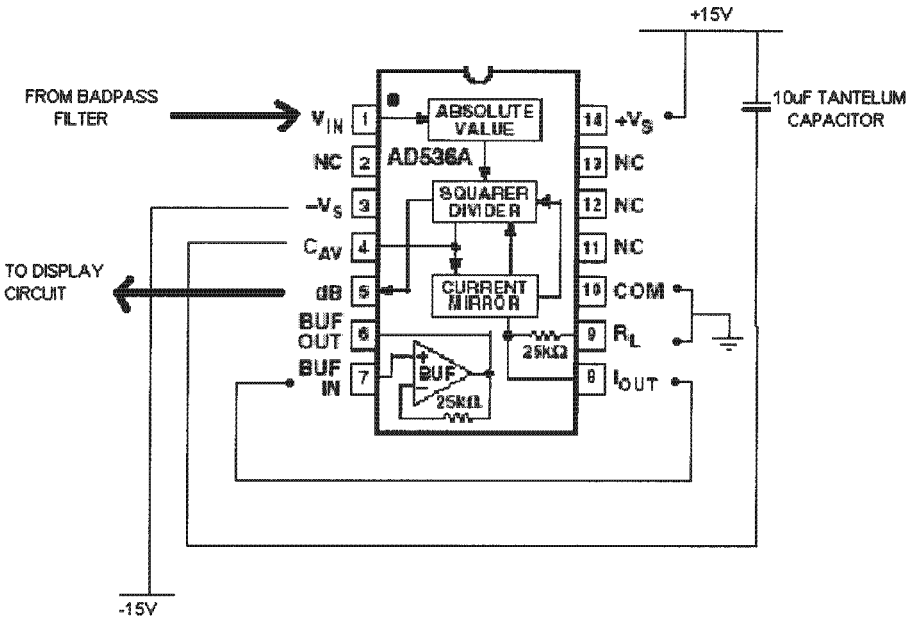

Figure 4.6 RMS to DC Converter

From the RMS converter the DC signal is fed to the ICL 7107 chip which directly drives the LED displays. This chip offers the advantage of being easily calibrated as a volt meter with an accuracy of 0.01V.

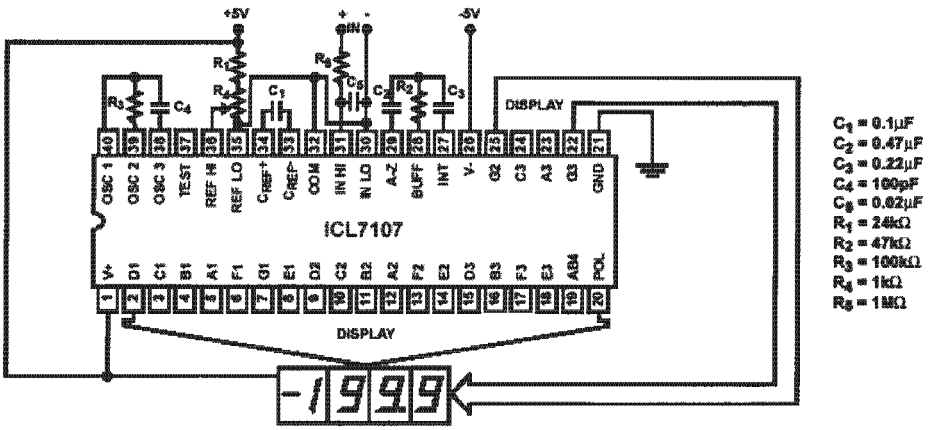

Figure 4.7 A/D Converter and LED Display Driver

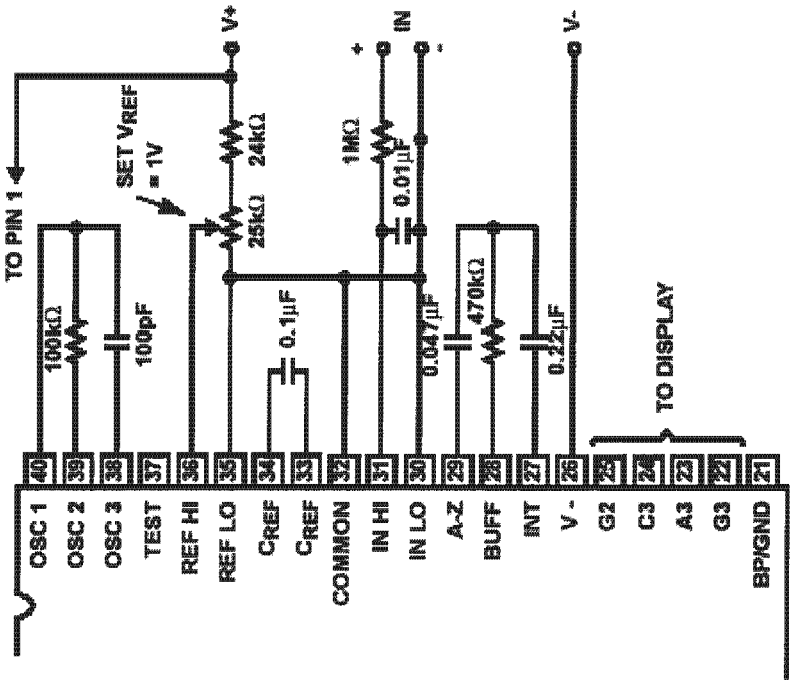

Figure 4.8 Circuit Connections for 2V Input voltage.

4.3 Power supply

4.3.1 Transmitter and Receiver Power Supply

The mains power supply has to be regulated down to $\pm$15V using a transformer rated at 18V-0V-18V with a current rating of 2A was used (Figure 4.9). The signal is then fed into a bridge rectifier circuit. Capacitors C1 and C2 are used to smooth the output of the bridge rectifier. 7815 and 7915 voltage regulators are then used to provide a stable $\pm$15V supply. The outputs of the voltage regulators are further smoothed using capacitors C3 and C4. For short circuit protection, diodes are connected in parallel to the capacitors [21].

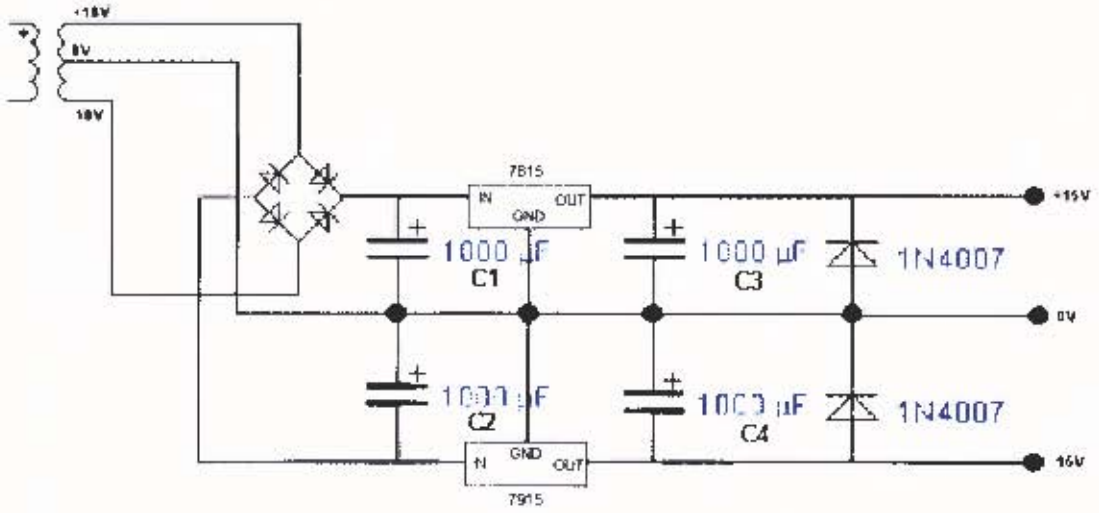

Figure 4.9 Power Supply of Transmitter and Receiver

4.3.2 ICL 7107 Power Supply

The voltage is further regulated to ± 5V for the ICL 7107 chip, using the same values of capacitors and diode as in the transmitter and receiver supply.

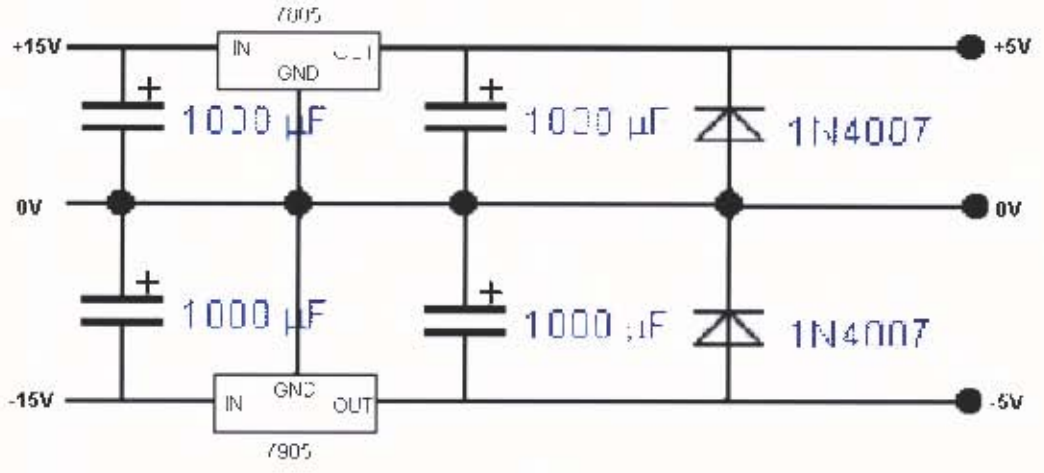

Figure 4.10 Power Supply to ICL 7107 Display Chip

4.4 Wave Propagation

4.4.1 Attenuator

A 10dB attenuator is used to reduce the power received by the detector diode, so as to avoid operating outside the square law region. Without using any attenuation and with zero attenuation in the waveguide, the detector diode is driven to saturation (see Figure 5.1). This attenuator provided 20dB isolation between the Gunn oscillator and the mineral sample. Thus reducing the reflections from the sample affecting the output power of the Gunn oscillator.

4.4.2 Higher Orders Modes in Waveguides

Waveguides can be rectangular, circular or a variety of other shapes. Their application usually defines the waveguide's particular shape.

A rectangular waveguide operating in the fundamental TE_{10} mode was used for this application because it offers the least possibility of propagation of higher order modes. All of the energy is concentrated into the fundamental Transverse Electric mode (TE_{10} mode), thus optimising measurement accuracy. This is better understood from Figure 4.11 and 4.12 below.

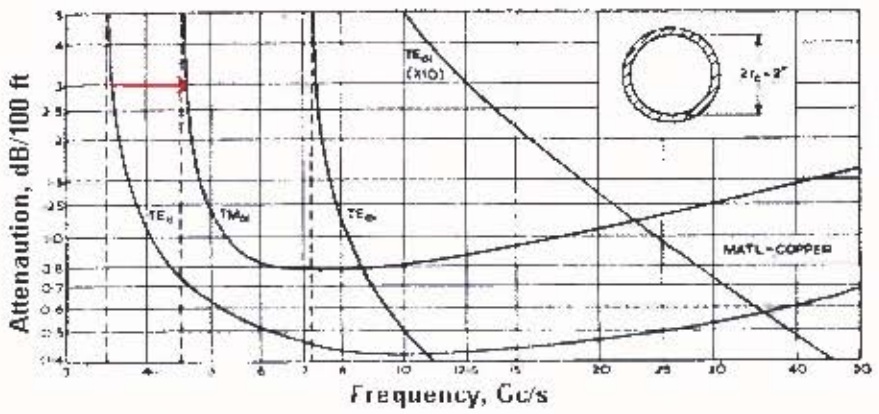

Figure 4.11 Attenuation of Circular Guided Modes as a Function of Frequency [24]

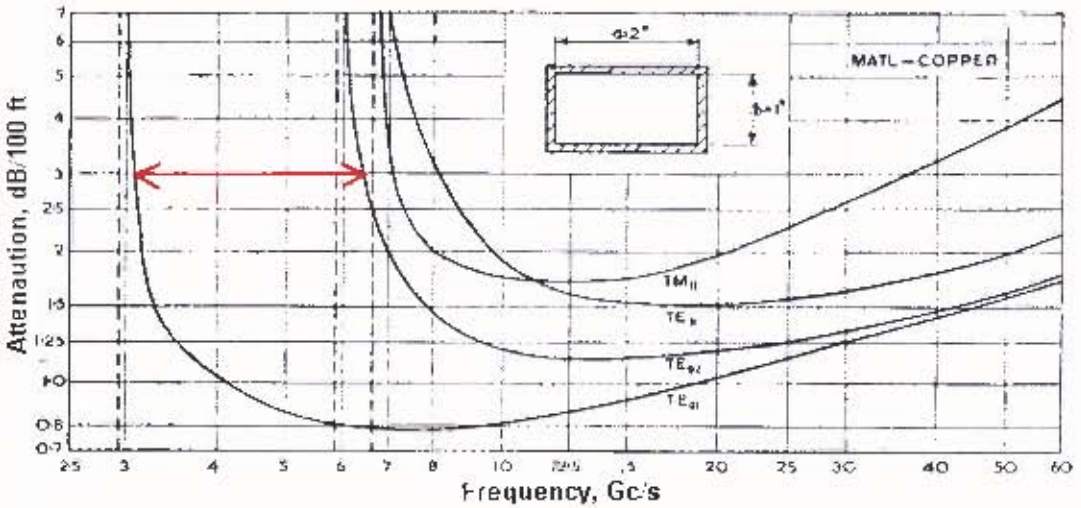

Figure 4.12 Attenuation of Rectangular Guided Modes as a Function of Frequency [24]

Comparing Figure 4.9 for circular waveguides and Figure 4.12 for rectangular waveguides, with a rectangular wave guide there is a greater frequency gap between the fundamental mode and the next mode than with a circular waveguide. Hence, there is less chance of higher order modes propagating in the rectangular waveguide.

4.5 Final Design

Figures 4.13 and 4.14 show the final design of the analyser. The transmitter, receiver and A/D converter are each encased in a separate aluminium box which is grounded to provide shielding from atmospheric interference. Waveguides with 90° bends were permanently fixed on the outside of the metal case and a 30cm piece of straight waveguides was used to store the sand sample while measurement were to be taken. It was found that the best way to mount the waveguide with the sand sample was in the upright position, as illustrated in Figure 4.16. In this configuration, any air gaps resulting from the sand sample settling resulted in a minimum change to attenuation measurement. Pieces of Teflon (has a very low dielectric loss factor) were used in the straight piece of waveguide and one of the 90° bend to act as stoppers to avoid sand getting into the 90° bends and the detector diode (see Figure 4.16).

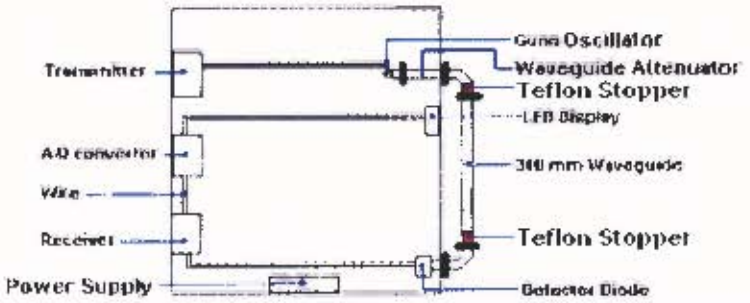

Inside View of Mineral Analyzer

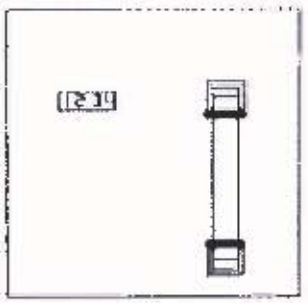

Front Elevation of Mineral Analyzer

Figure 4.13 Orthographic View of Mineral Analyzer

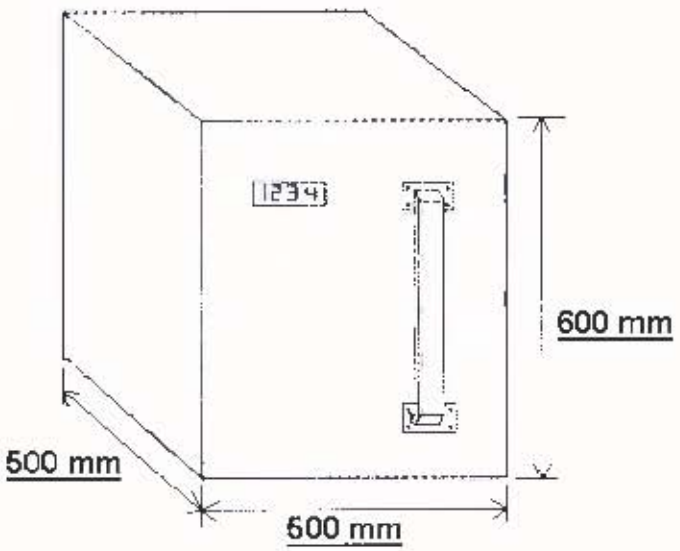

Figure 4.14 Isometric View of Mineral Analyzer

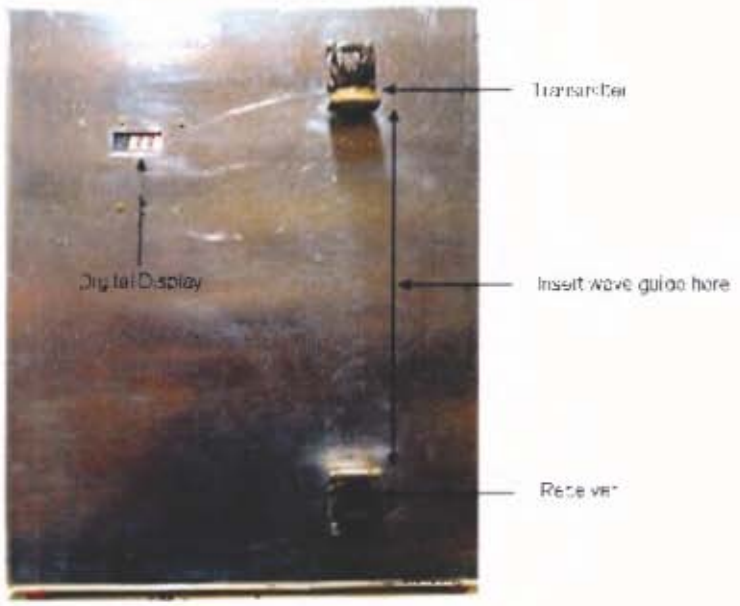

Figure 4.15 Front Photographic View of Analyzer

Figure 4.16 Method of Mounting Waveguide Filled with Mineral Sand

Chapter 5

5. Experimental Results and Methods of Calibration

5.1 Choosing Optimum Power to Supply Diode

The graph below (Figure 5.1) shows the output voltage, after the band pass filter, of the detector diode varies according to different power inputs (power inputs measured using a power meter). If the power exceeds 10mW, the diode starts to saturate and no longer follows the square law characteristics. Thus, an optimum power input of 10mW in the absence of a sand sample should be ideal and is easily achieved by a 10dB waveguide attenuator placed in-between the Gunn diode and waveguide (see Figure 5.2).

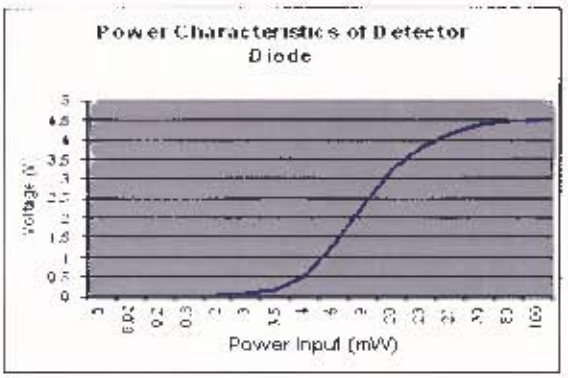

Figure 5.1 Characteristics of Detector Diode

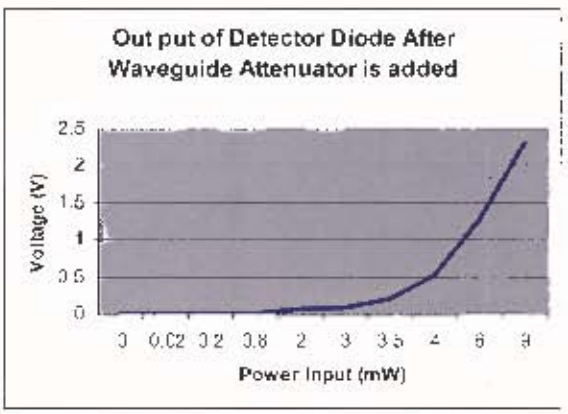

Figure 5.2 Output from Attenuation

5.2 Relationship between Attenuated Voltage and Percentage of Zircon

It has been established that the mineral samples consist of Zircon (insulator), Rutile (conductor) and Leucoxene (conductor). There are traces of other minerals but the percentages are so small that they can be ignored. Figure 5.3 shows a clear and distinct relationship between attenuated RMS voltage and the percentage of Zircon in the sand sample. Thus, as the percentage of Zircon is increased in the sample, the output detected voltage increases due to decreasing attenuation.

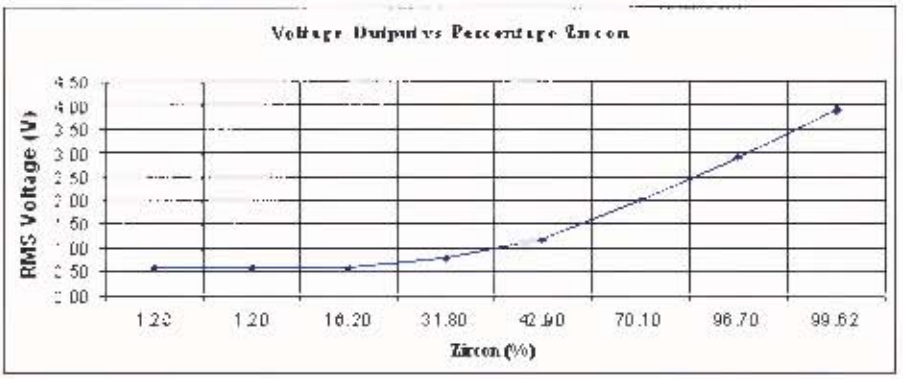

Figure 5.3 Graph of Voltage Output vs. Percentage Zircon

The graph above also indicates that samples with less than 31.8% Zircon will exhibit very high attenuation, which is approaching the limit of sensitivity of the system. However such low values are of little interest for this system. Figure 5.4 shows the relationship between attenuated RMS voltage and the percentage of conductors in the sample.

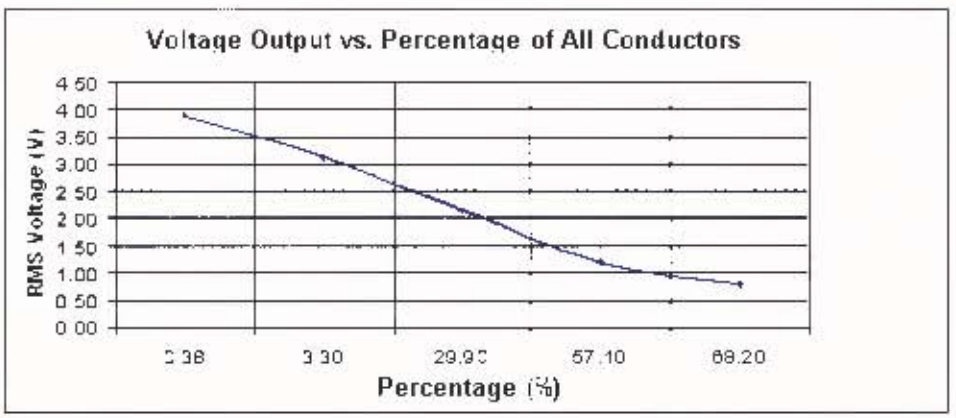

Figure 5.4 Graph of Voltage Output vs. Percentage Conductors and Semi- conductors

5.3 Method of Calibration

Once the results were obtained, the next step was to find a simple and accurate way to calibrate the system.

Since the graph in Figure 5.3 followed a polynomial function, it was decided to find the best fit curve, which could be interpreted using a mathematical function. This was achieved using Microsoft Excel and the curve is shown in Figure 5.5, where the best fit line is highlighted in red.

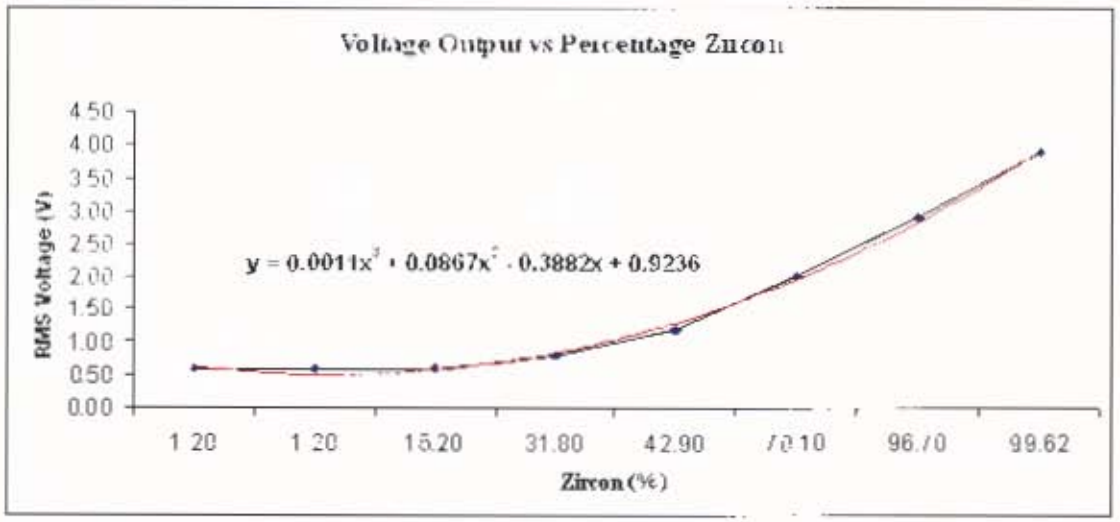

Figure 5.5 Best fit line for output Voltage vs. Percentage Zircon

The final step was to create a look up table which an individual may use to translate the voltage displayed into its corresponding percentage of Zircon. This is shown in Appendix i.

5.4 Conclusions Based on Results

A prototype instrument was built and delivered to the Namakwa Sands Separation Plant for long term on-site testing. The system was tested at the plant on different sand sample for eight months and showed an accuracy of ± 3%. It also showed that an effect due to

varying relative humidity was negligible. Thus, the system delivered had met the user requirements as a quick and reasonably accurate mineral analyzer.

The report from the plant showed that the technique worked well. However, for a production instrument there were major problems with this system:

- They preferred the instrument to have smaller dimensions.
- To measure the voltage of a particular sample, readings had to be taken at least five times to get the best average. This was because of the reflections caused by the sand sample in the waveguides (explained in section 5.4.1).

5.4.1 Inconsistency in Results Recorded

The measurements of voltage taken for a particular sample led to inconsistency between collected data. Hence, the readings had to be taken at least five times to get the best average. This was because of the reflections caused even after an attenuator was added to the instrument. The reflections were a result of the interface of the air to mineral and mineral to air impedance mismatches. This inconsistency in reading is shown in Table 5.1 with the Figures marked in blue.

Table 5.1 Mineral Composition of Samples Measured

No.	Zircon (%)	Rutile (%)	Leucox. (%)	Others (%)	voltage V1	voltage V2	voltage V3	Ave. voltage
1	99.62	0.19	0.08	0.11	3.54	3.80	4.30	3.88
2	96.70	1.20	0.90	1.20	3.16	2.93	2.61	2.90
3	70.10	16.10	9.70	4.10	1.97	1.95	2.09	2.00
4	42.90	23.50	4.60	29.00	1.19	1.20	1.18	1.19
5	31.80	33.00	25.80	9.40	0.78	0.80	0.79	0.79
6	16.20	51.90	26.00	5.90	0.59	0.59	0.59	0.59
7	1.20	48.20	46.80	3.80	0.58	0.58	0.58	0.58
8	1.20	69.30	28.20	1.30	0.58	0.58	0.58	0.58

5.4.1.1 Orientation of waveguide

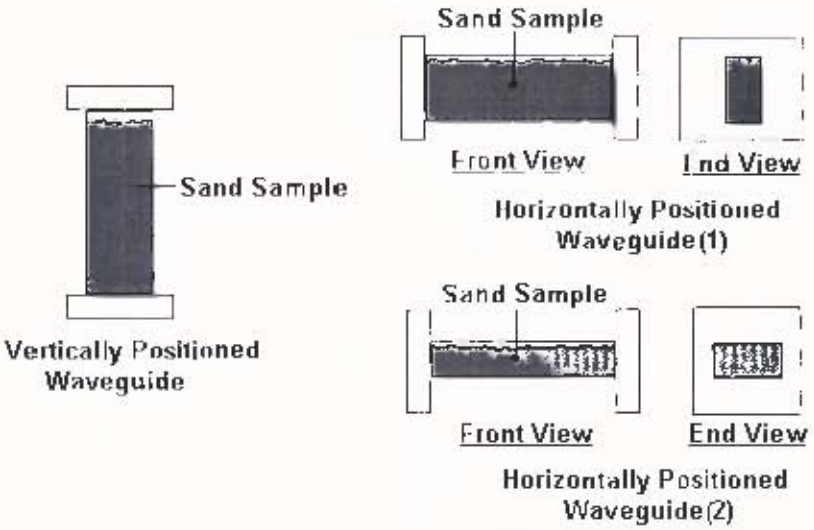

Figure 5.6 Orientation of Waveguide

Several results were recorded for the vertical and two horizontal orientations (Figure 5.6) of the waveguide and it was found that the vertical orientation showed the least variation in measured values.

5.4.1.2 Reflections in waveguide due to sand sample

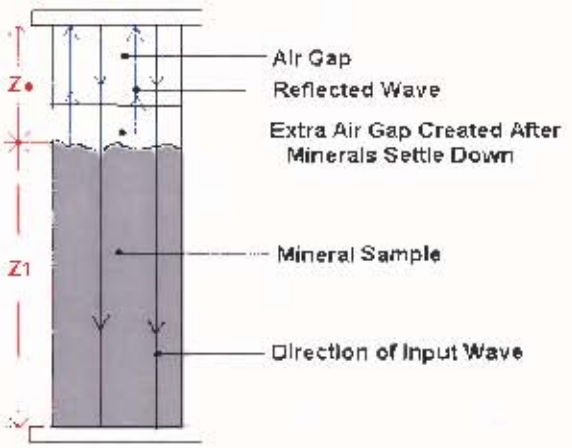

Figure 5.7 Impedance Mismatch (Zo AND Z1) of Waveguides

Figure 5.7 shows a waveguide filled with a sand sample. When the mineral (sand) sample is shaken, the air gap increases as the mineral settles down. This causes a relative phase change, which is different from the phase of the input wave and results in reflections. Reflections within the waveguide occur and injection lock the Gunn diode oscillator. This reduces the output power of the Gunn diode oscillator. This problem was solved by using a waveguide isolator between the Gunn diode oscillator and the mineral sample.

However, a variation in detected power levels existed as a result of the phase of the reflections at the second discontinuity changing as the sand sample settled and the sample length reduced. To reduce the variations in the output signal level, the length of the wave guide needed to be increased to increase the attenuation in the mineral sample. This variation should be less than 1% for an instrument with a required accuracy of 3%. The next subsection describes the method used to calculate this length.

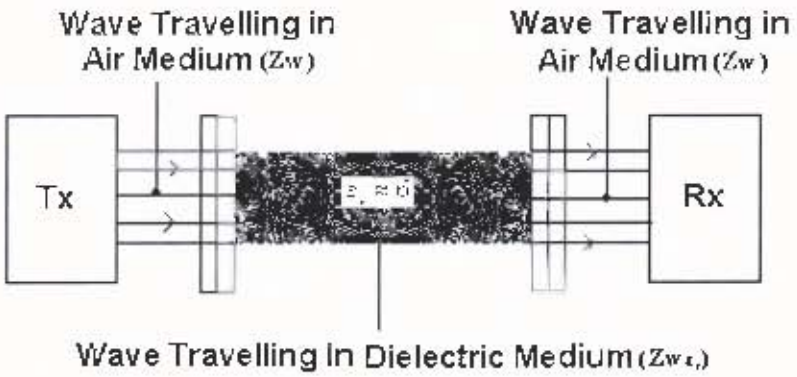

Figure 5.8 Wave Travelling in Different Media

To calculate the length needed, first the impedance of a wave travelling in a dielectric medium, Zw_{ε_r} of permittivity ε_r was found using the following Equation:

$$Zw\varepsilon_r = \frac{Zw}{\sqrt{\varepsilon_r}} \tag{5.1}$$

where Zw is the characteristic impedance of wave travelling in free space (wave impedance) and is equal to $120\pi = 377\Omega$(see Figure 5.8). The permittivity value of the

mineral samples is about 6 (this is the average value for of the minerals present in the sand sample). Hence Equation (5.1) becomes:

$$Zw\varepsilon_r = \frac{Zw}{2.45} \tag{5.2}$$

$$Zw\varepsilon_r = \frac{377}{2.45} = 153.9\Omega$$

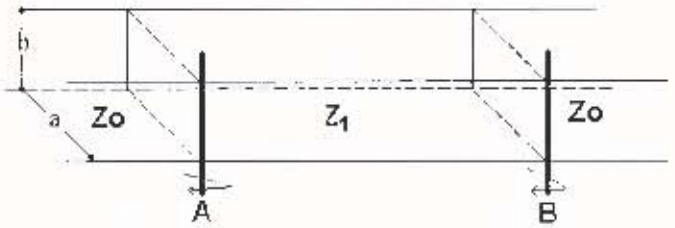

Figure 5.9 Cross Sectional View of Rectangular Waveguide

The characteristic Equation of a wave travelling in a waveguide full of air, Z_0, was calculated (see Figure 5.9):

$$Z_0 = Zw.\frac{\lambda_g}{\lambda_0}.\frac{b}{a} \tag{5.3}$$

a,b are dimensions of the cavity (see Figure5.9)
λ_0 *= wavelength in free space at 10.5GHz*
λ_g *= group wavelength*

$$\lambda_0 = \frac{c}{f} \tag{5.4}$$

f is the frequency of the wave
c speed of light

therefore $$\lambda_0 = \frac{3\times10^8}{10.5\times10^9} = 0.02857m$$

Equation (5.5) was used to calculate the group wavelength:

$$\frac{1}{\lambda_0^2} = \frac{1}{\lambda_g^2} + \frac{1}{\lambda_c^2} \tag{5.5}$$

where the cut-off wavelength $\lambda_c = 2 \cdot a$

$$= 2 \cdot 0.02286$$

$$= 0.04572m$$

$$\therefore \lambda_g = 0.03659m$$

substituting the values of λ_0, λ_g, Zw, a and b into Equation (5.3) gave the following:

$$Z_0 = 377 \times \frac{0.03659}{0.02857} \times \frac{0.01016}{0.02286}$$

$$= 214.6\Omega$$

The next step was to calculate the impedance of the wave in a dielectric medium in the waveguide, Z_1 (see Figure 5.10):

$$Z_1 = Zw\varepsilon_r . \frac{\lambda_{g\varepsilon r}}{\lambda_{0\varepsilon r}} . \frac{b}{a} \tag{5.5}$$

where the wavelength of signal in air in the waveguide, $\lambda_{0\varepsilon r}$, was:

$$\lambda_{0\varepsilon r} = \frac{\lambda_0}{\sqrt{\varepsilon_r}} = \frac{0.02857}{2.45} = 0.01166m \tag{5.6}$$

and the wavelength of signal in the dielectric in the waveguide, $\lambda_{g\varepsilon r}$, was:

$$\frac{1}{\lambda_{0\varepsilon r}^2} = \frac{1}{\lambda_{g\varepsilon r}^2} + \frac{1}{\lambda_c^2}$$

$$\therefore \lambda_{g\varepsilon r} = 0.01206m$$

substituting the values of $\lambda_{0\varepsilon r}$, $\lambda_{g\varepsilon r}$, $Zw\varepsilon_r$, a and b into Equation (5.5) gave:

$$Z_1 = 153.9 \times \frac{0.01206}{0.01166} \times \frac{0.01016}{0.02286}$$
$$= 70.75\Omega$$

thus the voltage wave standing ratio VSWR was:

$$VSWR = \frac{Z_0}{Z_1} = \frac{214.6}{70.75} \approx 3.0 \qquad (5.7)$$

and the reflection coefficient was:

$$|\rho| = \frac{VSWR - 1}{VSWR + 1} = \frac{2}{4} = 0.5 \qquad (5.8)$$

using the reflection coefficient, the **reflected power** at the air to mineral interface was:

$$|\rho|^2 = 0.25 \text{ or } 25\% \qquad (5.9)$$

therefore the power absorbed in load at junction A was $1 - |\rho|^2 = 0.75$ or 75% (5.10)

The loss due to reflections at junction A (see Figure 5.8) was:

$$-10\log_{10} 0.75 = 1.24dB \qquad (5.11)$$

Consequently the loss due to reflections at junction B was 1.24dB.

Hence if the mineral sample under test is loss free then the total loss due to reflection is when junctions A and B are in phase to give a value of 2.49dB. However, if junctions A and B are in anti-phase then the total loss due to reflections is 0 dB. This would give an output variation of 2.49dB.

Table 5.2 Table of Variation Power As function of Dielectric attenuation

Attenuation in Dielectric(dB)	Min Power (dB)	Max Power(dB)	Variation (dB)
0	0.00	2.49	2.49
1.5	0.67	1.82	1.15
3	0.97	1.52	0.55
6	1.18	1.31	0.13
8	1.22	1.27	0.05
8.5	1.23	1.26	0.03
10	1.24	1.25	0.01

For an instrument with an accuracy of 3%, required by Namakwa Sands Mineral Processing Company, an output variation should be about 1% maximum. This translates to a signal variation of 0.04dB. The final step was to measure the attenuation of almost pure Zircon (using a network analyser) sand sample as it had the most inconsistency in results recorded and compare it to the required attenuation in Table 2 to achieve 1% variation. In other words, if the maximum power at the receiving end was 1mW, the result recorded with a 1% variation would be anything between 0.99mW and 1mW or -0.044dB and 0dB.The maximum variation should be 0.04dB.

The attenuation of 99.62% pure Zircon sand sample was recorded to be 3.5dB. Thus to achieve a variation of less than 0.04dB, the attenuation of the 99.62% Zircon sand sample needed to be increased to 8.5dB (see Table 5.2). To improve the accuracy of the system the length of the waveguide needed to be increased by a factor of approximately 2.5 (from 300mm to 700mm). This would reduce the amount of reflections caused during measurements and improve repeatability. However, increasing the waveguide's dimension to two and a half times its present size would make the whole instrument much too large and hence impractical. The other solution would be to take several

measurements for a particular sand sample and find the average. This is, however, very time consuming and would lead to inefficiency in process control. Swept frequency techniques could be used in order to eliminate the reflections. However, the output power of a Gunn oscillator varies with frequency and in order to eliminate the power variation, a completely different measurement system is required. As a result other measuring techniques were investigated.

The resonant cavity perturbation technique was therefore looked at in order to enhance the loss and at the same time reduce the test sample's size. The Microwave Resonant Technique will be discussed in the next Chapter.

Chapter 6

6. Single Mode Resonant Cavity Technique

6.1 Introduction

The Microwave Cavity Perturbation technique involves the superposition of incident and reflected waves, in a metal cavity of high conductivity, to form a standing wave. As a result of the particular electromagnetic configuration that is established, an E-field maximum will occur at some point in the cavity and the H-field maximum will occur at a different point in the cavity. Placing the dielectric at the point of maximum E-field facilitates optimum transfer of energy into the dielectric. It is the measure of this absorption of the E field in the dielectric that forms the basis of Resonant Cavity Perturbation technique.

6.2 The Q- factor of a Resonant Circuit

In transmission line theory any value of impedance is easily realised as having transmission line characteristic impedance Zo terminated with a load impedance of Z_L as seen in Figure 6.1 below[15].

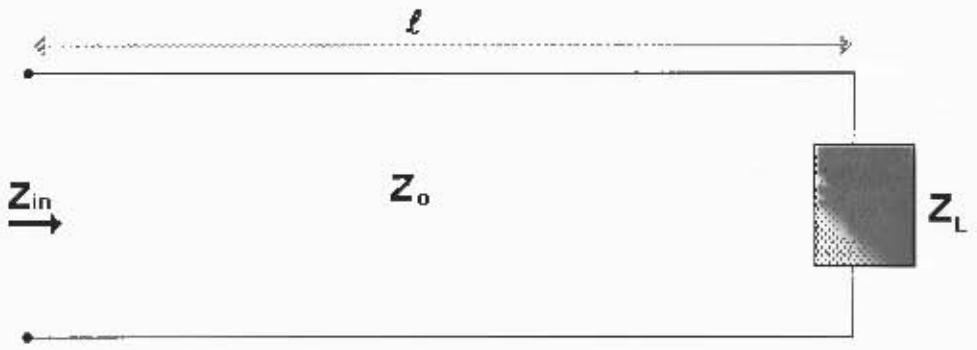

Figure 6.1 Transmission Line of Length ℓ Terminated in Z_L

Similarly, microwaves resonant circuits can be represented in the form of a parallel RLC circuit.

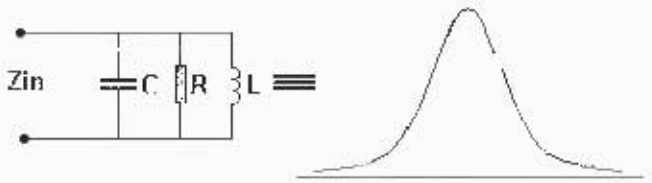

Figure 6.2 RLC Resonance Circuit

The magnitude response of the resonant circuit is shown in Figure 6.2. The measure of the quality of magnitude response is known as the Q-factor and is simply defined as [24]:

$$Q = \frac{2\pi.EnergyStored}{Energy \cdot Dissipated \cdot per \cdot Cycle} \tag{6.1}$$

For lumped circuits this becomes

$$Q = \frac{R}{\omega \ell} \tag{6.2}$$

ω = *resonant frequency*
ℓ = *inductance*
R = *resistance*

In resonant circuits the Q-factor can be measured from the resonance curve by taking the 3dB bandwidth (half power bandwidth) as indicated in the graph below (Figure 6.3).

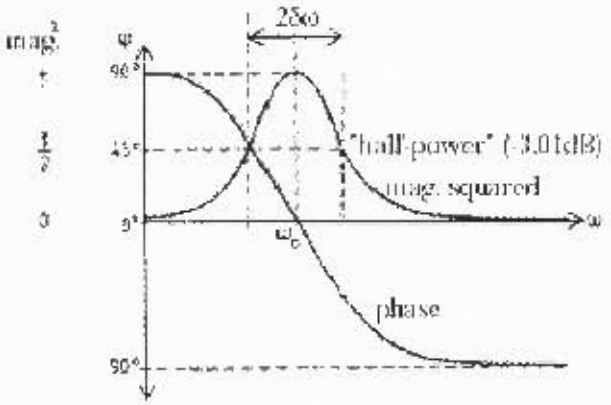

Figure 6.3 Measure of Q-factor [22]

For high-Q tuned circuit the Q-factor of the circuit in Equation (6.1) may be shown to be:

$$Q = \frac{\omega_o}{2 \cdot \delta\omega} = \frac{f_o}{\Delta f} \qquad (6.3)$$

f_o = *centre frequency*
Δf = *frequency change at 3dB's*

6.3 Microwave Resonant Circuits

Section 6.2 described circuits that consist of lumped inductors and capacitors and are only suited to operate at frequencies below 300MHz. At microwave frequencies these lumped circuits are replaced by distributive components. The advantage with these distributed components is that they result in much higher Q-factors, because energy storage is much greater in these circuits.

This section briefly looks into the three main types of microwave resonant circuits together with their advantages and disadvantages.

6.3.1 Microstrip Resonant Circuit

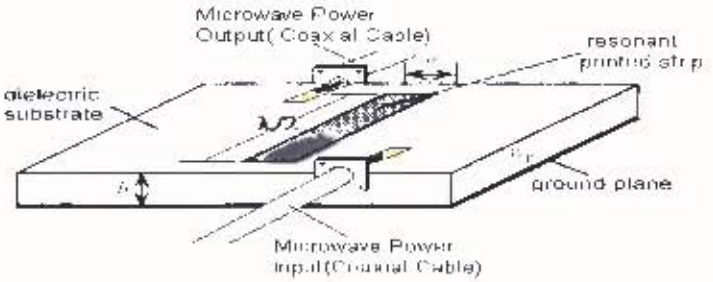

Figure 6.4 Microstrip Resonant System

The use of Microstrip as a resonant cavity structure for determining the loss tangent of mineral sample has a number of disadvantages:

- The Q-factor is limited to about 100.
- There is an increase in radiation loss with the increase in operating frequency.

- Precision connections are required to connect to Microstrip at microwave frequencies. These are not suited to operations in a mining environment.

Due to the disadvantages mentioned above, Microstrip Resonant Circuit is not considered further.

6.3.2 Coaxial Line Method

In this method the dielectric sample is placed in the centre of the coaxial line. The reflection coefficient and transmission coefficient (or change in Q-factors and frequency shift) are measured and hence the relative permittivity is calculated [12]. The setup of this circuit is shown in Figure 6.5.

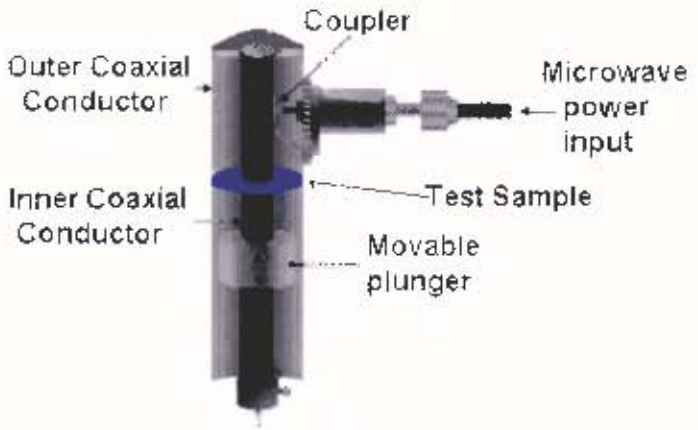

Figure 6.5 Coaxial Resonant Structure

The advantage of this system is that coaxial structures do not suffer the radiation losses that are characteristic of microstrip and consequently they have a better Q-factor than microstrip. However, since the system is used to measure a wide range of loss tangents, the Q-factor obtained may still not be high enough to carry out sensitive measurements. Further, precision connectors are also required to connect to coaxial circuits at microwave frequencies.

6.3.3 Waveguide Cavity

Section 6.1 noted that when an electromagnetic field is applied to a conducting cavity there will be points in that cavity where the E-field is at a maximum. This gives a response with a Q-factor governed by Equation:

$$Q = \frac{f_0}{\Delta f} \tag{6.4}$$

In cavity perturbation methods a dielectric is placed in the cavity at a region where the E-field is at a maximum. The introduction of this dielectric sample has two major effects:

- **Frequency shift** - Introducing a dielectric increases the relative permittivity and hence stored energy. This in turn increases the wavelength and therefore decreases the resonant frequency. The shift in frequency is proportional to the DC permittivity ϵ' or the real part of complex permittivity (see Chapter 2) and has been shown experimentally with the results obtained in Chapter 5, Sections 5.2 and 5.3.

- **Q-factor and attenuation** – The presence of a dielectric also increases the energy losses, causing a reduction in Q-factor and increase in attenuation. The change in Q is inversely proportional to the dielectric loss factor ϵ'', and the attenuation is directly proportional to the dielectric loss factor ϵ'' (refer to Figure 6.6).

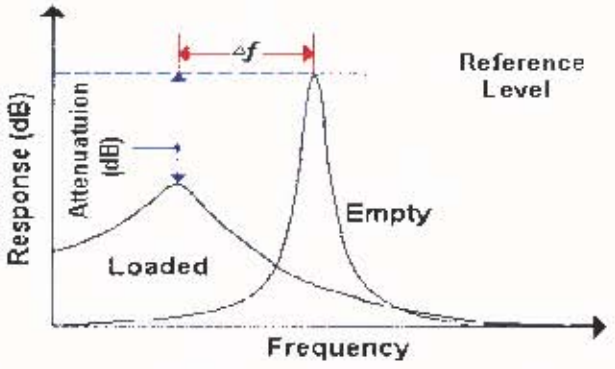

Figure 6.6 Resonant Changes Due to Introduction of Dielectrics Sample

By measuring the changes in Q-factor and frequency shift, the complex permittivity of samples can be measured.

There are a variety of shapes in which waveguides resonant cavities can exist. This thesis, however, is concerned with only the simplest of them. These are cylindrical and rectangular cavities in their fundamental modes.

6.3.3.1 TE_{010} Circular Cavity

Figure 6.7 shows the E-field of a cylindrical cavity excited in the fundamental mode. This is the TE_{010} mode, which has an e-field maximum along its central axis. For efficient energy transfer, the dielectric sample is placed along this axis as shown in Figure 6.7.

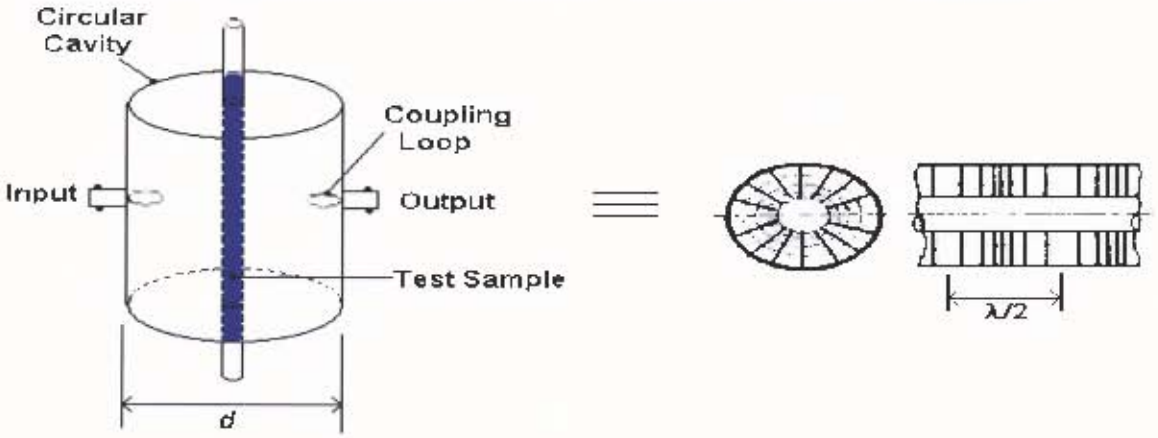

Figure 6.7 TE_{010} Circular Resonant Cavity

The dimensions of a circular cavity at a particular resonant frequency f operating in TE_{lmn} mode is calculated using the following Equation [24]:

$$(fd)^2 = \left(\frac{cx_{lm}}{\pi}\right)^2 + \left(\frac{cn}{2}\right)^2 + \left(\frac{d}{l_c}\right)^2 \qquad (6.5)$$

Where c is the speed of light, d is the diameter of the circular cavity. l is the number of tangential full periods, m is the radial half periods and n is the axial half period variation of field. x_{lm} is the mth root of $J_l'(x)=0$ for TE modes [24, pg195].

Which reduces to Equation (6.6) for TE_{010} mode [25]:

$$f = \frac{3.832c}{\pi \cdot d} \tag{6.6}$$

By connecting the setup shown in Figure 6.7 to a network analyser and measuring the frequency shift and change in Q-factor, the relative permittivity of the sample can be found by the following Equations [26]:

$$\varepsilon' = 1 - 0.539 \frac{Vo}{V} \frac{\Delta f}{fo} \tag{6.7}$$

where: Vo is the cavity volume and
V the specimen volume, and
f_o is the original resonant frequency
Δf is the frequency shift

and

$$\varepsilon'' = 0.269 \frac{Vo}{V} \left(\frac{1}{Q} - \frac{1}{Q'}\right) \tag{6.8}$$

Q is the quality factor of the cavity with the specimen
Q' is the quality factor of the cavity with no specimen

6.3.3.2 TE_{101} Rectangular Cavity

Exciting a rectangular cavity in the fundamental mode of TE_{101} produces a different E-field configuration to that of a circular cavity, but as in circular cavity the E-field is maximum at the centre and therefore the sample is also placed in the centre of the cavity. This can be seen from Figure 6.8 below [26].

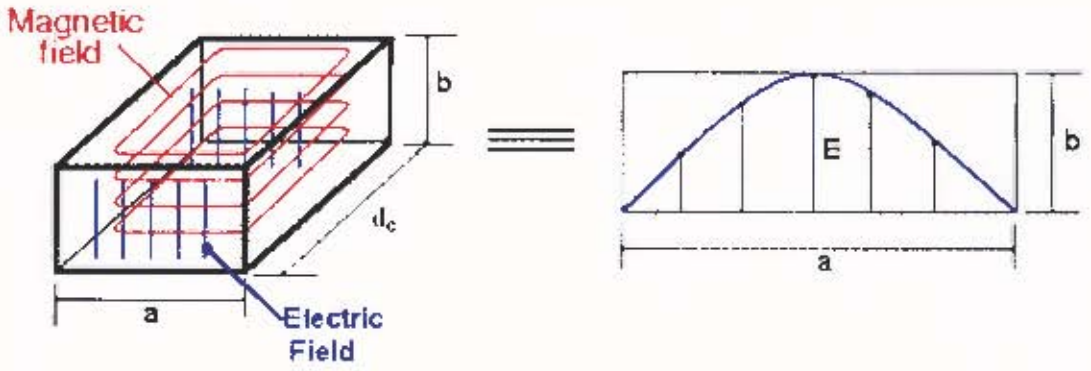

Figure 6.8 TE_{10} Rectangular Resonant Cavity

The dimensions of a rectangular cavity for a particular resonant frequency operating in TE_{mn} mode is calculated using the following Equation [25]:

$$f_c = \frac{1}{2} c \sqrt{\left(\frac{l}{a}\right)^2 + \left(\frac{m}{b}\right)^2} \qquad (6.9)$$

a, b are dimensions of the cavity (see Figure 6.8)
f_c is the cut-off frequency of cavity
c speed of light

which reduces to Equation (6.10) for TE_{10} mode:

$$\lambda_c = \frac{2}{\sqrt{\left(\frac{l}{a}\right)^2 + \left(\frac{m}{b}\right)^2}} \qquad (6.10)$$

2a for the fundamental mode

For dimension a and b the standard dimensions for rectangular waveguides can be used, as shown in Appendix iv. Dimension d_c can be found by finding the phase velocity (hence waveguide wavelength) using Equation (6.11)[15].

$$\frac{1}{\lambda_0^2} = \frac{1}{\lambda_g^2} + \frac{1}{\lambda_c^2} \tag{6.11}$$

$\lambda_0 = free\ space\ wavelength\ at\ resonance$

$\lambda_g = waveguide\ wavelength$

$\lambda_c = cut\text{-}off\ wavelength$

and $$d_c = \frac{\lambda_g}{2} \tag{6.12}$$

According to A.C. Metaxas, the relative permittivity of a sample in rectangular resonant cavity with TE_{101} mode can be found by using the 'Mehmet and McPhun, 1973' Equation [26]. This is shown below.

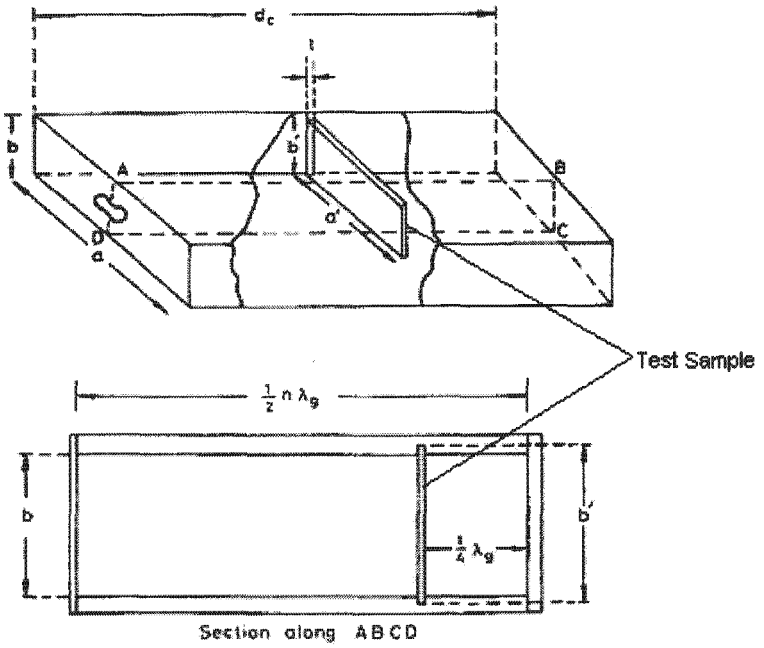

Figure 6.9 Cross Section of Resonant Cavity

$$\varepsilon' = 1 - A\left(\frac{\Delta f}{f_0}\right) \tag{6.13}$$

$$\varepsilon'' = A\left(\frac{1}{2Q} - \frac{1}{2Q_0}\right) \tag{6.14}$$

where

$$A = \frac{abd_c}{a'b't}\left[1 - \frac{a}{2\pi a'}\sin\frac{2\pi a'}{a}\right]^{-1} \tag{6.15}$$

ω_0 = *loaded resonant frequency*
$\Delta\omega$ = *frequency shift*
Q_0 = *unloaded Q value*
Q = *loaded Q value*
t = *the thickness of sample*

6.4 Conditions for Resonance

A resonant cavity can be translated using a quarter wave long transmission line with one end terminated in a short circuit and the other end terminated in an open circuit (see Figure 6.10).

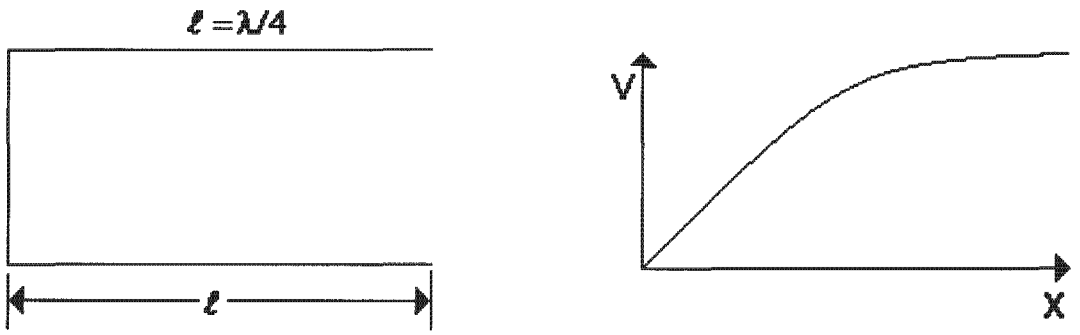

Figure 6.10 Conditions for Quarter Wavelength Resonance [25]

It is more efficient, however, to have a system terminated with short circuits on both ends, half a wavelength apart (Figure 6.11). Consequently, resonance can be achieved in systems at multiples of a quarter or half a wave length [25].

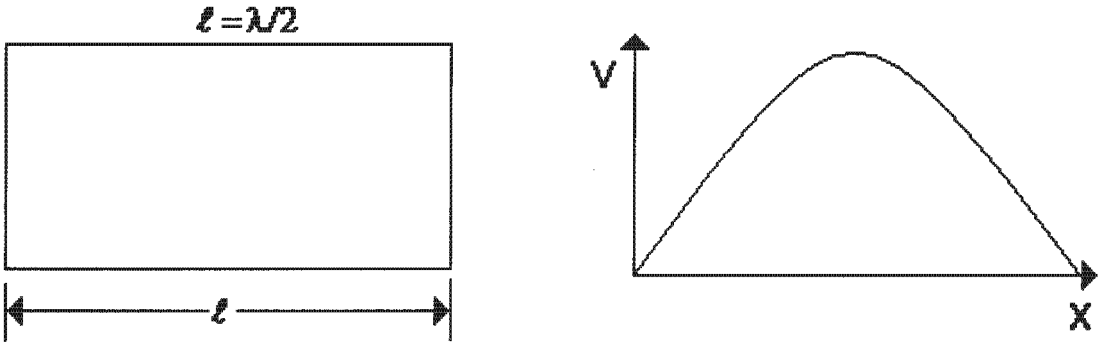

Figure 6.11 Conditions for Half Wavelength Resonance [25]

The Figure below shows the resonant length of a rectangular waveguide section which is half a wavelength long. Energy is reflected from each closed end of the waveguide section in the correct phase so as to sustain oscillations (see Figure 6.12).

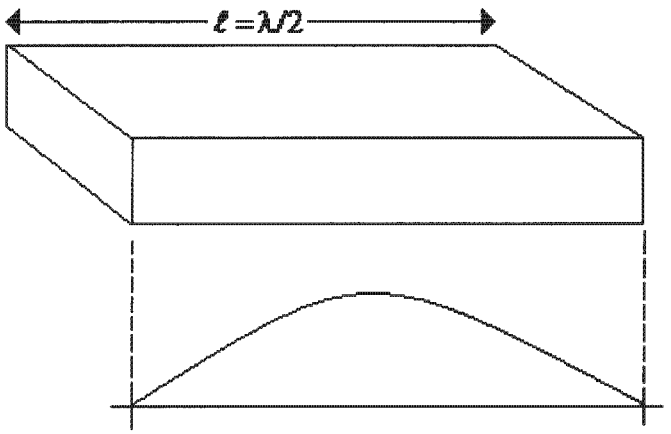

Figure 6.12 Resonant Section of Rectangular Waveguide

6.5 Coupling for Cavity Resonators

Excitation of the cavity can be achieved using coupling loops or apertures. Both of these methods are described briefly in this section.

6.5.1 Coupling Loops

Figure 6.13 shows the equivalent circuit when the coupling loop is inserted into a resonant cavity. The coupling loop acts as an antenna which converts radio frequency power into electromagnetic energy which can propagate in the cavity. When a current is applied, the loop produces a magnetic field in the direction of the xy plane (according to Figure 6.14) and thus produces a standing wave at a particular frequency [27].

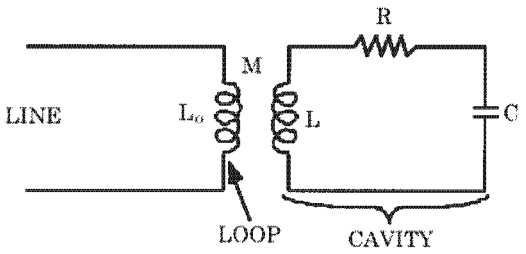

Figure 6.13 Equivalent Circuit of Cavity Coupling and Coupling Loop

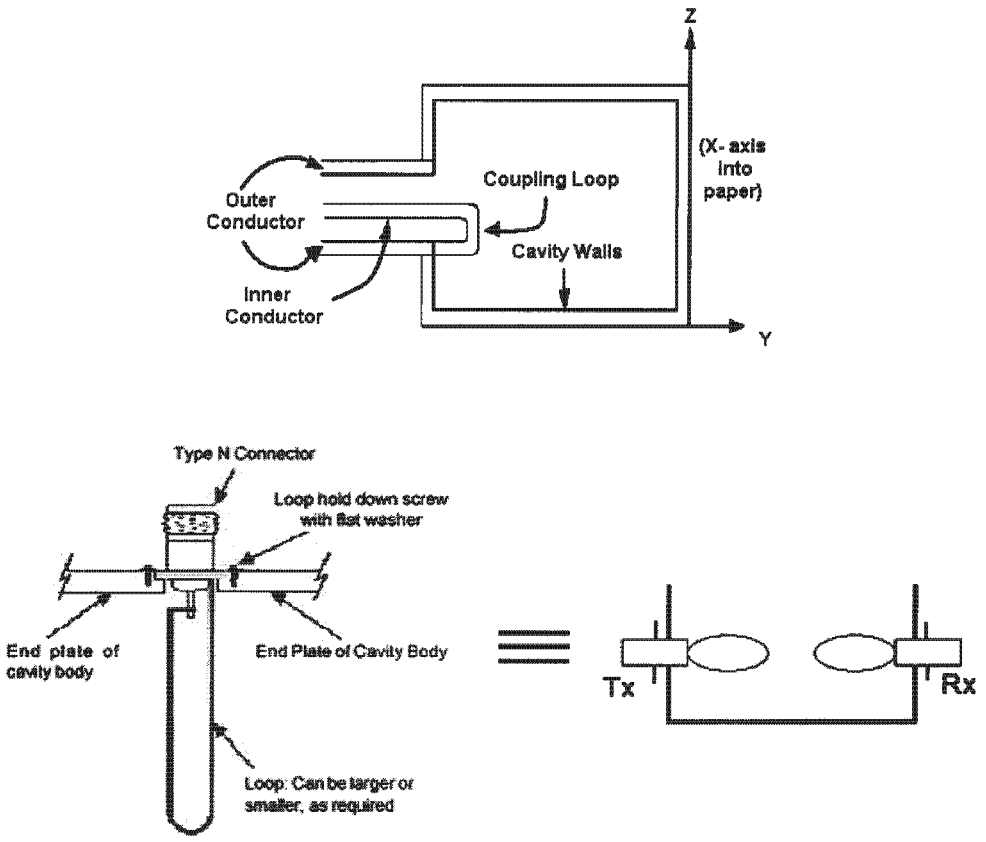

Figure 6.14 Coupled Cavity

The configuration in Figure 6.14 shows one of the simplest ways to couple into a cavity for both transmitting and receiving signals. Changing the orientation of the coupling loops or varying the dimensions of the loop affects the input and output impedance of the resonance cavity.

6.5.2 Aperture Coupling

This involves coupling the waveguide with small slots which allow injection of power into the cavity and the extraction of power from the other side (Figure 6.15). Combining the inductive and capacitive apertures shown in Figure 6.15 a and b gives rise to a resonant aperture shown in Figure 6.15c. For resonant cavities half a wavelength long, the apertures act as a band-pass filter, enabling only the frequencies whose wavelength is related to the cavity length to pass. These apertures are optimized experimentally to achieve the best Q-factor [25], [26].

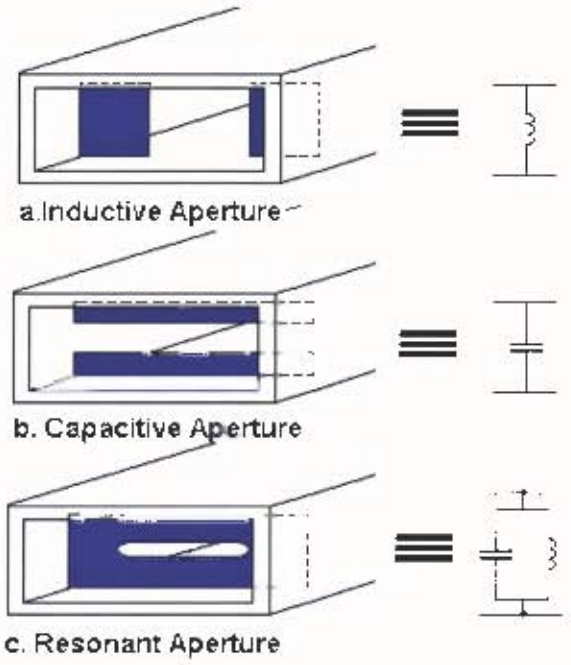

Figure 6.15 Aperture Coupling

6.6 Choice of Approach

After reviewing the theory behind microwave resonant structures, it is quite evident that using wave guide cavity perturbation would result in higher Q-factors than microstrip or coaxial structure. The rectangular waveguide cavity perturbation technique operating in its fundamental mode was chosen as opposed to a circular waveguide cavity for the following reasons:

- Higher mode propagation is less likely in rectangular guided structures.
- Rectangular waveguides were readily available

An operating frequency of 10.5GHz was first chosen to compare the measurements obtained in this system to the attenuation measurements reported in Chapter five. This resulted in resonant cavity being very small which is highly desirable in reducing the size of the equipment. However, it will be shown in the next Chapter that this required the mineral sample to be impractically small.

In order to increase the sample to a convenient size, a larger cavity was used. This resulted in a resonant frequency of about 1.5 GHz.

Chapter 7

7. Design of Cavity Perturbation System

At the end of Chapter five it was concluded that the microwave attenuation technique worked and fulfilled all of the user's operating requirements. However, on feedback from the client on the system's user-friendliness and, more importantly, physical size, other measuring techniques were investigated. In Chapter six resonant cavity techniques were discussed and it was concluded that rectangular cavity perturbation technique is the best option. This Chapter covers the design and implementation of the rectangular cavity technique operating in its fundamental mode.

7.1 TE_{101} Rectangular Resonant Cavity

An operating frequency of 10.5GHz was initially chosen in order to compare the accuracy and of the resonant system with that of the attenuation system. Standard X-band waveguide dimensions were used with the dimensions 22.86mm and 10.16mm.

To calculate the value of dimension d_c, first the cut-off wavelength was found using Equation (6.10):

$$\begin{aligned}\lambda_{cTE_{101}} &= 2 \cdot a \\ &= 2 \cdot 0.02286 \\ &= 0.04572m\end{aligned}$$

The resonant free space wavelength:

$$\lambda_o = \frac{c}{f_o} \qquad (7.1)$$

$$= \frac{3\times10^8}{10.5\times10^9}$$

$$= 0.02857m$$

Next Equation (6.11) was used to calculate the group wavelength:

$$\frac{1}{\lambda_0^2} = \frac{1}{\lambda_g^2} + \frac{1}{\lambda_c^2}$$

$$\therefore \lambda_g = 0.03659m$$

Therefore, the value of c using Equation (6.12) was (for **half** a wavelength resonant structure):

$$c = \frac{\lambda_g}{2}$$

$$= 0.01830m$$

7.1.1 Construction of Resonant Cavity

The cavity was made of two solid brass metal pieces which were tightly screwed together as shown in Figure 7.1. Although copper can be used instead of brass, to achieve higher Q-factors, it has the disadvantage of being very difficult to work with. The insertion hole is 5.5mm in diameter, as this was a reasonable size for the sand to pass through without clogging the tube.

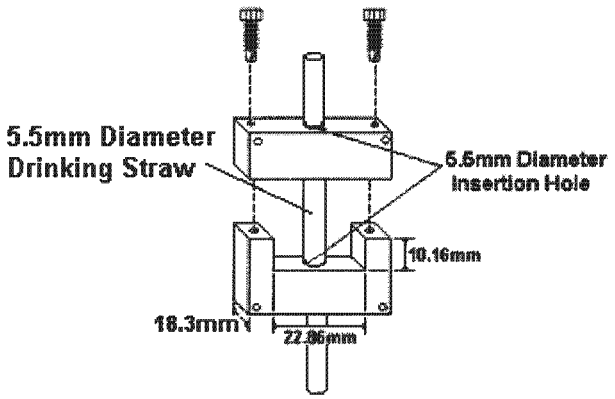

Figure 7.1 Blown-up Diagram for Construction of Cavity

Aperture coupling was chosen instead of loop coupling as it is much easier to construct for such small dimensions. The size of the aperture was determined experimentally. The plates were attached to the cavity by means of screws (see Figure 7.2).

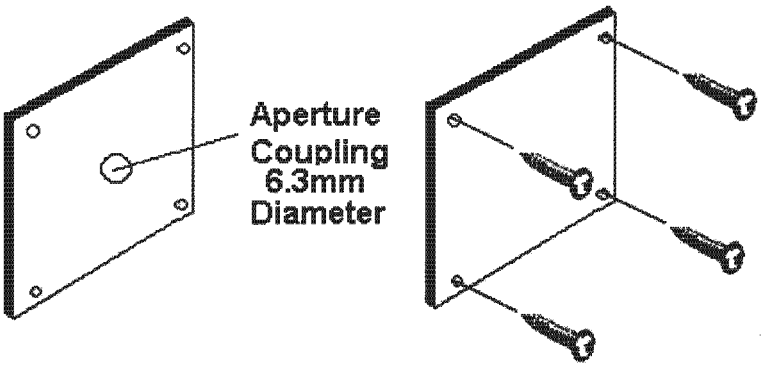

Figure 7.2 End Plates Aperture Coupled

The cavity was then connected to the network analyser as shown in Figure 7.3.

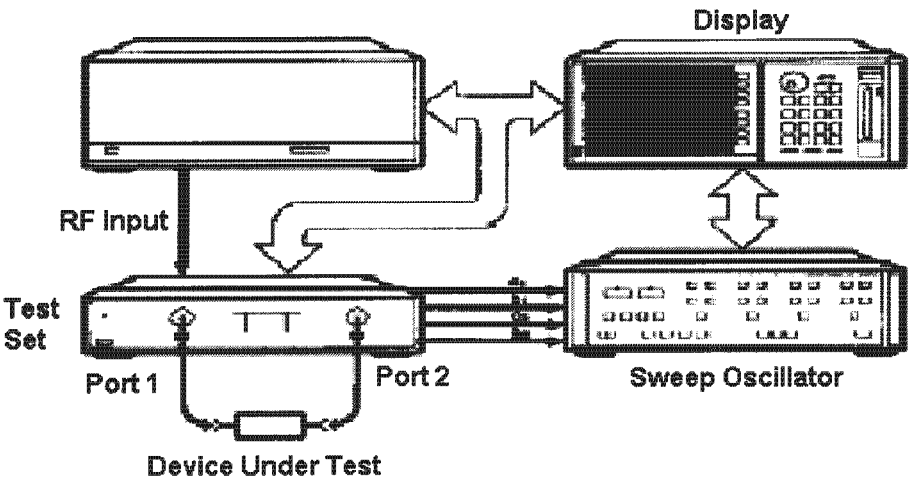

Figure 7.3 Network Analyser Setup for Measuring Cavity Response

The Q-factors of the empty (loaded with drinking straw, and no sand sample) cavity was measured as 1500. Measurements were taken using pure Zircon samples and it was discovered that there was a huge change in both resonant frequency and the Q-factor, when the mineral samples were placed in the resonant cavity.

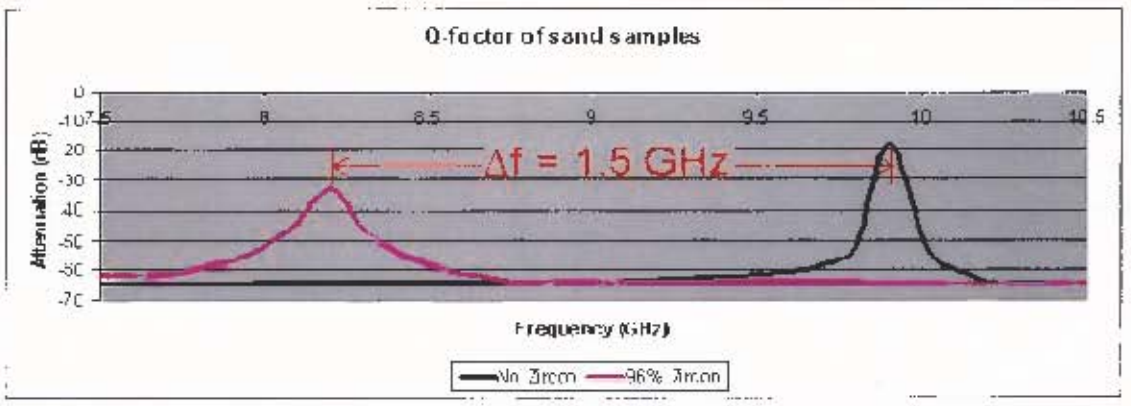

Figure 7.4 Graph Showing Magnitude Response of 96% Pure Zircon Sample

Thus, only relatively low loss Zircon samples that were purer than 95% could be measured (see Figure 7.4). The rest of the sand samples had resonant frequencies below the cut-off frequency of the X-band waveguide cavity and could not be measured. In order to reduce the change in the resonant frequency and the Q-factor it is necessary to reduce the coupling of the cavity. This could be achieved in 3 ways:

- Change the position of the insertion hole to be near the edge of the cavity instead of the centre to achieve the least amount of energy transfer possible, as shown in Figure 7.5.

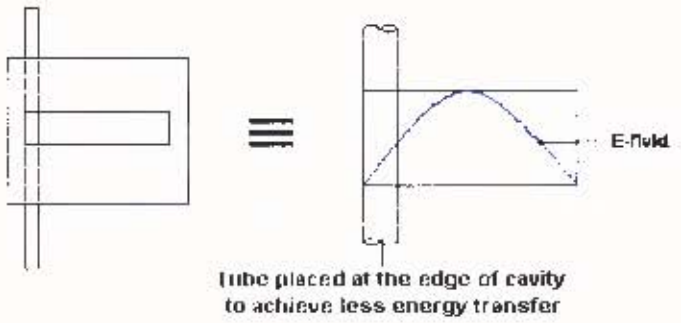

Figure 7.5 Positioning tube for least energy transfer

This system was built and tested. However with a 5.5mm diameter mineral sample it was still too strongly coupled and only samples that were greater then 85% Zircon could be measured.

- Reduce the diameter of the sample drastically to about 1mm or only partly insert it into the cavity. Sample tubes of less than about 5mm caused clogging of the mineral sample. Only partially inserting the samples resulted in inconsistent measurements.

- Reduce bring down the operating frequency to anything between 1GHz – 2GHz hence the 5.5mm diameter sample will occupy a much smaller percentage of the larger cavity, and it will have a much reduced effect on the resonant frequency and Q-factor. This was tried and details of construction are given in the next section.

7.1.2 Construction of Resonant Cavity operating between 1GHz to 2GHz

An aluminium box of suitable dimension to operate in the required region was readily available and thus used. The dimensions of the cavity are shown in Figure 7.6.

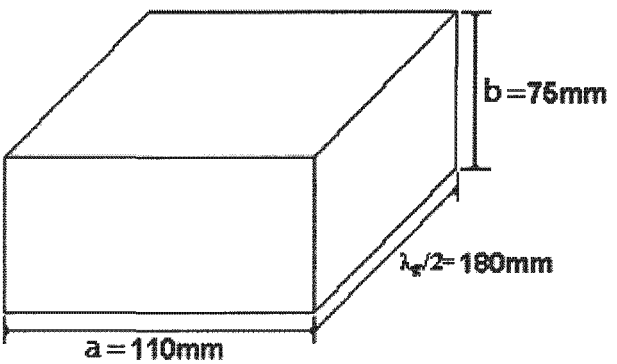

Figure 7.6 Rectangular Resonant Cavity Operating between 1GHz to 2GHz

The unloaded resonant frequency of the cavity is shown below (using Equation (6.11)).

$$\frac{1}{\lambda_o^2} = \frac{1}{\lambda_g^2} + \frac{1}{(2a)^2}$$

$$\frac{1}{\lambda_0^2} = \frac{1}{(36\times10^{-3})^2} + \frac{1}{(22\times10^{-3})^2}$$

$$\lambda_o = 187.7220034\times10^{-3}\,m$$

$$f_o = \frac{c}{\lambda_o} = 1.598107811GHz$$

$$where: c = 3\times10^8\,m/s$$

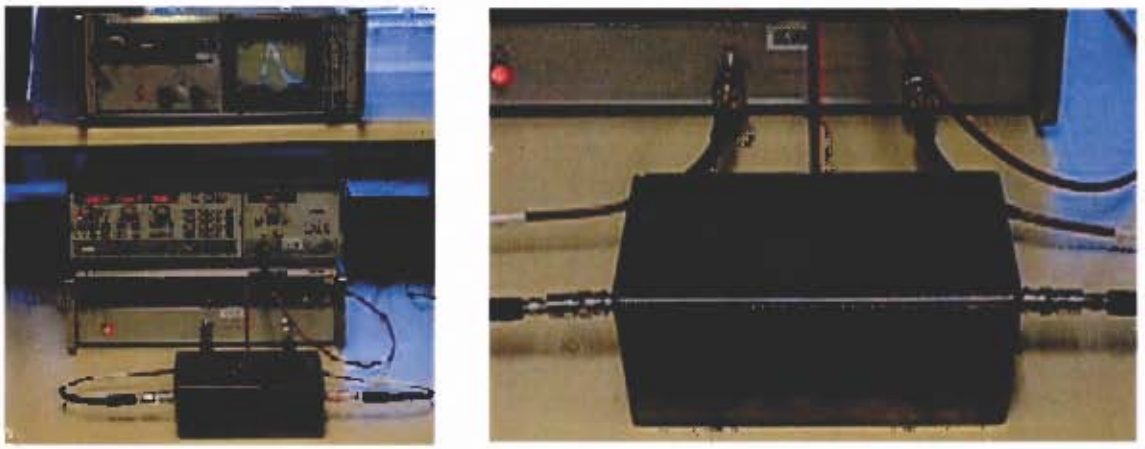

Figure 7.7 Rectangular Waveguide Resonant Cavity

The structure was coupled using copper coupling loops of 10mm diameter connected to BNC sockets (shown in Figure 7.7) to achieve a Q-factor of 1650. The insertion hole was made to be 5.5mm in diameter. The wall thickness of the tube containing the sand sample was about 0.25mm (drinking straw), resulting in the diameter of the sand sample being 5.0mm.

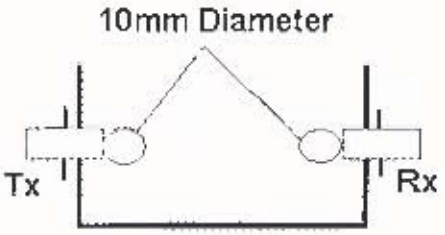

Figure 7.8 Method of Coupling

Although the above system was able to measure all of the sand samples available, the coupling was too weak to record significant changes between mineral samples. Thus, the diameter of the insertion hole was increased to 12mm and a 12mm diameter tube was used. This showed significant improvement. The results and the interpretation of the graphs obtained are discussed in the next Chapter. It is evident that a smaller cavity operating at a frequency of about 3GHz would have resulted in optimum coupling of the mineral samples with a tube diameter of 5.5mm. However, the physical size of the 1.598 GHz cavity was acceptable for the application and there was a significant advantage to using a 12mm diameter tube to avoid clogging of the sand samples in humid conditions.

Chapter 8

8. Experimental Procedure and Results

8.1 Introduction

As discussed in Chapter one, Zircon products normally come with two major impurities, which are conductors. The fist step was to experimentally determine the relative permittivity of each of the impurities and compare the results with that of pure Zircon. Further tests were carried out to test the feasibility of using cavity perturbation and to see the effect of varying impurities on Q-factor, frequency shift and attenuation measurements.

8.2 Permittivity Tests

These tests were performed in order to understand the electrical properties of the minerals concerned. The tests were done at an operating frequency of 1.5GHz with the 5.5mm diameter insertion hole. Table 8.1 shows the chemical compositions of the minerals under investigation. The chemical compositions of the four samples were provided by Namakwa Sands in their purest available.

Table 8.1 Chemical Composition of Minerals

Mineral	Chemical Composition	Percentages Tested
Zircon	$ZrSiO_4$	99.70%
Rutile	94% TiO_2, +/- 2% SiO_2	68.80%
Leucoxene	60 to 90% of TiO_2	54.00%
Ilmenite	46% TiO_2, +/- 50% Fe_2O_3	99.70%

The change in Q-factor and frequency shift measurements were taken and the dielectric loss and dielectric constants were calculated. Q1, Q2 and Q3 in tables 8.2 represent

separate Q-factor measurements taken for each mineral sample from which the average Q-factor was calculated. f1, f2 and f3 in table 8.3 represents separate resonant frequency measurements taken for each mineral sample from which the average resonant frequency was calculated.

Table 8.2 Dielectric Loss of Minerals

	Dielectric loss				
Sample	**Q1**	**Q2**	**Q3**	**Ave. Q-factor**	**ε''**
Zircon	2243	2245	2247	**2245**	**0.000599**
Rutile	1196.769	1196.077	1198.23	**1197.025**	**0.074693**
Leucoxene	1197.3	1198.38	1199.15	**1198.277**	**0.074527**
Ilmenite	174.8	178.632	175.92	**176.4507**	**0.992755**

Table 8.3 Dielectric Constant

	Dielectric Constant				
Sample	**f1(GHz)**	**f2(GHz)**	**f3(GHz)**	**Ave. f_0(GHz)**	E'
Zircon	1.5724	1.5715	1.5726	**1.572167**	**3.600547**
Rutile	1.5562	1.5566	1.5558	**1.5562**	**7.433354**
Leucoxene	1.5565	1.5564	1.5561	**1.556333**	**7.401348**
Ilmenite	1.5558	1.5569	1.5553	**1.556**	**7.481364**

These results were then checked with that of Pendock [1] in order to check the accuracy of the measurement and are shown in Table 8.4.

Table 8.4 Comparison between Measured and Referenced Values

Mineral	**Measured εr**	**Referenced εr**
Zircon	3.600547 + j0.000599	3.3 + j0.00081
Ilmenite	7.481364 + j0.992755	7.5 + j 0.91

The relative permittivity of each mineral was plotted on a complex plane in order to get a better understanding of their electrical properties (see Figure 8.1). The Figure indicates that there is a greater difference in the loss factor of the mineral than there was in their dielectric constants. These measurements indicate that it would be better to separate minerals by measuring the change in Q-factor rather than change in resonant frequency.

It can also be concluded that since Ilmenite is a very lossy material, the presence of a relatively small amount of Ilmenite in almost pure Zircon would have significant effects on the loss tangent. However, Ilmenite is normally present in very small quantities and should not affect the measurements taken.

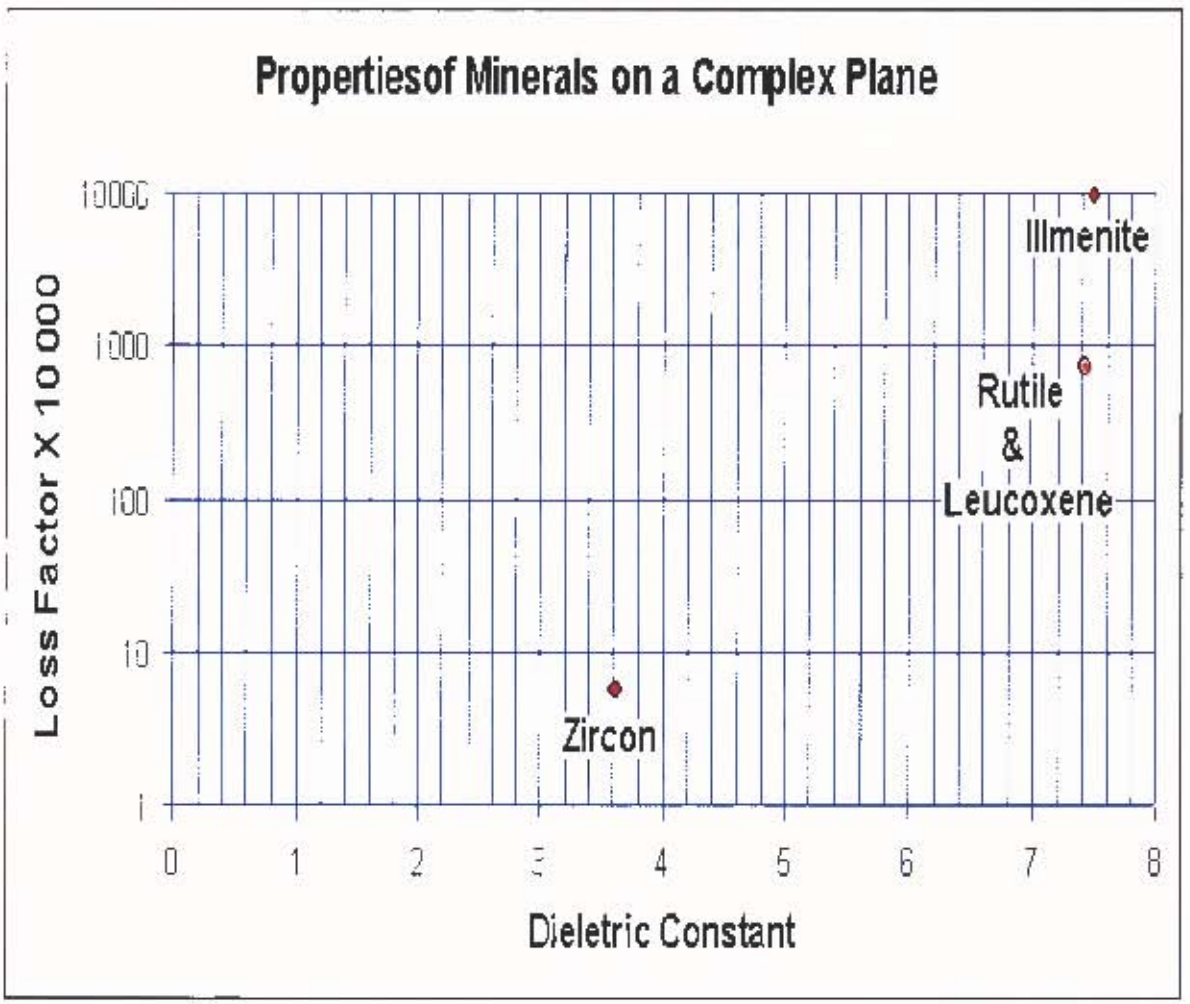

Figure 8.1 Mineral Plane

8.3 Sample Test Using 5.5mm Diameter Insertion Hole

The samples given by Namakwa Sands were in the form of powdered sand with different mineral contents in each sample (see table 8.5). The powdered form introduces a lot of air into the sample as compared to a solid sample. Hence, the relative permittivity of the powdered form would be less than that of a solid chunk of mineral.

Table 8.5 Mineral Compositions of Sand Samples

	Mineral content (%)			
Sample	**Zircon**	**Rutile**	**Leucoxene**	**Ilmenite**
uct 1	99.70	0.20	0.10	0.00
mic 33	89.86	1.05	3.15	0.35
mic 34	70.55	1.37	6.16	0.34
mic 37	66.11	11.96	17.28	1.99
mic 03	62.46	17.30	16.13	1.16
uct 4	58.38	19.94	18.21	1.16
mic 27	56.27	16.51	22.63	1.53
mic 06	47.88	29.34	18.92	1.54
mic 40	47.74	20.56	24.39	2.09
uct 5	44.90	27.50	24.70	0.60
uct 6	37.20	36.00	23.50	0.90
uct 7	27.16	39.10	31.34	0.60
uct 8	20.70	50.45	25.83	1.80
uct 9	14.50	51.50	31.20	0.90
uct 10	2.70	66.00	29.30	0.70

A problem arose when packing the sample in the insertion tube. The more densely packed the minerals, the greater the permittivity, adding to variations in readings taken. The best solution to this was to gently tap the samples to be measured; allowing the air gaps to be filled and greatly improving the consistency of readings.

Figure 8.2 shows the effects on Q-factor for different percentages of Zircon. From this graph it can be seen that there is not a distinct relationship between Q-factor and the variation in the percentage of Zircon. This is because the size of the insertion hole was too small and thus the effect of inserting the samples into the cavity was too small. The same can be concluded for the frequency shift and attenuation graphs shown in Figures 8.3 and 8.4.

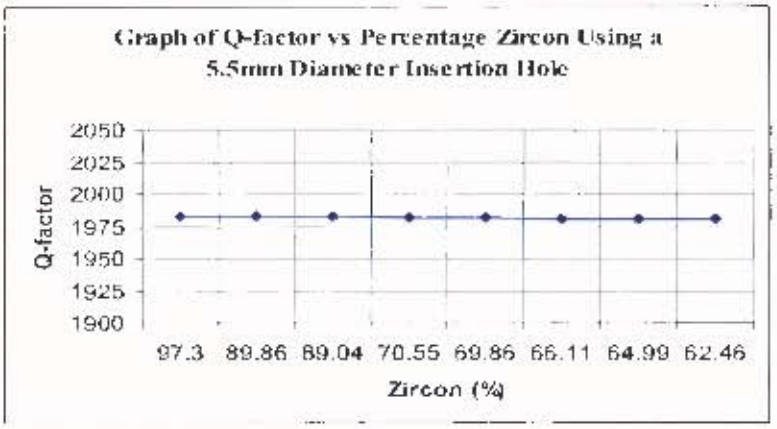

Figure 8.2 Graph of Change in Q-factor for different percentages of Zircon

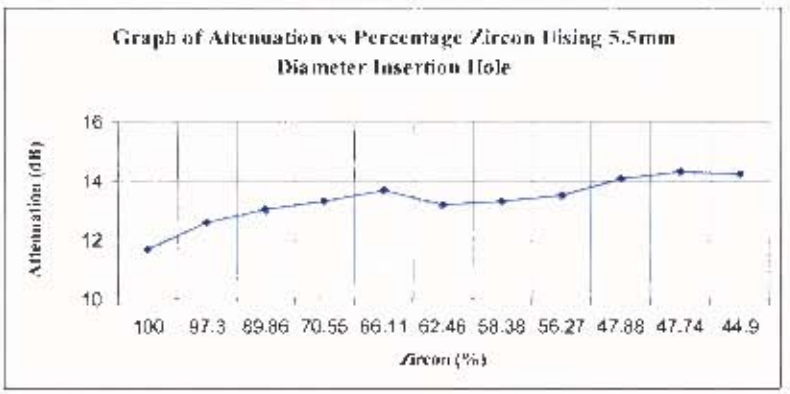

Figure 8.3 Graph of Change in Attenuation for different percentages of Zircon

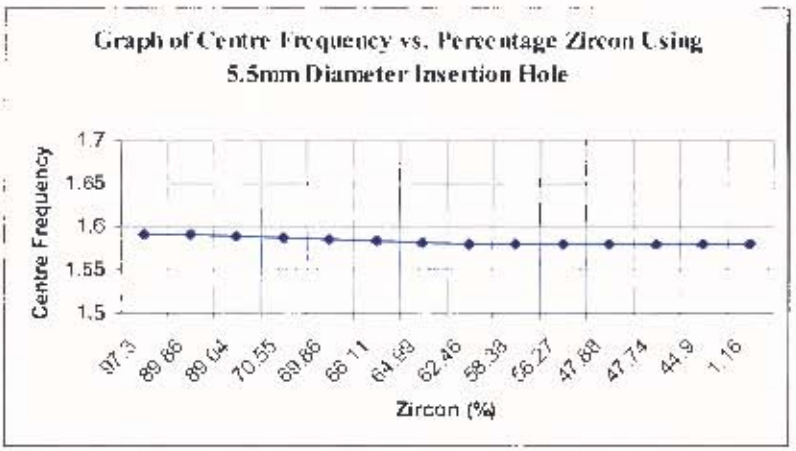

Figure 8.4 Graph of Change in Centre Frequency for different percentages of Zircon

8.4 Sample Test Using 12mm Diameter Insertion Hole (and a larger sample)

In order to achieve increased coupling the size of the insertion tube was increased to a 12mm diameter. The measurements were repeated and the graph of Q-factor responses is shown in Figure 8.5.

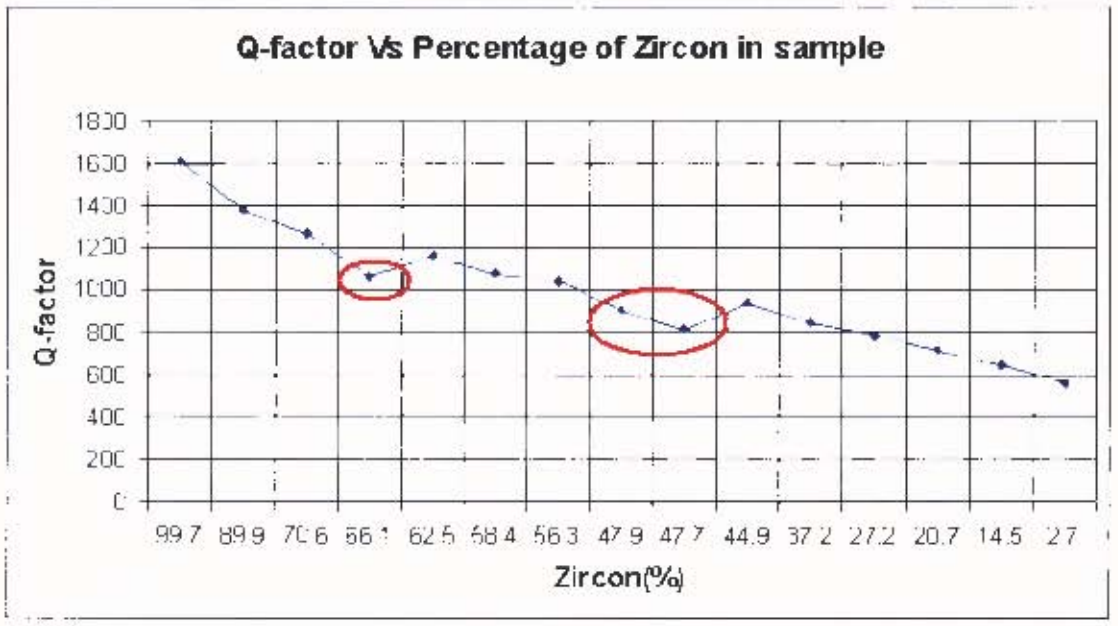

Figure 8.5 Graph of Change in Q-factor for different percentages of Zircon

From the graph above a distinct correlation can be made between the Q-factor and the percentage of Zircon. This correlation is good when the impurities are predominantly Rutile and Leucoxene. The samples highlighted in blue, in table 8.5, were deliberately added to show that if the percentage of Ilmenite is greater then 1.2% it will significantly increase the loss tangent and cannot be ignored. This is in Figure 8.5 (circled in red). This makes it very difficult to find a clear relationship for samples which contain more than 1.2% Ilmenite.

On the other hand if this effect is removed, a simple exponential decay trend line can be drawn. This effect is shown in Figure 8.6 where the contaminated samples were removed.

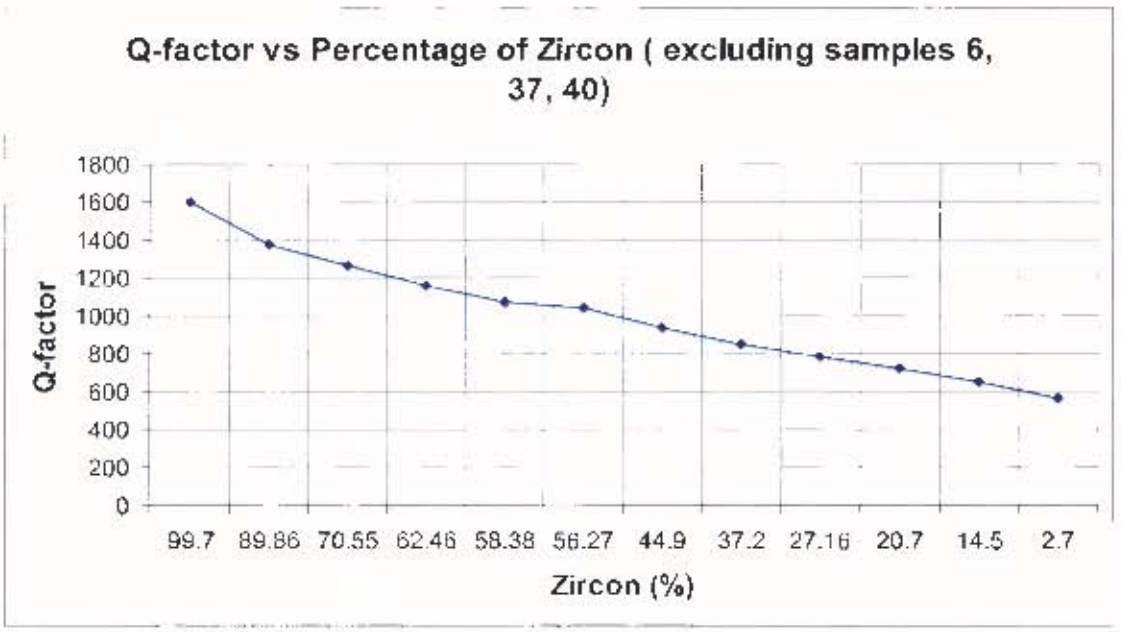

Figure 8.6 Graph of Change in Q-factor for different percentages of Zircon Excluding Sand Samples with more than 1.2% Ilmenite

The next two graphs (8.7 & 8.8) show the best fit line when the contaminated samples are present and when they are not.

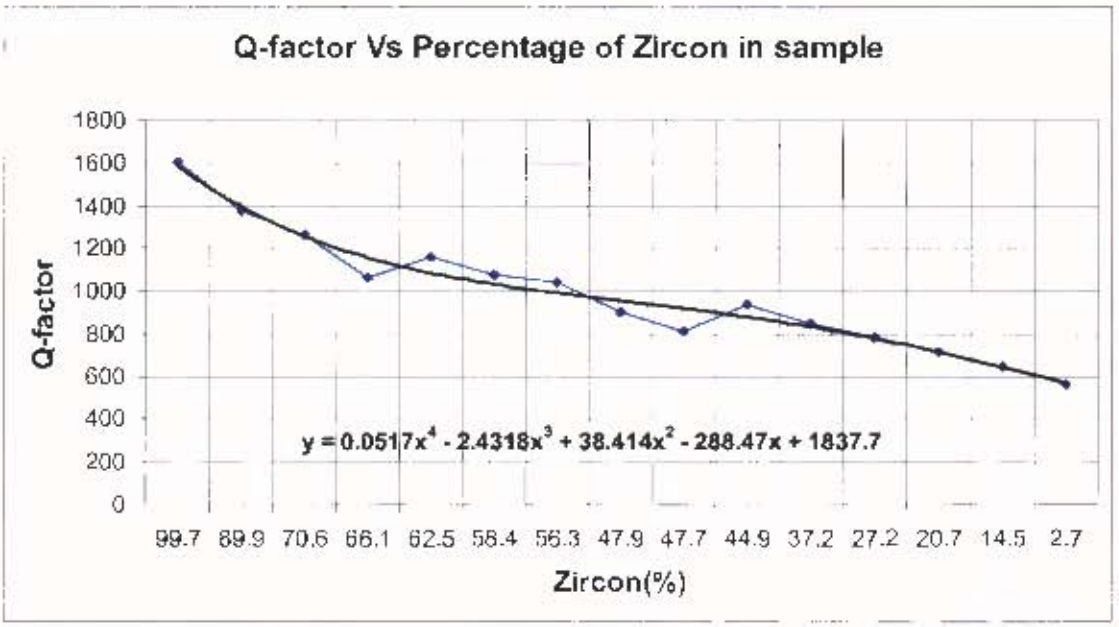

Figure 8.7 Graph of Best Trend Line to Represent Data

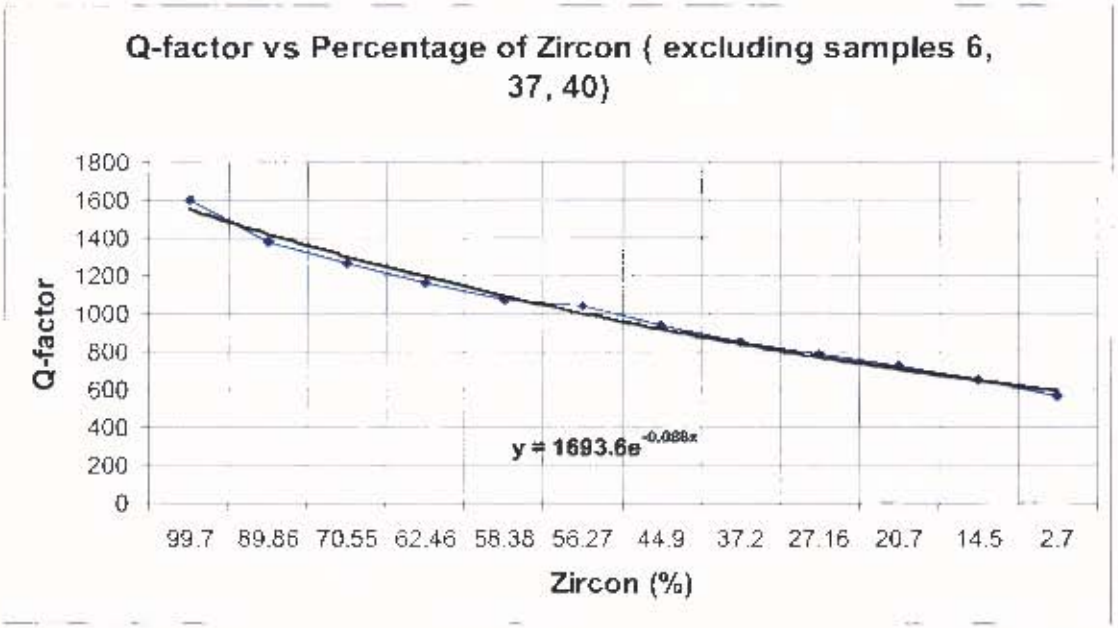

Figure 8.8 Graph of best fit Trend line to Represent Data Excluding Contaminated Sand Samples

It was further observed that the Equation of the line found in Figure 8.8 was far more simple when the contaminated samples were removed, compared to the Equation in Figure 8.8.

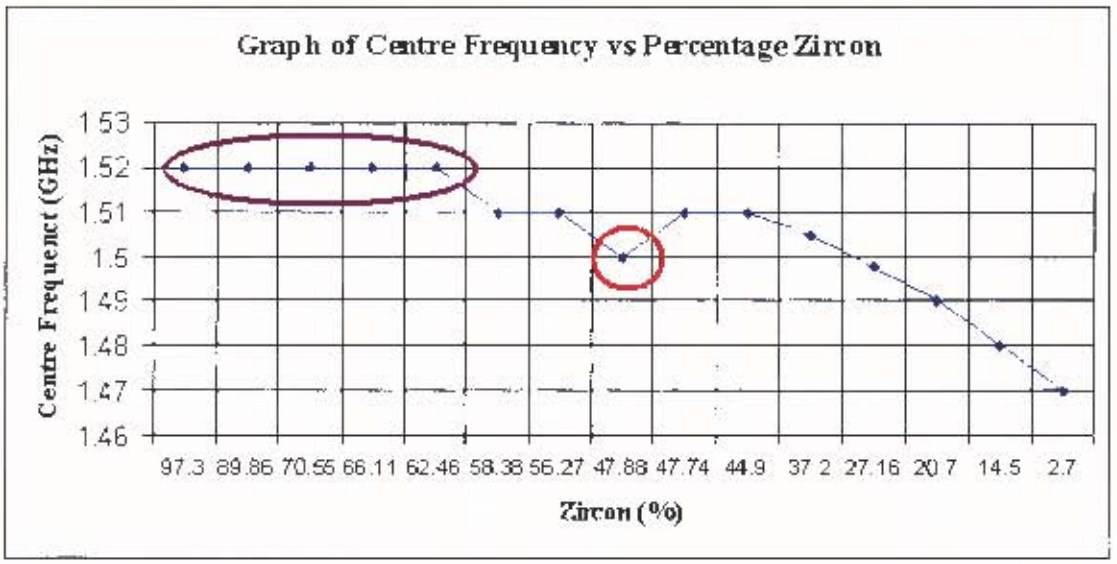

Figure 8.9 Graph of Change in Centre Frequency for different percentages of Zircon

The increase in volume of the mineral sample greatly improved the coupling and the consequent effect on Q-factor. Clearly there is not a good correlation between centre frequency reading and percentage Zircon (Figure 8.9). The area circled in purple shows an almost flat line which clearly indicates that frequency change measurements will not be able to distinguish between sand samples of varying Zircon content. Figures 8.10 shows an improvement in attenuation measurements with 12mm diameter sample. The effect of Ilmenite contaminated samples is also seen (circled in red).

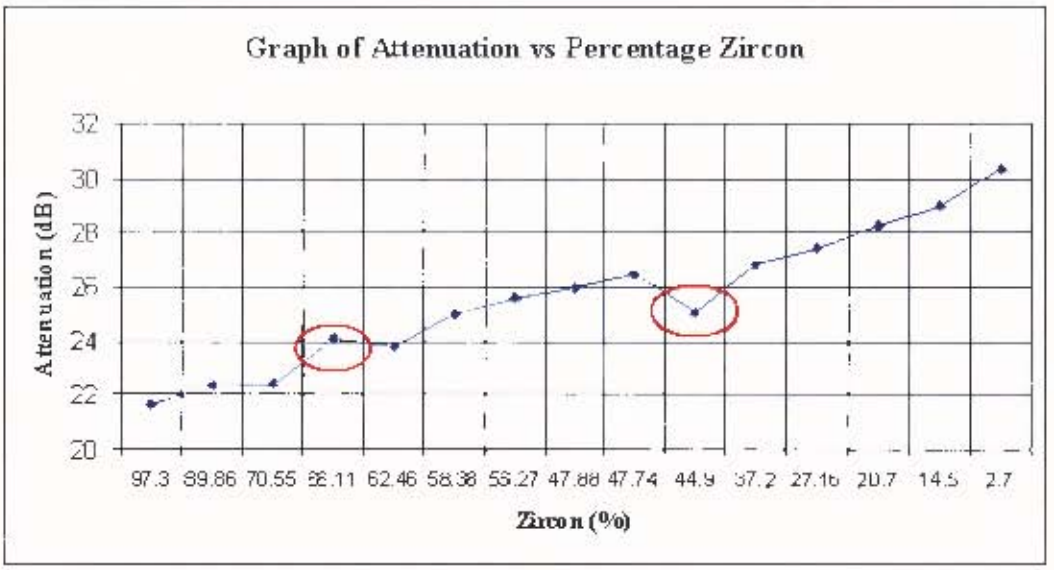

Figure 8.10 Graph of Change in Attenuation for different percentages of Zircon

8.5 Conclusions Based on Results Obtained

The resonant cavity perturbation technique proved to provide an acceptably accurate measuring technique to distinguish between different percentages of Zircon in samples. Repeatability is also consistent, provided the samples are tapped gently to fill most of the air gaps present. The effects of adding Illemnite are shown to change readings appreciably where it is more than 1.2% of the overall mix. however, Illemnite is not normally present in large amounts and should not have any significant effects. A clear correlation between the Q-factor and varying percentage of Zircon is shown in the form of an exponential decay curve in Figure 8.8. Figure 8.9 also indicates that any reading

taken to measure the dielectric constant of a sample by measuring the frequency shift is not a reliable measure of the percentage of Zircon in a sample. The attenuation curve shown in Figure 8.10 represents a better correlation with percentage of Zircon, although the Q-factor measurement was more accurate. However, in mine operating conditions the percentage of Ilmenite is normally less than 1.2 percent.

Final conclusions and comparisons between the attenuation measurement system described in Chapters 2 to 5 and resonant cavity measurement, described in Chapter 6, are made in the next Chapter.

Chapter 9

9. Conclusion and Recommendations

This thesis has investigated two microwave measuring techniques which were tested on various mineral sand samples provided by Namakwa Sands Mineral Processing Company. The samples contained Zircon product with two major impurities, Rutile, and Leucoxene. It was found that Ilmenite has a very high loss tangent and if it is present with more than 1.2%, it produced errors in the measurement system which has been calibrated for Rutile and Leucoxene impurities.

The first of the two methods, microwave attenuation techniques, was considered because of its simplicity. An operating frequency of 10.5GHz was chosen for the following reasons:

- Components were readily available at minimum expense.
- The range of attenuation measurements was about 30dB. This was an easily manageable dynamic range to achieve using a simple detector diode with good accuracy.

A Gunn diode oscillator was used to transmit the operating frequency of 10.5GHz and was modulated to 1KHz producing a 10V square wave supplying a current of 600mA. The receiver made use of the Schottky low-level detector operating in the square law region. The voltage output was read using the ICL 7107chip (A/D converter) and displayed on a LED screen. This system showed a clear correlation between attenuated voltages and the percentage of impurities in the sand sample, showing an accuracy of ± 3%. This method also indicated that change in relative humidity had insignificant affects on the measurements taken. Thus all of the user requirements were met. However, feedback indicated that this method did not provide consistent readings when measured. This was a direct result of the reflections from the interface between the air to mineral

sample. In order to reduce the inconsistency in the measurements a long waveguide was required. This ensured that the reflections from the second mineral to air interface was sufficiently attenuated to have a negligible effect on the measurements. However, the long waveguide resulted in an unacceptable large size of the instrument. Therefore a large number of readings had to be taken and an average found.

A second method, resonant cavity perturbation technique, was consequently developed in order to improve the consistency in readings and reduce the analyser's physical size. A 1.598 GHz rectangular waveguide cavity operating in TE_{101} mode was chosen and the system was excited using coupling loops. The result obtained showed a great improvement in the consistency of the results recorded. The resonant cavity is also substantially smaller than the waveguide used in the attenuation system. This analyser was also able to calculate the complex permittivity of the various minerals in the samples provided.

The experimental data obtained further indicated that if Ilmenite was present in quantities greater than 1.2%, then it would have significant effects on the readings taken since it is an extremely lossy material. It was also found that any microwave system that measured the dielectric constant as opposed to dielectric loss factor would not work as there was not much difference between the dielectric constants of the minerals.

As a result of the findings and conclusions of this report, the following recommendations are made:

- A major problem with the microwave attenuation technique arose from the reflections at the air to mineral interface. This could be eliminated using a sweep oscillator as opposed to a fixed oscillator and averaging the measurements over the frequency range.
- Further studies should be carried out in order to understand the hygroscopic nature of the sample and the relationship of inbound moisture content and relative humidity.

- A network analyser was used for the resonant cavity technique. It is recommended that a much cheaper version of the network analyser for this system in order to have a cost effective system. This system need be no more expensive or complex than that used in the attenuation system.
- A suitable method of packing the sand sample should be investigated to achieve greater consistency.

List of References

[1] http://www.rbm.co.za/mining.htm

[2] http://www.rbm.co.za/market.htm

[3] http://www.outokumpu.com/files/Technology/Documents/Physical%20Separation/Technical%20Papers/ManyusesofREBA.pdf

[4] http://en.wikipedia.org/wiki/Infra-red_spectroscopy

[5] http://en.wikipedia.org/wiki/X-ray_photoelectron_spectroscopy

[6] http://www.earthsci.unibe.ch/people/scherrer/micro-XRF/XRFinstrument/xrf.htm

[7] http://www.alschemex.com/learnmore/learnmore-techinfo-principles-analyticalmethodologies.htm

[8] http://www.tscm.com/rf_absor.pdf

[9] http://demining.jrc.it/aris/events/mine99/program/P66-71/p66-71.htm

[10] http://www.people.virginia.edu/~lz2n/mse209/Chapter19-p3.pdf

[11] J.C Anderson, 'Dielectrics', Reader in Electrical Engineering Imperial College, Ph.D, (1964), pp 21-38

[12] Graeme Pendock, 'An investigation of minerals using microwave measurements of complex permittivity', MSc Thesis in Electrical Engineering, Department Of Electrical Engineering, University of Cape town April 1990.

[13] B.K.P. Schaife, 'Complex Permittivity', The English Universities Press, 1971

[14] J.Vincent, 'Moisture Measurement in Sand Using Attenuation Of microwave Irradiation', Undergraduate Thesis, Department Of Electrical Engineering, University of Cape town, 3 June 1991.

[15] Dennis Roddy, 'Microwave Technology', 1996 by Prentice-Hall.

[16] E.I.Parkomenko, 'Electrical Properties of Rocks', Plenum Press, 1967.

[17] M.Broek, 'Ore Level Detector'. MSc thesis, Department Of Electrical Engineering, University Of Cape Town, 1990.

[18] D.Roddy, 'Microwave Technology', Prentice Hall, 1986.

[19] G.H.Bryant, 'Principles of Microwave Measurement', 1988 Peter Peregrinus Ltd.

[20] P.A.Matthews & I.M.Stephenson, 'Microwave Components', Butler & Tanner Ltd, Frame and London, 1968.

[21] Paul Horowitz and Winfield Hill, 'The Art of Electronics ',Cambridge, {Eng.} New York Cambridge University Press, 1980.

[22] http://nucl.phys.s.u-tokyo.ac.jp/widmann/hfs-lit/cavity-bead-pull.pdf

[23] Reinmut K.Hoffmann, 'Handbook of Microwave Intergrated Circuits', Library of Congress Cataloging-in- Publication Data, 1987.

[24] A.F. Harvey, 'Microwave Engineering',Academic Press London and New York, 1963.

[25] Stephen F. Adam, 'Microwave Theory and Applications', Prentice-Hall,INC. 1969.

[26] A.C.Metaxas & R.J. Mederith, 'Industrial Microwave Heating', Peter Peregrinus Ltd, London, 1993.

[27] http://wug.physics.uiuc.edu/courses/Phys301/301exp/E44/E44.pdf

[28] http://www.flyash.info/2001/benef1/16bittn.pdf

[29] X. K. Ridley and T. B. Watkins, ' The Possibility of Negative Resistance Effect Semiconductors' Proc. Phys. Soc. (London), 73, August 1961.

Appendix i

Look-up table for Microwave Attenuation System

Voltage	Percentage
0.79	32.18925831
0.80	32.44501279
0.81	32.70076726
0.82	32.95652174
0.83	33.21227621
0.84	33.46803069
0.85	33.72378517
0.86	33.97953964
0.87	34.23529412
0.88	34.49104859
0.89	34.74680307
0.90	35.00255754
0.91	35.25831202
0.92	35.51406650
0.93	35.76982097
0.94	36.02557545
0.95	36.28132992
0.96	36.53708440
0.97	36.79283887
0.98	37.04859335
0.99	37.30434783
1.00	37.56010230
1.01	37.81585678
1.02	38.07161125
1.03	38.32736573
1.04	38.58312020
1.05	38.83887468
1.06	39.09462916
1.07	39.35038363
1.08	39.60613811
1.09	39.86189258
1.10	40.11764706
1.11	40.37340153
1.12	40.62915601
1.13	40.88491049
1.14	41.14066496
1.15	41.39641944
1.16	41.65217391
1.17	41.90792839
1.18	42.16368286

Voltage	Percentage
1.19	42.41943734
1.20	42.67519182
1.21	42.93094629
1.22	43.18670077
1.23	43.44245524
1.24	43.69820972
1.25	43.95396419
1.26	44.20971867
1.27	44.46547315
1.28	44.72122762
1.29	44.97698210
1.30	45.23273657
1.31	45.48849105
1.32	45.74424552
1.33	46.00000000
1.34	46.25575448
1.35	46.51150895
1.36	46.76726343
1.37	47.02301790
1.38	47.27877238
1.39	47.53452685
1.40	47.79028133
1.41	48.04603581
1.42	48.30179028
1.43	48.55754476
1.44	48.81329923
1.45	49.06905371
1.46	49.32480818
1.47	49.58056266
1.48	49.83631714
1.49	50.09207161
1.50	50.34782609
1.51	50.60358056
1.52	50.85933504
1.53	51.11508951
1.54	51.37084399
1.55	51.62659847
1.56	51.88235294
1.57	52.13810742
1.58	52.39386189

Voltage	Percentage
1.59	52.64961637
1.60	52.90537084
1.61	53.16112532
1.62	53.41687980
1.63	53.67263427
1.64	53.92838875
1.65	54.18414322
1.66	54.43989770
1.67	54.69565217
1.68	54.95140665
1.69	55.20716113
1.70	55.46291560
1.71	55.71867008
1.72	55.97442455
1.73	56.23017903
1.74	56.48593350
1.75	56.74168798
1.76	56.99744246
1.77	57.25319693
1.78	57.50895141
1.79	57.76470588
1.80	58.02046036
1.81	58.27621483
1.82	58.53196931
1.83	58.78772379
1.84	59.04347826
1.85	59.29923274
1.86	59.55498721
1.87	59.81074169
1.88	60.06649616
1.89	60.32225064
1.90	60.57800512
1.91	60.83375959
1.92	61.08951407
1.93	61.34526854
1.94	61.60102302
1.95	61.85677749
1.96	62.11253197
1.97	62.36828645
1.98	62.62404092
1.99	62.87979540
2.00	63.13554987
2.01	63.39130435

Voltage	Percentage
2.02	63.64705882
2.03	63.90281330
2.04	64.15856777
2.05	64.41432225
2.06	64.67007673
2.07	64.92583120
2.08	65.18158568
2.09	65.43734015
2.10	65.69309463
2.11	65.94884910
2.12	66.20460358
2.13	66.46035806
2.14	66.71611253
2.15	66.97186701
2.16	67.22762148
2.17	67.48337596
2.18	67.73913043
2.19	67.99488491
2.20	68.25063939
2.21	68.50639386
2.22	68.76214834
2.23	69.01790281
2.24	69.27365729
2.25	69.52941176
2.26	69.78516624
2.27	70.04092072
2.28	70.29667519
2.29	70.55242967
2.30	70.80818414
2.31	71.06393862
2.32	71.31969309
2.33	71.57544757
2.34	71.83120205
2.35	72.08695652
2.36	72.34271100
2.37	72.59846547
2.38	72.85421995
2.39	73.10997442
2.40	73.36572890
2.41	73.62148338
2.42	73.87723785
2.43	74.13299233
2.44	74.38874680

Voltage	Percentage
2.45	74.64450128
2.46	74.90025575
2.47	75.15601023
2.48	75.41176471
2.49	75.70627000
2.50	76.07615894
2.51	76.40728477
2.52	76.7384106
2.53	77.06953642
2.54	77.40066225
2.55	77.73178808
2.56	78.06291391
2.57	78.39403974
2.58	78.72516556
2.59	79.05629139
2.60	79.38741722
2.61	79.71854305
2.62	80.04966887
2.63	80.38079470
2.64	80.71192053
2.65	81.04304636
2.66	81.37417219
2.67	81.70529801
2.68	82.03642384
2.69	82.36754967
2.70	82.69867550
2.71	83.02980132
2.72	83.36092715
2.73	83.69205298
2.74	84.02317881
2.75	84.35430464
2.76	84.68543046
2.77	85.01655629
2.78	85.34768212
2.79	85.67880795
2.80	86.00993377
2.81	86.34105960
2.82	86.67218543
2.83	87.00331126
2.84	87.33443709
2.85	87.66556291
2.86	87.99668874
2.87	88.32781457

Voltage	Percentage
2.88	88.65894040
2.89	88.99006623
2.90	89.32119205
2.91	89.65231788
2.92	89.98344371
2.93	90.31456954
2.94	90.64569536
2.95	90.97682119
2.96	91.30794702
2.97	91.63907285
2.98	91.97019868
2.99	92.30132450
3.00	92.70105263
3.01	92.91157895
3.02	93.12210526
3.03	93.33263158
3.04	93.54315789
3.05	93.75368421
3.06	93.96421053
3.07	94.17473684
3.08	94.38526316
3.09	94.59578947
3.10	94.80631579
3.11	95.01684211
3.12	95.22736842
3.13	95.43789474
3.14	95.64842105
3.15	95.85894737
3.16	96.06947368
3.17	96.28000000
3.18	96.49052632
3.19	96.70068000
3.20	96.80074400
3.21	96.89970646
3.22	96.99719704
3.23	97.09321574
3.24	97.18776256
3.25	97.28083750
3.26	97.37244056
3.27	97.46257174
3.28	97.55123104
3.29	97.63841846
3.30	97.72413400

Voltage	Percentage
3.31	97.80837766
3.32	97.89114944
3.33	97.97244934
3.34	98.05227736
3.35	98.13063350
3.36	98.20751776
3.37	98.28293014
3.38	98.35687064
3.39	98.42933926
3.40	98.50033600
3.41	98.56986086
3.42	98.63791384
3.43	98.70449494
3.44	98.76960416
3.45	98.83324150
3.46	98.89540696
3.47	98.95610054
3.48	99.01532224
3.49	99.07307206
3.50	99.12901500
3.51	99.14533589
3.52	99.16179456
3.53	99.17805101
3.54	99.19410524
3.55	99.20995725
3.56	99.22560704
3.57	99.24105461
3.58	99.25629996
3.59	99.27134309
3.60	99.28618400
3.61	99.30082269
3.62	99.31525916
3.63	99.32949341
3.64	99.34352544
3.65	99.35735525
3.66	99.37098284
3.67	99.38440821
3.68	99.39763136
3.69	99.41065229
3.70	99.42347100
3.71	99.43608749
3.72	99.44850176
3.73	99.46071381

Voltage	Percentage
3.74	99.47272364
3.75	99.48453125
3.76	99.49613664
3.77	99.50753981
3.78	99.51874076
3.79	99.52973949
3.80	99.54053600
3.81	99.55113029
3.82	99.56152236
3.83	99.57171221
3.84	99.58169984
3.85	99.59148525
3.86	99.60106844
3.87	99.61044941
3.88	99.61962816
greater than 3.88V = 100 %	

Appendix ii

Data Collected from Resonant Cavity Test

DATA COLLECTED WITH THE 5.5MM DIAMETER INSERTION HOLE.

	Q-Factor				
Sample ID	**Test 1**	**Test 2**	**Test 3**	**Test avg.**	**% Zircon**
uct 1	1982.60	1982.75	1982.75	1982.70	97.30
mic 33	1982.63	1982.75	1982.63	1982.67	89.86
mic 35	1982.75	1982.63	1982.63	1982.67	89.04
mic 34	1981.63	1981.63	1981.62	1981.62	70.55
mic 38	1981.75	1980.75	1981.25	1981.25	69.86
mic 37	1980.63	1980.75	1980.50	1980.63	66.11
uct 3	1980.13	1980.75	1980.75	1980.54	64.99
mic 03	1980.63	1980.13	1980.63	1980.46	62.46
uct 4	1759.78	1759.67	1759.11	1759.52	58.38
mic 27	1759.00	1759.82	1759.44	1759.42	56.27
mic 06	1758.33	1757.44	1757.78	1757.85	47.88
mic 40	1757.89	1757.55	1757.44	1757.63	47.74
uct 5	1757.11	1755.60	1757.67	1756.79	44.90

	Attenuation(att.)				
Sample ID	**Test 1**	**Test 2**	**Test 3**	**Att. Avg**	**% Zircon**
uct 1	13.20	11.80	12.80	12.60	97.30
mic 33	13.60	12.20	13.30	13.03	89.86
mic 35	13.40	12.20	13.30	12.97	89.04
mic34	14.00	12.40	13.50	13.30	70.55
mic 38	13.40	12.70	13.70	13.27	69.86
mic 37	14.00	13.80	13.30	13.70	66.11
uct 3	14.40	12.10	13.90	13.47	64.99
mic 03	13.40	12.60	13.60	13.20	62.46
uct4	13.80	12.40	13.70	13.30	58.38
mic 27	13.80	12.80	14.00	13.53	56.27
mic 06	14.60	13.20	14.50	14.10	47.88
mic 40	14.60	13.80	14.50	14.30	47.74
uct 5	14.10	14.10	14.50	14.23	44.90

	Centre fequency(Fc) in GHz				
Sample ID	**Test 1**	**Test 2**	**Test 3**	**Fc avg**	**%Zircon**
uct 1	1.59	1.59	1.59	1.59	97.30
mic 33	1.59	1.59	1.59	1.59	89.86
mic 35	1.59	1.59	1.59	1.59	89.04
mic34	1.59	1.59	1.59	1.59	70.55
mic 38	1.59	1.58	1.58	1.58	69.86
mic 37	1.58	1.58	1.58	1.58	66.11
uct 3	1.58	1.58	1.58	1.58	64.99
mic 03	1.58	1.58	1.58	1.58	62.46
uct4	1.58	1.58	1.58	1.58	58.38
mic 27	1.58	1.58	1.58	1.58	56.27
mic 06	1.58	1.58	1.58	1.58	47.88
mic 40	1.58	1.58	1.58	1.58	47.74
uct 5	1.58	1.58	1.58	1.58	44.90

DATA COLLECTED WITH THE 12mm DIAMETER INSERTION HOLE.

Q-factor					
Sample	**Q1**	**Q2**	**Q3**	**Q-factor**	**Zircon**
uct 1	1605.00	1610.00	1615.00	1610.00	99.70
mic 33	1390.00	1390.00	1390.00	1390.00	89.86
mic 34	1300.00	1306.00	1295.00	1300.33	70.55
mic 37	1088.00	1090.00	1093.00	1090.33	66.11
mic 03	1160.00	1174.00	1167.00	1167.00	62.46
uct 4	1086.00	1088.00	1087.00	1087.00	58.38
mic 27	1025.00	1030.50	1034.50	1030.00	56.27
mic 06	882.00	890.00	886.00	886.00	47.88
mic 40	810.00	810.00	810.00	810.00	47.74
uct 5	913.00	907.00	911.00	910.33	44.90
uct 6	855.00	852.00	852.00	853.00	37.20
uct 7	790.00	792.00	788.00	790.00	27.16
uct 8	706.00	712.00	713.00	710.33	20.70
uct 9	633.00	633.00	633.00	633.00	14.50
uct 10	577.00	578.00	576.00	577.00	2.70

Centre Frequency (fc) in GHz					
Sample	**fc1**	**fc2**	**fc3**	**Average**	**%Zircon**
uct 1	1.52	1.52	1.53	1.52	97.30
mic 33	1.52	1.52	1.52	1.52	89.86
mic 34	1.52	1.52	1.53	1.52	70.55
mic 37	1.51	1.51	1.52	1.52	66.11
mic 03	1.51	1.51	1.52	1.52	62.46
uct 4	1.51	1.51	1.51	1.51	58.38
mic 27	1.50	1.51	1.51	1.51	56.27
mic 06	1.50	1.50	1.50	1.50	47.88
mic 40	1.51	1.51	1.51	1.51	47.74
uct 5	1.50	1.51	1.51	1.51	44.90
uct 6	1.50	1.51	1.50	1.50	37.20
uct 7	1.51	1.49	1.49	1.50	27.16
uct 8	1.48	1.49	1.48	1.49	20.70
uct 9	1.48	1.48	1.49	1.48	14.50
uct 10	1.47	1.47	1.48	1.47	2.70

ATTENUATION (dB's)					
Sample ID	**Att-1**	**Att-2**	**Att-3**	**Attenuation**	**%Zircon**
uct 1	20.00	20.00	25.00	21.67	97.30
mic 33	21.50	20.00	25.20	22.23	89.86
mic 34	21.55	20.20	25.00	22.25	70.55
mic 37	22.00	22.20	28.00	24.07	66.11
mic 03	22.00	21.55	28.00	23.85	62.46
uct 4	23.00	22.00	30.00	25.00	58.38
mic 27	22.96	24.20	30.00	25.72	56.27
mic 06	24.00	24.00	30.54	26.18	47.88
mic 40	24.50	24.00	31.00	26.50	47.74
uct 5	23.00	22.20	30.00	25.07	44.90
uct 6	24.50	24.00	32.00	26.83	37.20
uct 7	25.00	25.20	32.00	27.40	27.16
uct 8	26.50	25.20	33.00	28.23	20.70
uct 9	27.00	27.00	33.00	29.00	14.50
uct 10	29.00	28.00	34.00	30.33	2.70

Appendix iii

Reference Table of Rigid Rectangular Waveguide Data [24]

		Inside dimensions, in					
British R.C.S.C type	American E.I.A. type	Width	Depth	TE_{01} Cut-off, Gc/s	Operating range, Gc/s	Attenuation,dB/100 ft	Power rating, kW
WG 1	WR 1800	18·000	9·000	0·327	0·41-0·61	0·0334	115,000
WG 2	WR 1500	15·000	7·500	0·393	0·51-0·75	0·0438	85,000
WG 3	WR 1150	11·500	5·750	O·517	1·61-0·96	1·0614	45,000
WG 4	WR 975	9·750	4·875	0·605	0·75-1·12	0·0807	33,000
WG 5	WR 770	7·700	3·850	0·765	0·96-1·45	0·120	21,500
WG 6	WR 650	6·500	3·250	0·908	1·12-1·70	0·154	14,800
WG 7	WR 510	5·100	2·550	1·154	1·45-2·20	0·222	9,300
WG 8	WR 430	4·300	2·150	1·375	1·70-2·60	0·286	6,500
WG 9 A	WR 340	3·400	1·700	1·737	2·20-3·30	0·450	4,200
WG 10	WR 284	2·840	1·340	2·080	2·60-3·95	0·555	2,800
WG 11 A	WR 229	2·290	1·145	2·579	3·30-4·90	0·750	2,000
WG 12	WR 187	1·872	0·872	3·155	3·95-5·85	1·047	1,200
WG 13	WR 159	1·590	0·795	3·710	4·90-7·05	1·259	900
WG 14	WR 137	1·372	0·622	4·285	5·85-8·20	1·700	620
WG 15	WR 112	1·122	0·497	5·260	7·05-10·0	2·338	420
WG 16	WR 90	0·900	0·400	6·56	8·20-12·4	3·24	250
WG 17	WR 75	0·750	0·375	7·87	10·0-15·0	3·92	205
WG 18	WR 62	0·622	0·311	9·49	12·4-18·0	5·21	145
WG 19	WR 51	0·510	0·255	11·57	15·0-22·0	7·00	95
WG 20	WR 42	0·420	0·170	14·08	18·0-26·5	10·9	52
WG 21	WR 34	0·340	0·170	17·37	22·0-33·0	12·8	43
WG 22	WR 28	0·280	0·140	21·10	26·5-40·0	17·3	28
WG 23	WR 22	0·224	0·112	26·35	33·0-50·0	24·0	18
WG 24	WR 19	0·188	0·094	31·4	40·0-60·0	31·3	14
WG 25	WR 15	0·148	0·074	39·9	50·0-75·0	44·7	8
WG 26	WR 12	0·122	0·061	48·4	60·0-90·0	59·7	5
WG 27	WR 10	0·100	0·050	59·0	75·0-110	80·7	3·8
WG 28		0·0800	0·0400	73·8	90·0-140	113	2·3
WG 29		0·0650	0·0325	90·9	110-170	154.00	1·5
WG 30		0·0510	0·0255	115·8	140-220	225.00	0·90
WG 31		0·0430	0·0215	137·5	170-260	286.00	0·65
WG 32		0·0340	0·0170	173·3	220-325	405.00	0·42

PLEASE FOLLOW THESE INSTRUCTIONS

- **Switch on machine**
- **Leave idle for one hour before use**
- **Fill funnel with sand sample**
- **Place finger over outlet of funnel**
- **Gradually fill waveguide until full**
- **Make sure sand is level with top of waveguide**
- **Slide waveguide in from left between two terminals**
- **Do not touch waveguide (This disturbs sand level)**
- **Tighten screws on bottom plate (anti clockwise direction)**
- **Tighten screws on top plate (same direction)**
- **Do not tighten screws too much (thread damage)**
- **Measurements to be taken are only for products in region of 70 to 100% pure Zircon**

Instruction Guide

The device is required to be switched on and to be left idle for at least an hour before use.

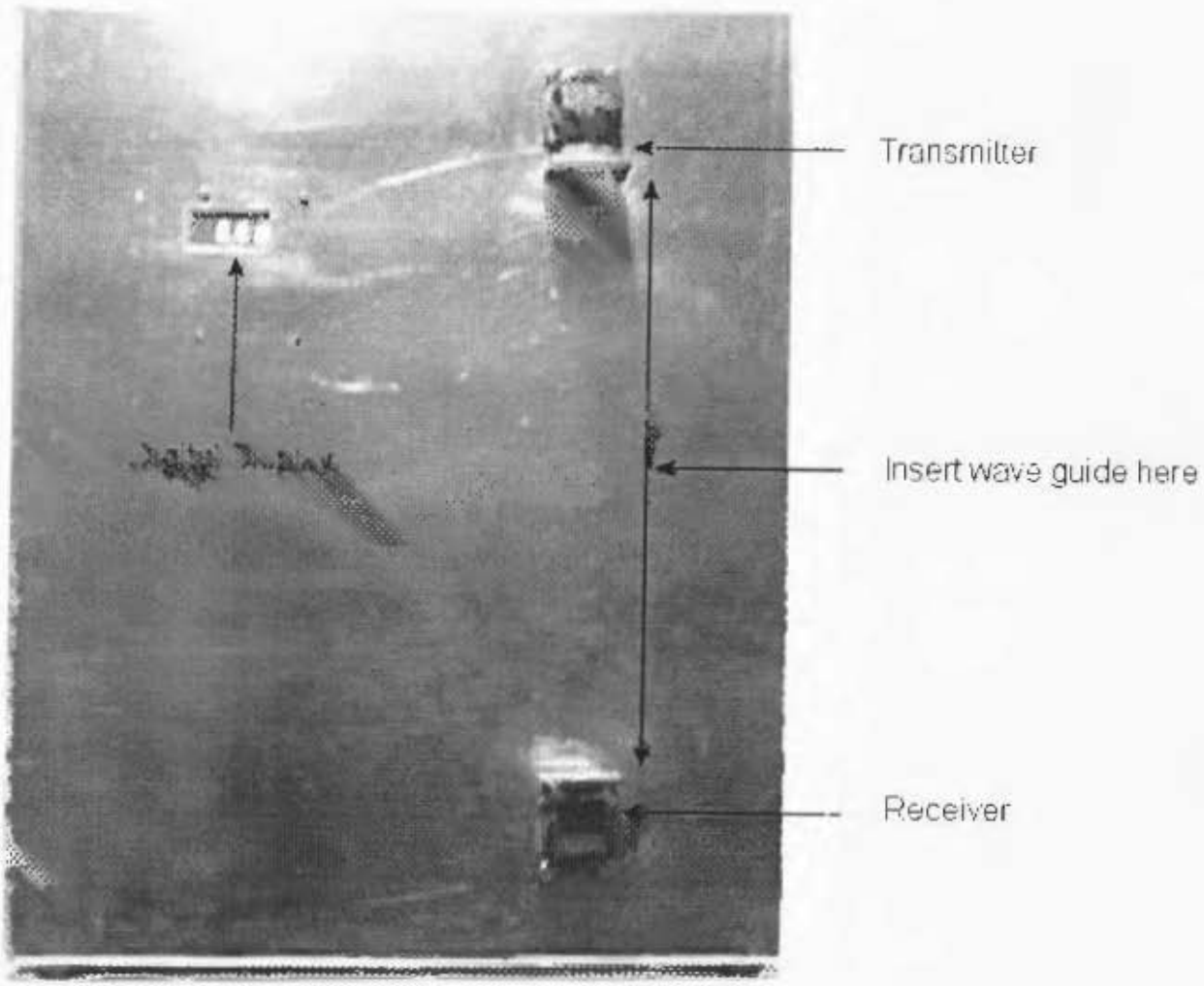

Digital Display:

2 decimal point digital display.

Transmitter and Receiver

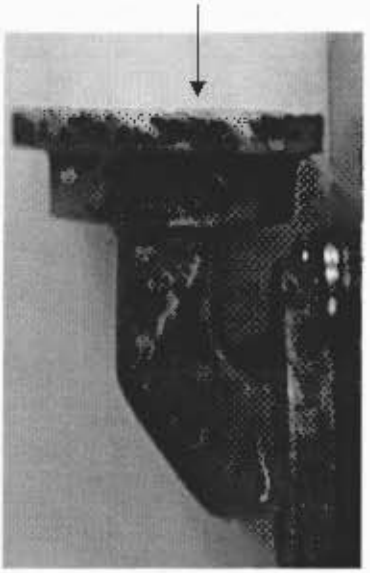

Waveguide

A copper waveguide that is to be used to contain the sand is to be placed between the transmitter and receiver shown above.

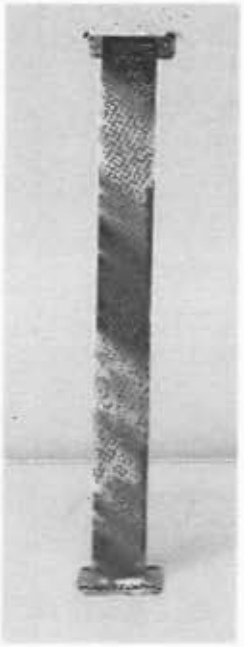

Filling the waveguide:

1. Fill funnel with selected sand sample (see below).

2. Fill waveguide until a heap of sand forms at the mouth (see below).

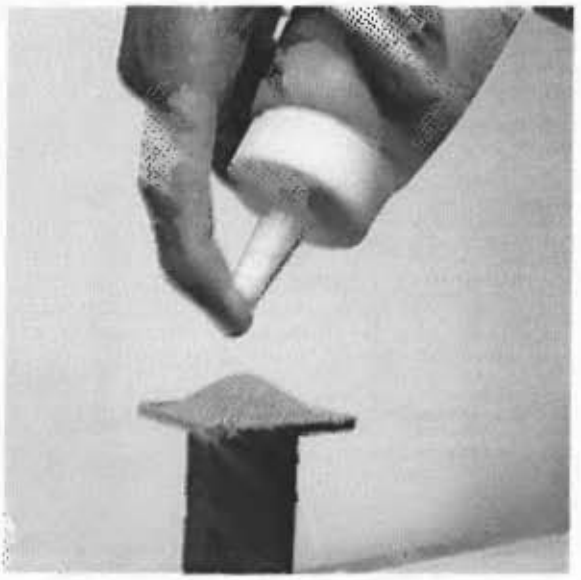

3. Hit waveguide on a flat hard surface to allow the contents to settle. **(Note: do not use a surface that can absorb any impact, this will affect the contents and the final results).**

4. The total volume of the sand will decrease (see below).

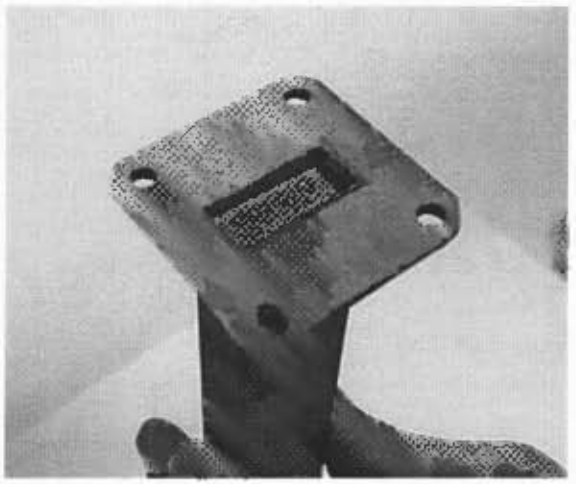

Add more off the sample to the waveguide while hitting the waveguide on the table surface.

5. When the waveguide is compacted enough leave a heap of sand on the mouth. **(Discretion must be used when determining how compact the sand is. However, consistency must be maintained for all sample readings.)**

   Using a ruler, clear the excess sand from the mouth.

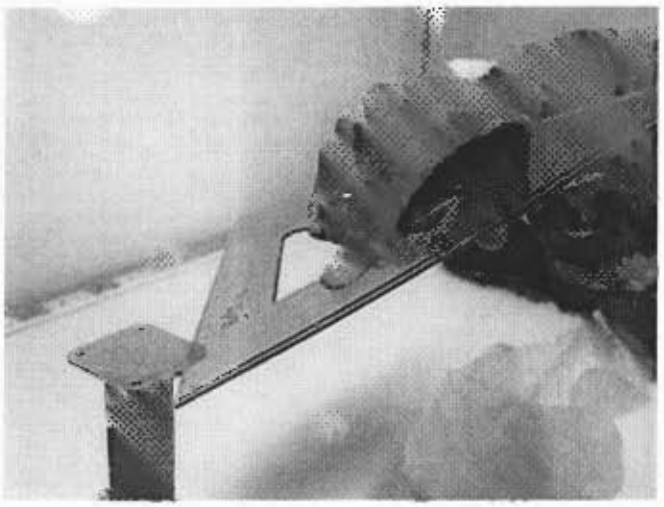

6. Insert the waveguide into the unit (Note: Insert the waveguide between the transmitter and the receiver from the left side, as indicated in the image below)

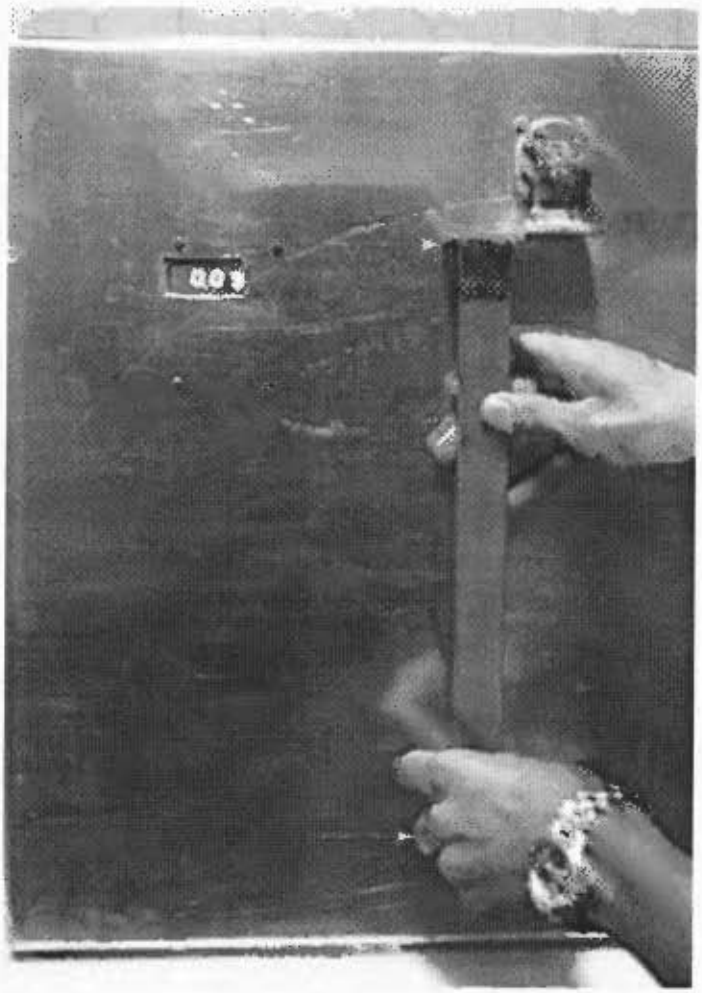

7. Line the holes up carefully without disturbing the waveguide, or the unit itself. (Note: any violent movement disturbing the waveguide will result in spurious results).

8. Insert the 4 mm into the transmitter as shown below.

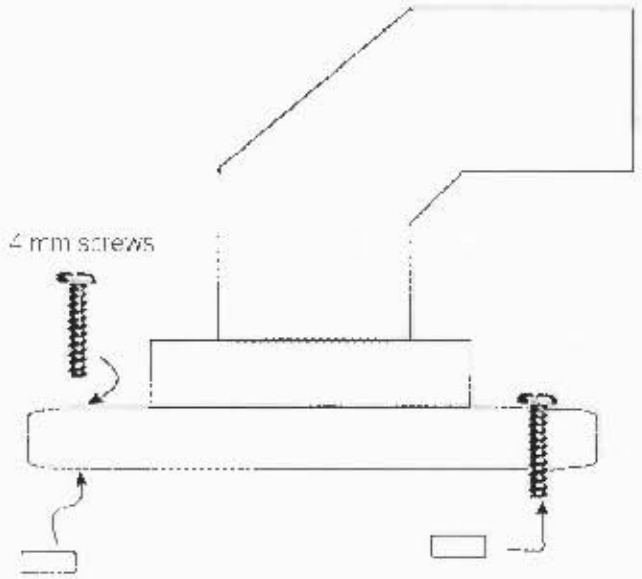

Insert the same size screws into the receiver.

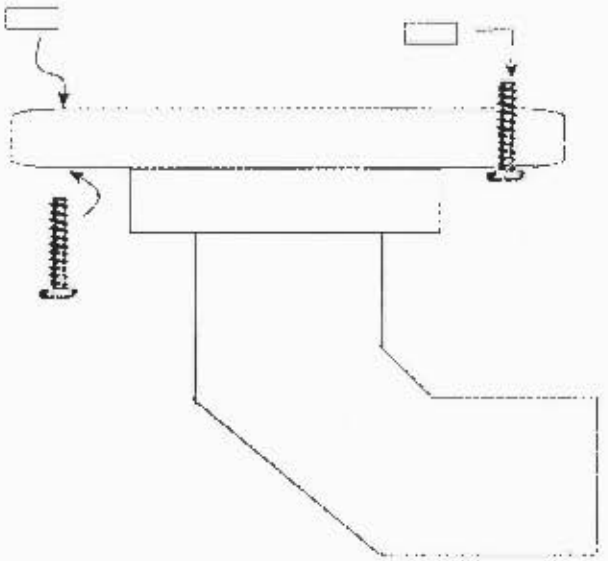

(Note: The direction of the insertion of the screws is important. Any variation in this arrangement will result in spurious results).

9. Tighten the screws:

When tightening the screws the sequence used to tighten the screws for the transmitter must be the same as the receiver. The screws of the receiver must be tightened first.

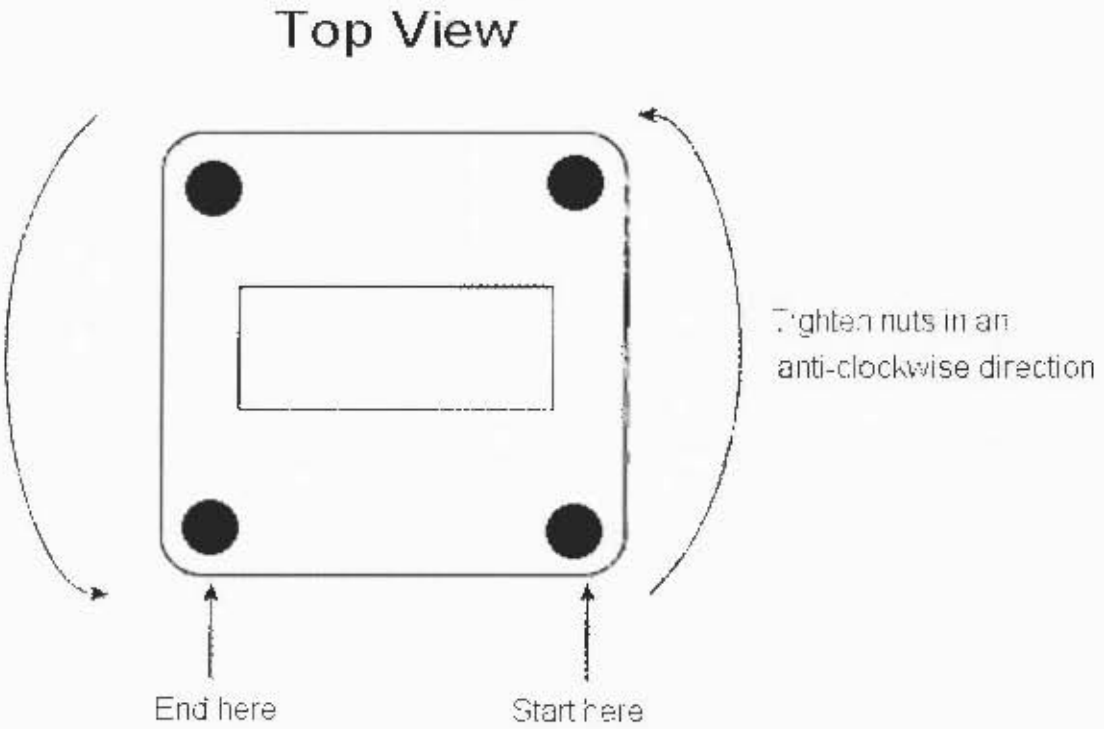

The diagram shown above is the top view of the transmitter and the receiver.

(Note. The last screw to be tightened must be at the position in the diagram above labelled "end here". The screws should not be tightened too much so as to avoid stripping of the thread.)

10. Reading the results:

The output of the system can be read off the digital display.

11. Removing the waveguide:

To see if the readings that were accurate. the waveguide must be removed carefully. The level of the contents determines the accuracy of the reading.

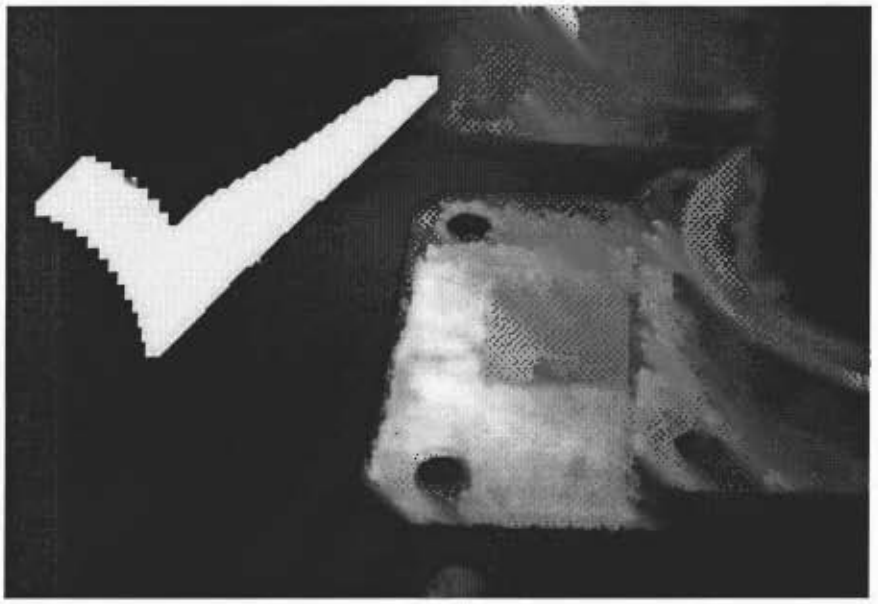

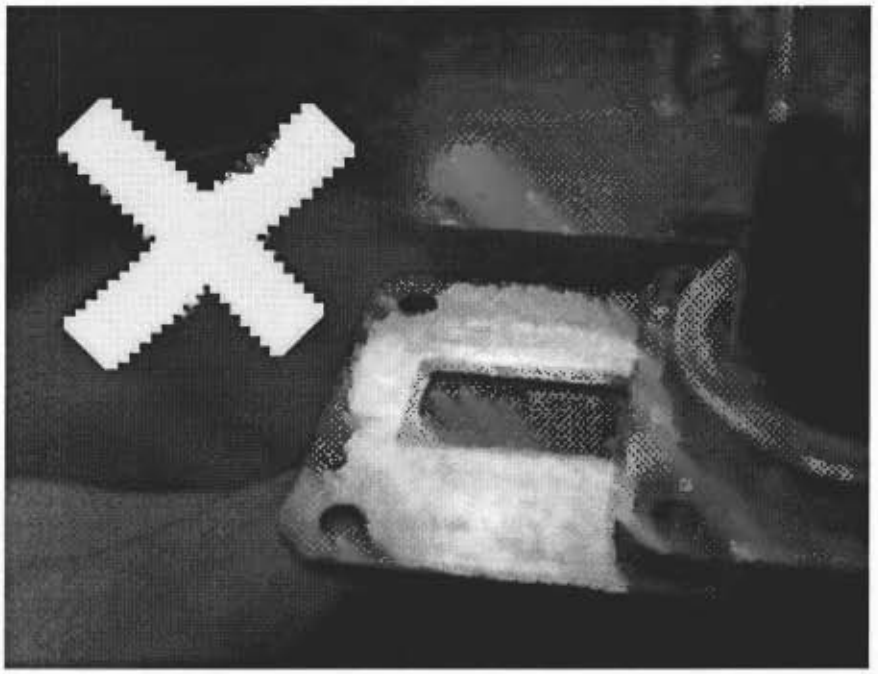

Once the waveguide is secure and a stable result is obtained on the screen the reading should be recorded.

Please note that readings should only be taken for products within 70% to 100% Zircon.